ROYAL SOCIETY
OF CHEMISTRY

REVIEW ARTICLE

Check for updates

The coming of age of water channels for separation membranes: from biological to biomimetic to synthetic

Yu Jie Lim, †[abc] Kunli Goh †[a] and Rong Wang *[ab]

Water channels are one of the key pillars driving the development of next-generation desalination and water treatment membranes. Over the past two decades, the rise of nanotechnology has brought together an abundance of multifunctional nanochannels that are poised to reinvent separation membranes with performances exceeding those of state-of-the-art polymeric membranes within the water–energy nexus. Today, these water nanochannels can be broadly categorized into biological, biomimetic and synthetic, owing to their different natures, physicochemical properties and methods for membrane nanoarchitectonics. Furthermore, against the backdrop of different separation mechanisms, different types of nanochannel exhibit unique merits and limitations, which determine their usability and suitability for different membrane designs. Herein, this review outlines the progress of a comprehensive amount of nanochannels, which include aquaporins, pillar[5]arenes, I-quartets, different types of nanotubes and their porins, graphene-based materials, metal– and covalent–organic frameworks, porous organic cages, MoS_2, and MXenes, offering a comparative glimpse into where their potential lies. First, we map out the background by looking into the evolution of nanochannels over the years, before discussing their latest developments by focusing on the key physicochemical and intrinsic transport properties of these channels from the chemistry standpoint. Next, we put into perspective the fabrication methods that can nanoarchitecture water channels into high-performance nanochannel-enabled membranes, focusing especially on the distinct differences of each type of nanochannel and how they can be leveraged to unlock the as-promised high water transport potential in current mainstream membrane designs. Lastly, we critically evaluate recent findings to provide a holistic qualitative assessment of the nanochannels with respect to the attributes that are most strongly valued in membrane engineering, before discussing upcoming challenges to share our perspectives with researchers for pathing future directions in this coming of age of water channels.

[a] Singapore Membrane Technology Center, Nanyang Environment and Water Research Institute, Nanyang Technological University, 637141, Singapore. E-mail: rwang@ntu.edu.sg

[b] School of Civil and Environmental Engineering, Nanyang Technological University, 639798, Singapore

[c] Interdisciplinary Graduate Programme, Graduate College, Nanyang Technological University, 637553, Singapore

† These authors contributed equally to this work.

1. Introduction

Nature does many magnificent things with molecules and fluids at the molecular scale and in a very efficient and structured manner. One example is aquaporins (AQPs), biological water protein nanochannels prominently known for their superb transport of water ($>10^9$ molecules per s) with the ability to reject all solutes.[1–6] However, reproducing the impressive, yet complex behaviours observed in AQPs is not an easy feat because the behaviour of fluids and ions at the nanoscale departs in many aspects from classical continuum mechanics.[7–9] In the past four decades, nanoscale science and technology, often termed nanotechnology, has opened up the possibility of manipulating matter at the level of single atoms as well as the ability to study the properties of materials at the nanoscale. One of the critical outcomes of nanotechnology is the discovery and creation of nanochannels, which are referred to as solid-state channels with cavities that act as confined spaces for the selective transport of small molecules at the sub-nanometre scale.[10–13] In an interesting contrast, the exploration of mass and momentum transport at the ångström scale has steadily emerged over the past 15–20 years.[14,15] Since then, nanochannel research has undergone a quantum leap that is evidenced by the abundance of nanochannels studied in the literature (Fig. 1). Over the past two decades, various emerging water channels such as pillar[5]arenes, graphene and nanotubes have been reported,

This journal is © The Royal Society of Chemistry 2022

Chem. Soc. Rev., 2022, **51**, 4537–4582 | **4537**

with experimental and simulation studies confirming the fast water transport properties of these nanochannels.[16–19]

Nanochannels have important applications in energy and environmental sciences such as catalysis, membrane separation, chemical sensing or batteries and fuel cells, of which water separation membranes occupy the largest market share (Fig. 2a). From the statistics presented in Fig. 2b, it is evident that water nanochannel research and water nanochannel membrane research have become increasingly important with a huge boom over the past 20 years, and the increasing trend is expected to continue in the coming years. This is because, driven by the grand challenge of freshwater scarcity, membrane-based technology has since become the mainstream method to generate freshwater, owing to its easy operation and reasonable water production cost

when compared to other technologies (Fig. 2a). Today, seawater reverse osmosis (SWRO), as the prevalent membrane-based technology, is used for desalinating up to 102 million m^3 of freshwater per day, which is sufficient to support the livelihoods of more than 300 million people in the world.[10] While state-of-the-art membrane technologies such as SWRO are capable of producing huge amounts of freshwater, desalination plants still consume a large amount of power and hence they are consistently challenged by the need to be less energy-intensive.[10]

Freshwater production at the water–energy nexus should therefore entail a minimal energy consumption such that water provision does not come at the expense of considerable energy sources.[38] Current state-of-the-art water purification and desalination membranes are the thin film composite (TFC) type that was invented about 50 years ago.[39] The materials and fabrication methods to synthesize TFC membranes are mainly based on empirical approaches which do not allow us to fine-tune their material properties with ångström-scale precision. For example, commercially available desalination membranes can attain fairly decent permeability and selectivity (salt rejection of ~99.5%), but empirical evidence has suggested that no revolutionary performance enhancement can be further obtained because of the permeability–selectivity tradeoff.[10,40] From the polymer chemistry perspective, dense polymeric membranes for RO and gas separation are plagued by this tradeoff because of the solution-diffusion mechanism, in which dense polymeric materials with higher free volumes (or pore size) tend to be more permeable to diffusing species, but that comes at the expense of selectivity because their ability to exclude ions at the molecular scale is compromised.

In the past 10–15 years, nanotechnology has opened up new avenues to develop next-generation materials that can be precisely designed at the molecular scale, presenting a paradigm shift in membrane transport phenomena from the conventional solution-diffusion mechanism to molecular sieving effects.[40–42]

Yu Jie Lim

Yu Jie Lim received his BEng (First Class Honours) in Chemical Engineering from the National University of Singapore in 2018. He was awarded the Water Graduate Scholarship by Singapore's National Research Foundation (administered by PUB, Singapore's National Water Agency) to work on the fabrication of next-generation water separation membranes incorporating nanochannels. He is currently a final year PhD student working under the supervision of Professor Rong Wang at the Singapore Membrane Technology Centre, Nanyang Technological University. His research interests focus on the exploration of nanochannel chemistry and membrane science to design novel membranes with better separation capabilities.

Kunli Goh

Kunli Goh received his BSc (Hons) in Chemistry from the National University of Singapore in 2004. He served as a Chemistry Subject Head in a high school in Singapore before returning to pursue his PhD degree in the Sustainable Earth Program at the Interdisciplinary Graduate School of Nanyang Technological University in 2016. He is currently a Senior Research Fellow in Professor Rong Wang's research group at the Singapore Membrane Technology Centre. His research interests focus on the synthesis, functionalization, and nanoarchitectonics of advanced functional materials for developing next-generation gas separation and water treatment membranes.

Rong Wang

Rong Wang is Full Professor and President's Chair in Civil and Environmental Engineering at Nanyang Technological University, Singapore. She received her PhD in Chemical Engineering from the Chinese Academy of Sciences in 1992. She has been the Director of the Singapore Membrane Technology Centre since 2012 and an elected Fellow of Academy of Engineering Singapore. She specializes in novel membrane development for water desalination and gas separation with a particular focus on the use of nanochannels and nanomaterials to advance the performance of current state-of-the-art membranes. She is an Editor-in-Chief of the Journal of Membrane Science – the flagship journal of the membrane community.
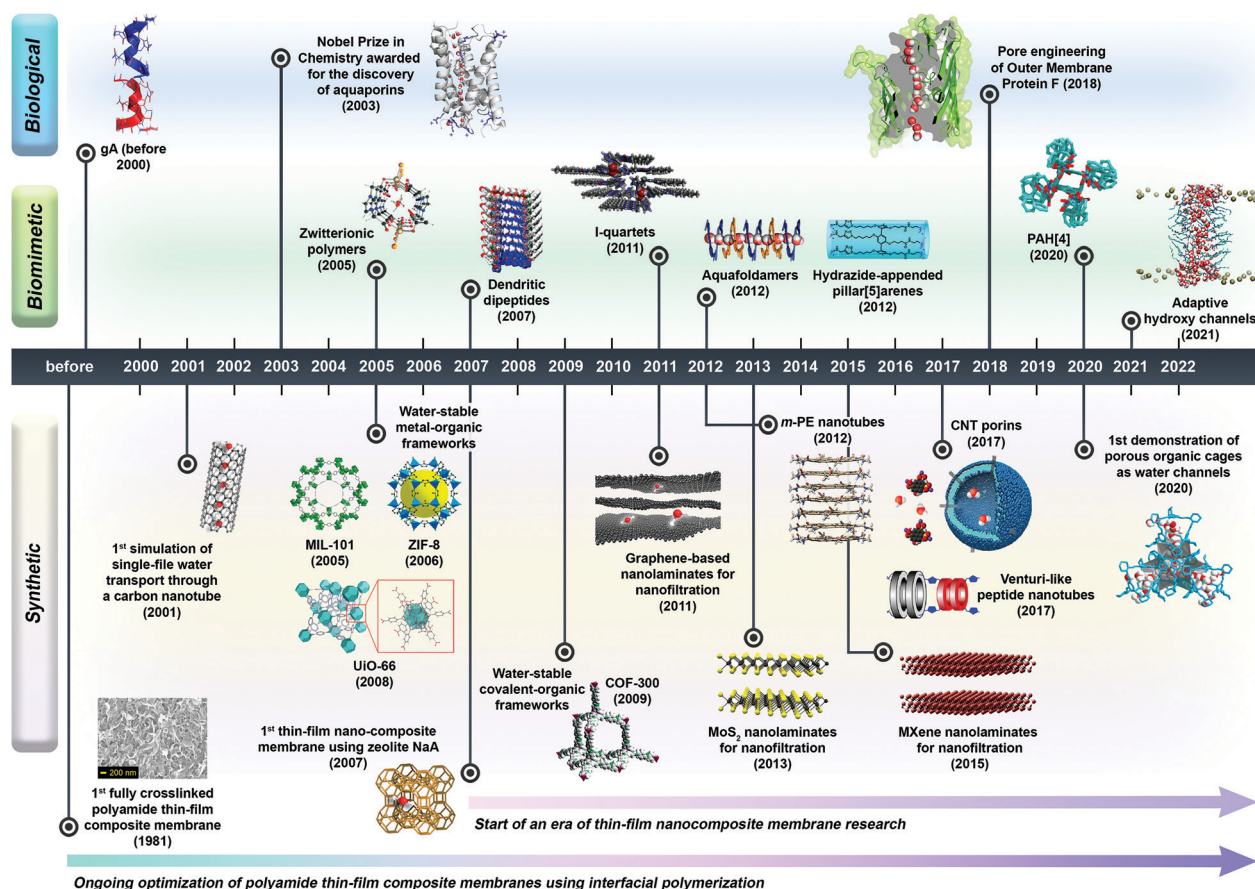
Fig. 1 The evolution of water nanochannels presented in the form of a timeline of the major advances in biological, biomimetic and synthetic nanochannel research. The schematic diagrams or chemical structures of the nanochannels were reproduced from the literature with copyright permissions from the respective publishers. They include: aquaporins (AQP-1),[20] dendritic dipeptides,[21] I-quartets,[22] pillar[5]arenes,[20] aquafoldamers,[23] hydroxy channels depicted in a hydrated lipid bilayer environment,[24] UiO-66,[25] ZIF-8,[26] m-phenylene ethynylene (m-PE) nanotubes,[27] COF-300,[28] MoS$_2$,[29] and carbon nanotube (CNT) porins,[30] American Chemical Society; zwitterionic polymers (top view)[31] and MXenes,[32] Wiley-VCH; β-barrel Outer Membrane Protein F,[33] peptide-appended hybrid[4]arene (PAH[4]),[34] and porous organic cages,[35] Springer Nature; thin-film composite membranes, carbon nanotubes, zeolites, and graphene nanolaminates,[10] Elsevier; and MIL-101[36] and Venturi-like peptide nanotubes,[37] Royal Society of Chemistry. The structural rendering of gramicidin A (gA) was made with a PyMOL molecular visualization system (PDB code: 1MAG).

Next-generation membranes are based on the concept of using compelling nanomaterials as key components in a bid to supplement membranes with the desired characteristics, such as enhanced permeability and selectivity and decreased fouling propensity.[10,43] The most prominent type of nanomaterial is nanochannels, which can be defined as hollow nanostructures with one of their cross-sections in the 0.1–100 nm range. Empirical evidence suggests that advanced membranes incorporating water channels can outperform current state-of-the-art polymeric membranes.[10]

Hence, we argue that there are three main reasons that support the growth and future development of nanochannel-enabled membrane research. First, supramolecular chemistry and nanotechnology have created new opportunities to fabricate nanochannels of nanometric size with manifold shapes and geometries (Fig. 1). From biological channels such as AQPs to biomimetic channels such as pillar[5]arenes and I-quartets, to synthetic channels such as carbon nanotubes (CNTs) and

graphene, these nanochannels have the ability to reach the ångström-scale confinement for nanofluidics to occur.[40,44,45] Second, advances in simulation and characterization techniques have emerged such that they allow researchers to study not only mass or ionic transport, but also the nature of fluids at the nanoscale. This is clearly manifested by the many unusual properties and behaviours that were reported in water nanochannels such as AQPs, graphene and CNTs.[9,40,46] Third and most importantly, these fundamental scientific discoveries provide innovative solutions for membrane science, especially against the recurring permeability–selectivity tradeoff commonly observed in polymeric membranes.

1.1 Concept and classification of water nanochannels

Nanochannels can be of one-dimensional (1D), two-dimensional (2D) or three-dimensional (3D) type. In the current literature, short nanochannels (<1 nm in length) are sometimes termed nanopores.[48,49] Overall, because these nanochannels can act as
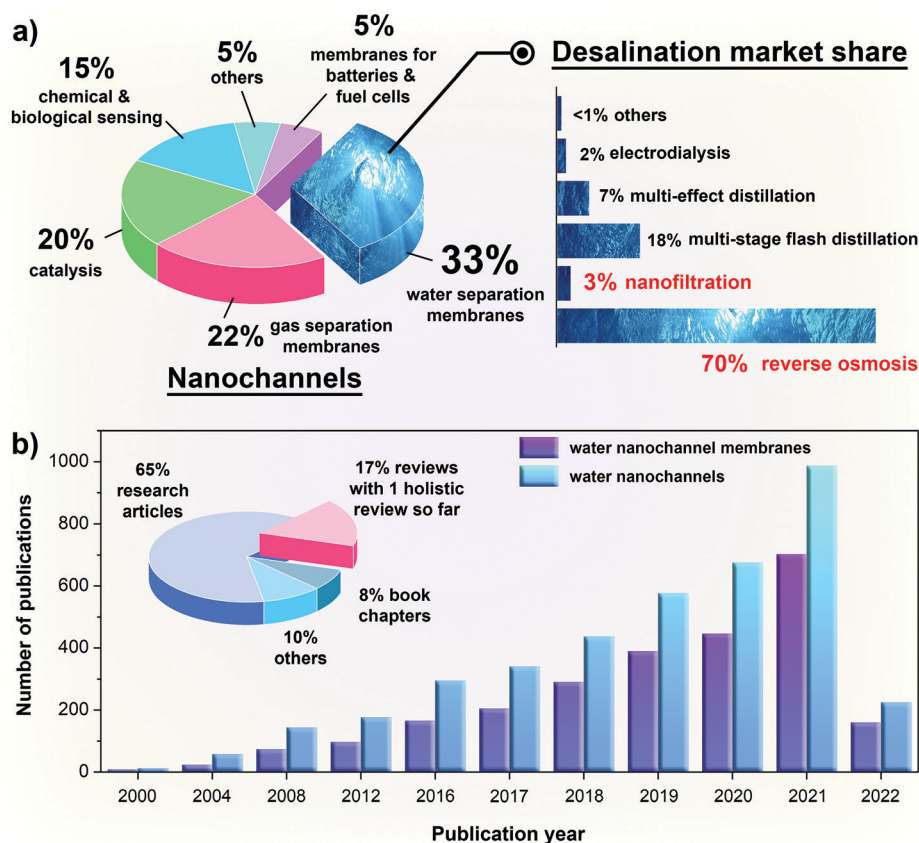
This journal is © The Royal Society of Chemistry 2022

Chem. Soc. Rev., 2022, **51**, 4537–4582 | **4539**

that are produced by segmental packing and motion are not included in this review because they do not possess persistent cavities.

1.2 The coming of age of water nanochannels

One of the most important discoveries of nature is the water channel membrane protein aquaporin (AQP), which is prominently reflected by the award of the Nobel Prize in Chemistry to Peter Agre and Roderick MacKinnon back in 2003 (Fig. 1).[45] AQPs have been frequently investigated in the areas of biological and medicinal research and serve as synthetic templates for physical property characterization and transport modelling.[6,51,52] Coupled with biophysical studies on ion channels that exhibit high selectivity, these inspirations from nature have motivated researchers to construct biomimetic nanochannels capable of mimicking the transport properties of AQPs. One of the most unique features of AQPs is their single-file transport of water molecules, which can be successfully reproduced by some biomimetic nanochannels like pillar[5]arenes.[53] The earliest type of biomimetic water nanochannel is zwitterionic polymers that seek to mimic the 1D water wire in AQPs,[31] but no water permeability test was conducted. Since then, many biomimetic channels with novel architectures have emerged over the past 15 years (Fig. 1), with experimental results and molecular dynamics simulation confirming their high water permeabilities and selectivities.[54,55] On top of designing novel channel architectures, it is also worthy of note that some research studies seek to develop nanochannels with enhanced performance based on existing templates, typically by the modification of the channel pore size or chemical properties.[7,53] Overall, biological channels have provided a guideline for us to synthesize biomimetic channels, which have led to the burgeoning development of water nanochannels in the past two decades.

For synthetic nanochannels, there have been no fewer developments as compared to biomimetic channels, with supramolecular chemistry and nanotechnology triggering an ascending growth in the development of water nanochannels in the past two decades. As compared to biomimetic channels, many investigations focussed on the synthesis of new channels exhibiting not only attractive mass transport properties, but also superior hydrolytic stability (as will be elaborated in Section 2). As compared to their biological or biomimetic counterparts, synthetic channels come in two other forms – 2D nanochannels and 3D nanopores – besides their ubiquitous 1D nanotubular structure. Some representative examples of 2D nanochannels and 3D nanopores include graphene oxide and zeolites, respectively. Today, research focus is slowly gearing towards 2D nanochannels with the recent interest in 2D materials as well as other dimensional nanochannels, including 0D porous organic cages (Fig. 1).

1.3 Scope and outline of the current review

Recently, a few reviews have provided an enlightening overview on the structural design and synthesis of nanochannels and 2D nanomaterials from a materials science point of view, highlighting some prospective applications in membrane technology related to gas separation,[40,56,57] ion separation,[16,58] electrochemistry[59] and batteries and fuel cells.[13,60] However, the focus of the current review is distinctly different as we seek to discuss the prospects of next-generation membranes incorporating biological, biomimetic and synthetic water channels, with critical discussions made to compare and contrast the three types of nanochannels in terms of chemistry and transport performance. We intentionally organize state-of-the-art channels into biological, biomimetic and synthetic types, in a bid to distinguish their strengths and weaknesses that will allow for better tailored membrane designs and for unlocking the full potential of the water channels. This review of the water channels also provides readers with a wider breadth of knowledge to make data-driven decision when selecting channels that suit their needs of maximizing membrane separation performances. Also, the grasping of these key concepts has profound implications for the nano-architectonics of rationally designed channels into optimized platforms for areas beyond membranes, such as but not limited to thin film processing and functional nanocomposites for energy storage, catalysis, and CO_2 capture applications.

As the concept of nanochannel-enabled membranes is still in its infancy with applications currently hampered by practical issues related to the efficiency, scalability and stability of the nanochannels and their eventual membranes,[5] there is a need to look for answers across interdisciplinary domains. Herein, this review provides a holistic summary on the recent chemistry, synthesis, and practical applications of water nanochannels, mainly with a multifaceted focus on biological, biomimetic and synthetic channels to address current challenges. Firstly, the basic chemistry and synthesis strategies of the nanochannels are discussed using conceptual knowledge, experimental results and molecular dynamics simulations, so as to present a comprehensive discussion on the transport properties of the nanochannels. Secondly, membrane nanoarchitectonics incorporating water nanochannels will be reviewed, starting from the fabrication methods and separation mechanisms that are explained using concepts from membrane science and polymer chemistry. Thirdly, various membrane designs incorporating water nanochannels will be outlined, and some general guidelines for the selection of a suitable membrane design based on the nanochannel properties are covered in detail. Finally, we present various perspectives looking forward, giving multidisciplinary insights into resolving current limitations with nanochannels and nanochannel-enabled membranes as well as strategic future endeavours where we expect water nanochannels to make a meaningful contribution to membrane research.

2. Basic chemistry and intrinsic transport properties

We first begin the discussion by introducing the basic chemistry and structural characteristics of the three overarching types of water nanochannels, emphasizing the specific traits and transport properties that are relevant to the fabrication and chemistry of the resulting next-generation membranes. In addition, we briefly

This journal is © The Royal Society of Chemistry 2022

Chem. Soc. Rev., 2022, **51**, 4537–4582 | **4541**

touch on certain important concepts regarding the mass transport properties of water nanochannels to promote a natural pivot into the subsequent in-depth discussions in Sections 3 and 4.

2.1 Biological channels

Biological membranes are selectively permeable membranes that create intracellular compartments (*i.e.*, the cell is separated from the external environment) consisting of a bilayer of lipid molecules (Fig. 3a).[6,61] They contain an ordered arrangement of passive transport channels, together with active co-transporters and pumps with various functions. The presence of various biological activities occurring in the amphiphilic matrix indicates the possibility of designing a biomimetic membrane with multiple functions. One of the core components in biological membranes is membrane proteins because they conduct processes necessary for cell viability (*e.g.* water, ion and nutrient transport across cell membranes).[6,62] There are various types of membrane proteins such as membrane protein channels, group trans-locators, and electron carriers, of which the first type is elaborated in this review because of its desired characteristics for separation such as the selectivity for small molecules, high specificity and fast water transport (Fig. 3b). Different types of membrane protein channels have been explored in the fabrication of water separation membranes, with the most common one being aquaporins (AQPs).[63,64]

2.1.1 Aquaporins (AQPs). AQPs are from a family of intrinsic proteins that permit fast water transport across the membrane of biological cells in the presence of an osmotic gradient. AQPs are important because of their ability to regulate cellular osmotic pressure and facilitate water transport between cells.[4,6] It is well known that AQPs usually assemble into tetramers whereby each individual protein subunit contains a water pore that is formed by several membrane-spanning alpha helices (Fig. 3c–e).[51] Empirical evidence has shown that classical AQPs can attain high water permeability and high monovalent ion selectivity (water–salt selectivity $> 10^9$).[6] Because of their excellent water permeability coupled with near perfect selectivity (including proton exclusion), AQPs serve as a benchmark for other biomimetic and synthetic water channels in terms of the structure–function relationships and transport performance. It is noted that various isoforms of AQPs exist (refer to Table 1).[51] For water-based membrane separation, prominent AQPs include human AQP-1 and bacterial AQP-Z, of which the latter is of interest in membrane fabrication because of its enhanced stability and easier processability as compared to the former.[66,67] Stopped-flow measurements (Fig. 3b and f) have shown that the water permeability of AQP-1 is ~2 times higher than that of AQP-Z (refer to Table 1) and most fundamental studies are based on the former.[65] It is must be noted that the permeability values are similar even in different matrices but the reconstitution efficiency might vary. Herein, the basic chemistry and structure of AQP-1 are discussed.

The excellent selectivity of AQPs coupled with their high water permeability can be attributed to four inherent characteristics: (1) a main hydrophobic interior, (2) an hourglass structure (~2 nm in length) that tapers down to a tight constriction zone with a mean diameter of ~0.28 nm, (3) a series of amino acid residues (asparagine–proline–alanine (NPA)) that lies at the entrance of the constriction zone and (4) plenty of inward-facing carbonyl groups (Fig. 3e).[4,51,73] Firstly, a nanochannel that has an extremely hydrophobic internal wall can induce a slip boundary condition (because of little frictional force with water molecules) such that viscosity is the only limiting factor in the transport of molecules. In the case of AQPs, water is channelled into a single file (*i.e.*, 1D water wire) such that the hydrogen bond-number is reduced from four to two and the bulk water viscosity is dissipated.[20] Secondly, the tight constriction zone of 0.28 nm is approximately the size of a hydrated water molecule,[52] which means that solutes can be rejected *via* a size exclusion mechanism, whereas water molecules undergo a transient-dipole reorientation/rotation before entering the constriction zone. Thirdly, solute and ion transports are hindered due to Donnan and dielectric exclusion effects. Here, the Donnan effect refers to the electric interaction between ions and nanochannels (*e.g.* exclusion of co-ions when the sign of their charge coincides with that of the residues in the constriction zone), whereas dielectric exclusion refers to the hindered transport of ions through the nanochannel due to the solvation energy barrier of ions into the nanochannel. In layman terms, the dielectric effect can be thought of as an energetic penalty that solutes have to compensate for while transferring from a solvent with a high dielectric constant (*e.g.* bulk water) to a medium with a low dielectric constant (*e.g.* nanopore). Readers are referred to the literature for detailed discussions on these two mechanisms.[74–76] For AQPs, the positive poles at the centre of the nanochannel (induced by the two asparagine–proline–alanine (NPA) bearing helices) as well as the positively charged arginine within the constriction zone restrict cation transport, whereas the pore-accessible carbonyl oxygen atoms restrict anionic transport.[51,52] Protons are also completely rejected by AQPs due to the electrostatic repulsion effect by the NPA motif and the arginine in the constriction zone, or the breaking of the water wire (because of the rotation of water molecules). In short, the large entrance effects due to site restriction and charge repulsion enable AQPs to reject all solutes.

Molecular dynamics simulations have further revealed some unique features of AQPs with regard to the influence of channel shape and hydrogen bonding when water permeates through the channel. First, it is postulated that hourglass or cone-shaped nanostructures with relatively short constriction zones possibly mitigate the large energy barrier present at the entrance of the water-selective pore.[77] For AQPs, the small cone angles of around 10–30° can reduce the resistance to transport when transitioning from the funnel to constriction zone.[73] To put it into perspective, the smaller the channel length (or the length of the constriction zone), the higher the optimal funnel angle. Another interesting point to note for biological water nanochannels is that they have different numbers of hydrogen-bonding sites at the pore mouths and channel cavity, including AQPs that convey only water as well as water and glycerol (*i.e.*, aquaglyceroporin, GlpF). Empirical evidence in
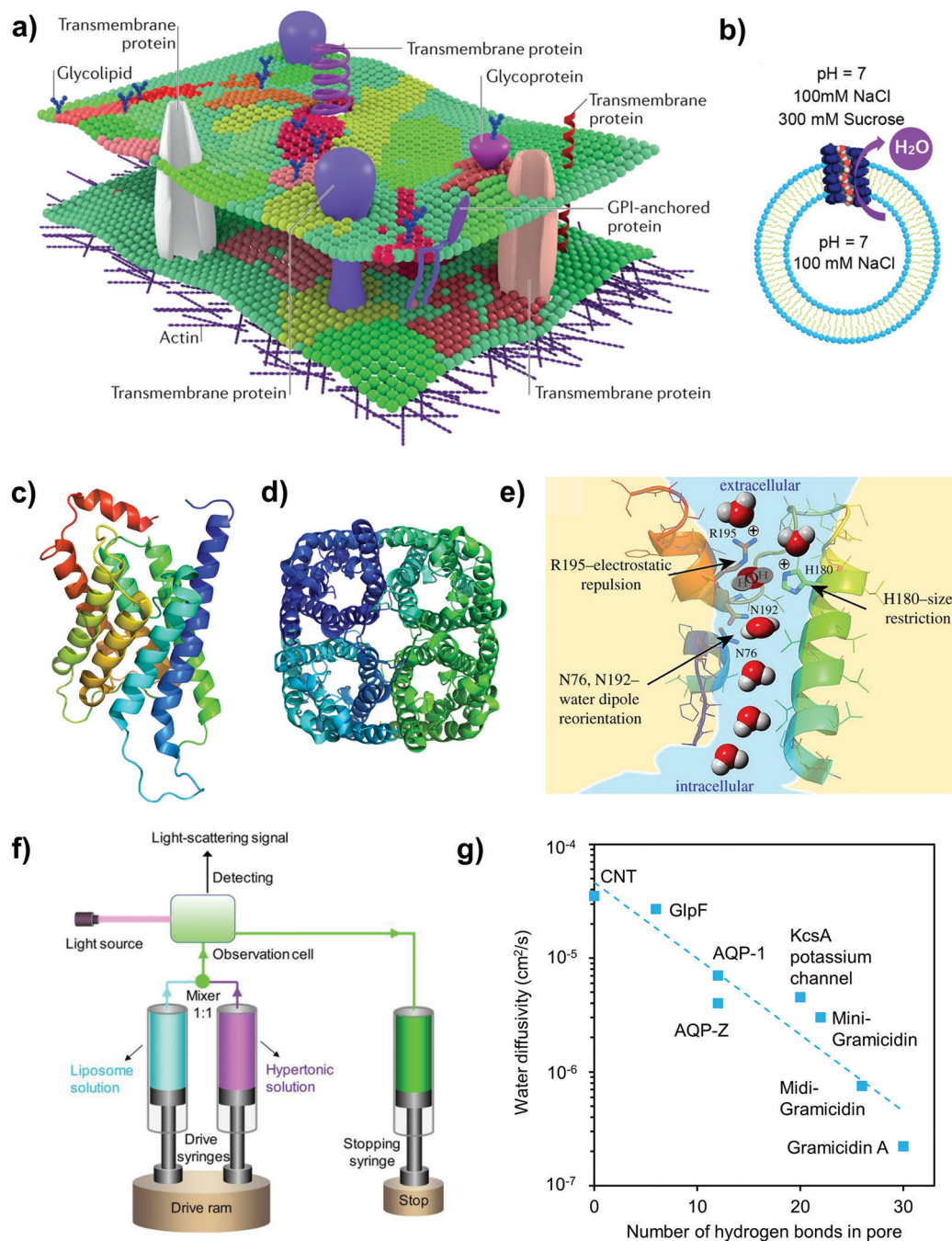
Fig. 3 (a) A schematic illustration of some components in the cell (plasma) membrane, consisting of lipids and transmembrane protein channels. Reproduced from ref. 61 with permission from Springer Nature Limited, copyright 2017. (b) Schematic illustration of the outward movement of water through a water nanochannel embedded in liposomes, in which the stopped-flow test was conducted under hypertonic conditions (draw solution: sucrose). Reproduced from ref. 55 with permission from American Chemical Society, copyright 2020. (c) The side view of aquaporin-1 (AQP-1) outlining its hourglass shape. (d) AQP-Z tetramer. The structural renderings in (c) and (d) were made with a PyMOL molecular visualization system (https://www.pymol.org). The protein sequences were taken from the Research Collaboratory for Structural Bioinformatics Protein Data Bank (RCSB PDB; https://www.rcsb.org/). The PDB codes used for AQP-1 and AQP-Z tetramers are 1J4N and 2ABM, respectively. (e) A schematic illustration of water transport through AQP-1, whereby the extracellular and the intracellular vestibules of the AQP-1 channel contain water in the bulk solution. Reproduced from ref. 51 with permission from The Royal Society (United Kingdom), copyright 2018. (f) A brief illustration of the stopped-flow light scattering experiment under hypertonic conditions. The water nanochannels are first embedded into liposomes and the latter are exposed to a hypertonic solution to induce the shrinkage of the lipid vesicles, with the shrinkage rate acting as an indicator of the water transport rate across the channel. Reproduced from ref. 53 with permission from Wiley-VCH, copyright 2019. (g) The relationship between the water diffusivity and the number of hydrogen bonds the water wire may form with residues lining the nanochannel pore (data points were extracted from ref. 65).

Table 1 Summary of promising water nanochannels that have the potential to be used in the development of next-generation water separation membranes

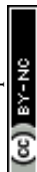| Water nanochannels	Pore constriction diameter (nm)	Reported single-channel permeability ($\times 10^{-14}$ cm^3 s^{-1})	Notable transport properties	Typical channel permeability measurement method	Ref. (year)
Biological channels					
AQP-1	0.3	52.8	Fast water transport with rejection of all solutes and protons	Vesicle size change	65 (2015)
AQP-Z	0.28	28.8			
RsAQP-Z	0.28	42.9			6 (2021)
GlpF	0.34	190	Can transport water and glycerol	Vesicle size change	65 (2015)
gA[a]	0.4	1.6	Can transport water and small cations such as Na$^+$ and K$^+$	Patch clamp studies	68 (2006)
MidiGramicidin[a]	0.4	5.6	—		
MiniGramicidin[a]	0.4	22	—		
Biomimetic channels					
Peptide-appended pillar[5]arenes	0.5	1.0	Fast water transport and with the ability to exclude solutes with molecular cutoffs >420 Da	Vesicle size change	69 (2015)
pR-PH	0.5	3.93	Fast water transport with salt exclusion	Vesicle size change	53 (2019)
PAH[4]	0.5–0.7 (transient void windows)	11	Fast water transport with salt exclusion	Vesicle size change	34 (2020)
Aqf-1	0.28	9.23	Fast water transport with salt exclusion (sodium chloride and potassium chloride; NaCl and KCl, respectively)	Vesicle size change	55 (2020)
Aqf-2	0.21 × 0.27 (cuboidal pore)	0.66	Fast water transport (single-file)	Vesicle size change	55 (2020)
Polypyridine-based foldamers	0.28	4.81	Rapid transport of protons and water, with near-perfect exclusion of ions	Vesicle size change	23 (2020)
Foldamers with lipid anchors	0.46–0.67	60.14	Fast water transport with salt (NaCl and KCl) and proton exclusion	Vesicle size change	7 (2021)
Synthetic nanotubes					
Wide CNTP	1.35	5.9	Fast water transport, but is permeable to Na$^+$/K$^+$ ions and other protons	Vesicle size change	2 (2017)
Narrow CNTP	0.68	68	Fast water transport with Na$^+$, K$^+$ and Cl$^-$ ion exclusion	Vesicle size change	70 (2012)
m-PE nanotubes	0.64	2.6 (open state)	Transports both water and ions	Molecular dynamics simulation	71 (2015)
CPN[b]	0.76	7			
mCPN-Ala[b]	0.65	4.5			
mCPN-Lys[b]	0.65	8.8			
mCPN-Gly[b]	0.70	18			

[a] The pore diameter of gA was obtained based on its pore size in a lipid bilayer from ref. 72. [b] The pore diameters were extracted from ref. 73 using atomic simulation images, whereas the channel permeabilities were converted to cm^3 s^{-1} for standardization purposes (readers are referred to ref. 73 for detailed information).

Fig. 3g suggests that there is an inverse correlation between the diffusivity of water through the nanochannels and the number of hydrogen-bonding sites within the channel itself (i.e., a reduced number of sites can lead to higher water permeability because of fewer interactions between the channel cavity and water wire).[65] In terms of the pore diameter of AQPs, the constriction zone correlates with permeability (e.g. GlpF has higher permeability than AQP-1 because of its greater pore diameter of $\sim$0.34 nm (refer to Table 1)).[52]

However, it must be noted that there is no correlation between constriction size and permeability (refer to Table 1) when comparing channels of different chemistries because other factors such as the hydrophobicity and the nature of functional groups inside the cavity are also crucial factors that control the nanochannel's permeability. We would also like to point out that the single-channel permeability values reported in Table 1 should not be compared with one another because of the different conditions adopted in the testing or simulation experiments, including but not limited to the osmotic pressure difference, temperature and encapsulating lipid to nanochannel molar ratios in stopped-flow tests as well as the operation mode (which can be shrinking or swelling of the channel-containing vesicles). For example, the single-channel permeability is known to be lower at high lipid-channel ratios because of the channel's lower solubility in the lipid bilayer membrane.[55] A recent critical review also pointed out that some of the values reported in stopped-flow tests are dramatically higher (than their true values) due to erroneous fitting procedures,[73] and hence the values in Table 1 cannot be a valid comparison.

2.1.2 Other types of membrane protein channels. Besides the ubiquitous AQP water channel, some other types of biological channels have been studied for synthetic membrane

4544 | Chem. Soc. Rev., 2022, 51, 4537–4582

This journal is © The Royal Society of Chemistry 2022

applications, which include gramicidin A (gA) and the β-barrel family of protein channels. First, linear gramicidins are peptides generated by the rod-shaped soil bacterium *Brevibacillus brevis* in which its anti-microbial mechanism is known to be related to the formation of transmembrane channels conducting ion permeation.[78] In nature, gramicidins exist as a mixture, with the major component being gramicidin A (gA) that is prominently known to fold into a β-helical shape (Fig. 4a), and

the symmetrically shaped water channel is formed by the transmembrane dimerization of two gA subunits in lipid bilayers (Fig. 4b).[79] In the gA structure, the peptide planes of the β-strand that line the aqueous pore are sufficiently narrow to support the single-file transport of water molecules and is also known to be selective to some monovalent cations (*e.g.* Cs^+ and Li^+);[80] some transport properties of the gA channel are summarized in Table 1.
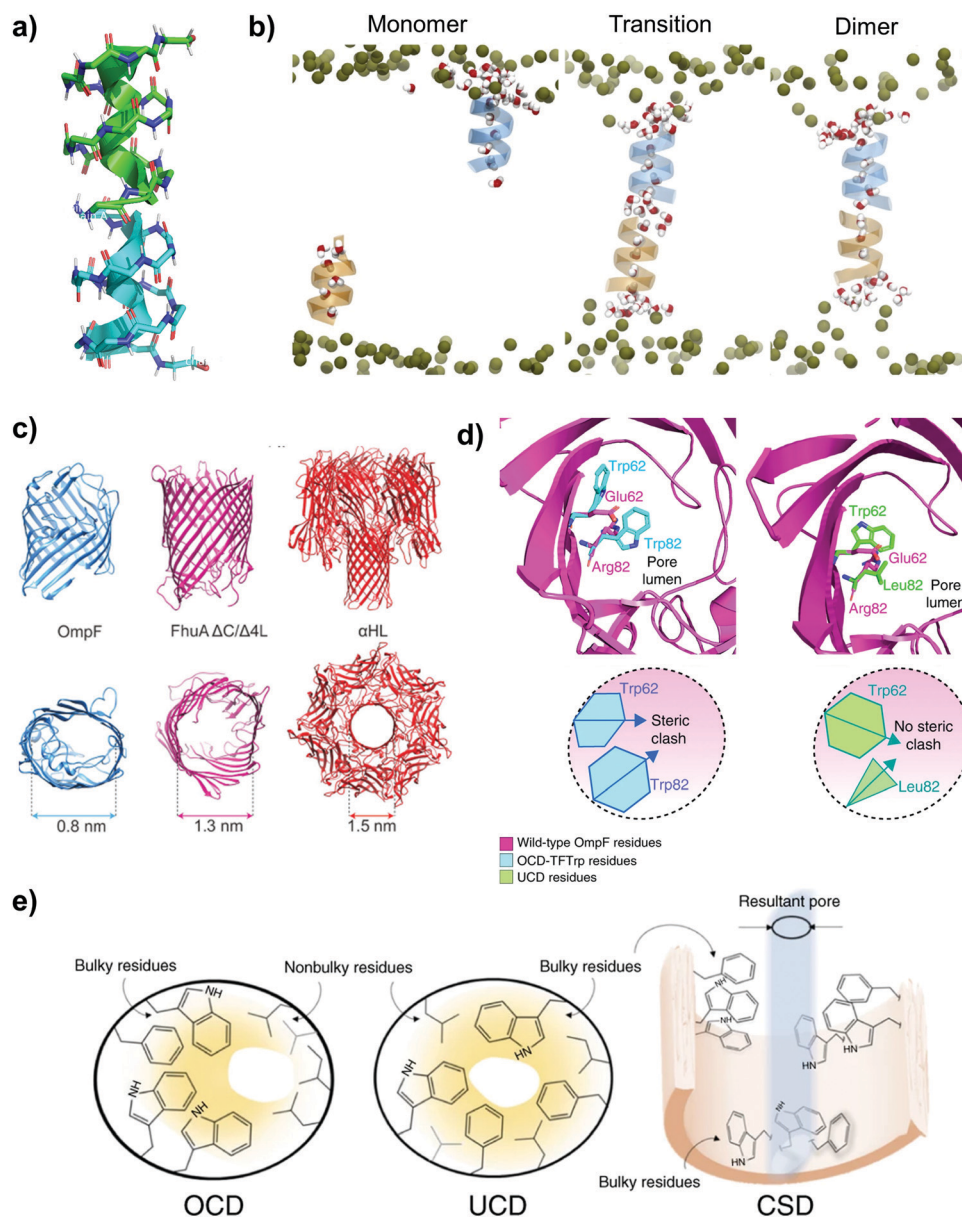
Fig. 4 (a) Gramicidin A (gA). The structural rendering was made with a PyMOL molecular visualization system (PDB code: 1MAG). (b) A schematic illustration of water molecules and their orientation under three scenarios: gA monomers, the transition state and after the formation of gA dimers. Reproduced from ref. 79 with permission from Elsevier, Cell Press, copyright 2019. (c) The structures of three β-barrel channel proteins: OmpF, FhuA ΔC/Δ4L and αHL. Reproduced from ref. 50 with permission from Springer Nature, copyright 2021. (d) The modification of nanochannels' pore size in OmpF due to the presence of different residues. Left: The presence of off-center pore closure design-only Trp mutations (OCD-TFTrp) residues induces steric clash, resulting in the pointing away of some side chains from the pore lumen. Right: The presence of uniform pore closure design (UCD) residues does not induce steric clash, resulting in smaller pore sizes. (e) The three types of pore geometries of OmpF are shown. Left: Off-center pore closure design (OCD); middle: uniform pore closure design (UCD) and right: cork-screw design (CSD). (d) and (e) reproduced from ref. 33 with permission from Springer Nature, copyright 2018.

This journal is © The Royal Society of Chemistry 2022

Chem. Soc. Rev., 2022, **51**, 4537–4582 | 4545

As compared to AQPs, β-barrel membrane proteins have higher stability and mutation tolerance, which are some of the desired traits needed for membrane fabrication. Within living organisms, β-barrel membrane proteins are used to exclude large molecules such as proteins while allowing the selective permeation of small molecules and ions (*e.g.* antibiotics and sugars).[50,81] The β-barrel structure consists of a robust scaffold that is highly stable thermodynamically, and more importantly, it is structural sturdy because of the low enthalpies of denaturation of the transmembrane domains. β-Barrel membrane proteins which have been explored for water-based membrane separation are typically pore-forming, such as: (1) outer membrane protein F (OmpF) from *E. coli*, (2) an engineered version of a bacterial ferrichrome outer membrane transporter (FhuA ΔC/Δ4L) from *E. coli*, in which its passive pore is formed due to the removal of the central alpha helical plug and (3) alpha-hemolysin (αHL), a self-assembled protein toxin from *Staphylococcus aureus* that forms pores in cell membranes (Fig. 4c).[50,81] These three types of membrane protein channels have been explored for water separation because of their ability to support water transport. αHL has a circular pore size of ∼1.5 nm, whereas OmpF and FhuA ΔC/Δ4L have elliptical pore shapes, with their narrowest side measuring 0.8 nm and 1.3 nm, respectively.[50,81]

The most typical and straightforward approach to enhancing the selectivity of nanochannels is to reduce their pore size, but that comes at the expense of permeability. To overcome this tradeoff, some researchers have proposed to modify the pore profile and chemistry of membrane protein channels while maintaining a similar pore size. Chowdhury *et al.* explored the possibility of fine-tuning the pore sizes of biological channels (specifically, OmpF) by designing their interior cavity with three distinct types of pore geometry within the stable β-barrel of the bacterial channel porin (Fig. 4d and e).[33] This work proposed to replace the residues of the pore wall with more hydrophobic groups so as to minimize the hydrogen bonding between the pore and water wire in a bid to synthesize protein channels with higher permeability. In general, experimental and molecular dynamics simulation results showed that a narrower pore with greater internal hydrophobicity typically has higher water permeability because of fewer interactions between the residues in the cavity and the water wire.[33,65]

2.2 Biomimetic and bioinspired channels

While biological water channels such as AQPs can be expressed and purified *via* well-established bioprocessing methods, their stability is an issue that has yet to be resolved.[5,40,50,73] No matter what, protein channels are still prone to denaturation and will lose functionality eventually. It must be highlighted that the stability of AQPs during membrane fabrication and operation is something that has not been validated also. Moreover, biological water channels might not provide the best pore-loading efficiency and functionality from a membrane science perspective. These limitations of natural biological channels have motivated researchers to come up with biomimetic water channels that seek to mimic the functions and

transport properties of biological channels.[53,55] Moreover, some biomimetic channels have higher compatibility with and solubility in organic solvents used in industrial membrane fabrication. Overall, biomimetic channels present another degree of freedom to tune their performance for target applications (for example, the rejection of monovalent salts in desalination membranes). In general, biomimetic water channels can be classified into two main types: unimolecular channels and self-assembled channels. A brief summary outlining the key differences between the two aforementioned channels is presented in Table 2. To facilitate easy referencing and comparison between the three overarching types of water channels (biological, biomimetic and synthetic), we also summarized some of their key information in Table 2.

2.2.1 Unimolecular channels. Supramolecular chemistry has opened the doors to the development of unimolecular biomimetic channels that seek to mimic the transport properties of biological channels. The most researched class of unimolecular channels is pillar[*n*]arenes (Fig. 5a), which are macrocycles (*i.e.*, cyclic macromolecules) composed of hydroquinone units chemically linked in the *para*-position by methylene bridges (where '*n*' denotes the number of units).[105] This unique class of macrocycles was named pillararenes because of their pillar-like shape consisting of 'arene' (benzene) moieties. The central component of pillararene channels is the pillararene ring in which the orientation of the benzene rings is orthogonal with respect to the macrocycle plane. Because of their high π-electron density induced by the electron-rich hydroquinones in the macrocycle, pillararenes are known to exhibit superb host–guest chemistry such that they can form association complexes (*via* chemical bonds) with electron-deficient species.[106–108] In the pillararene family, pillar[5]arene is the most structurally stable, and higher homologues (*i.e.*, pillar[6–15]arenes) can be synthesized *via* the expansion of the pillar[5]arene ring. One of the most facile methods to synthesize pillar[5]arenes is *via* the condensation reaction between 1,4-dimethoxybenzene and paraformaldehyde in the presence of a suitable Lewis acid as a catalyst (refer to Table 2). Currently, there are manifold reaction schemes to synthesize pillararenes and their derivatives; readers interested in the detailed synthesis schemes are referred to a comprehensive review on this topic.[82]

Besides their facile synthesis and high yield under optimized conditions,[82] another advantage of pillar[5]arenes is their versatile functionality whereby their structure can be modified for specific purposes (*e.g.* by attaching side chains onto the central ring).[20,111,112] Pillar[5]arenes are typically attached with side chains (*e.g.* hydrazide units) such that they are long enough (∼5 nm) to span the entire lipid bilayer (∼3.7 nm), with their tubular structure stabilized by the intramolecular hydrogen bonds of the adjoining hydrazide chains.[82,113] Currently, the most widely studied unimolecular water channel is the peptide-attached pillar[5]arene (Fig. 5a), whose pore diameter and length are determined by the macrocycle (∼0.5 nm) and the span of the peptide-appended arms.[69] A recent study also outlined the possibility of synthesizing a new type of hybrid pillararene–gramicidin nanochannel that

4546 | *Chem. Soc. Rev.*, 2022, **51**, 4537–4582

This journal is © The Royal Society of Chemistry 2022

Table 2 A summary and comparison of the structural characteristics, synthesis methods and parameters of the three overarching types of water nanochannels

Channel type and classification	Specific examples (pore size range)[a]	Structural characteristics and constituents	Typical synthesis method(s)	Synthesis parameters that control its structural tunability
Biological channels				
Natural proteins	AQPs (0.28 nm)	Proteins consisting of a bundle of six transmembrane α-helices	N/A	N/A
Biomimetic channels				
Unimolecular nanotubes	Pillar[5]arenes and their derivatives (~0.5 nm)	Macrocycles consisting of hydroquinone units linked with methylene bridges	Condensation reaction followed by the deprotection of methoxy groups[53,82]	Kinetic and thermodynamic factors of reaction, functional groups of the attaching units
	PAH[4] (transient void windows of 0.5–0.7 nm)	Cluster-forming organic nanoarchitecture consisting of 8 peptide appendages on macrocycles	Molecular construction strategy involving the appending of side chains onto the macrocycle[34]	Functional groups and building blocks of the side chains
	Foldamers (0.280.67 nm)	Spiral, crescent-shaped oligomer subunits with complementary chain-end functionalities	Sticky end-mediated strategy[55,83] and one-pot polymerization[7,23]	Oligomer subunits and functional groups, coupling reagents, polymerization temperature
Self-assembled	I-quartets (0.26 nm)	Stacks of four imidazoles and two water molecules that mutually stabilize to form water wires	Reaction of histamine with isocyanate under dissolution with heating[84]	Reactants, composition of the dissolving mixture and reaction temperature
Synthetic 1D nanotubes				
CNTs/CNTPs	Single-walled CNTs (0.8–2 nm)	Cylindrical large molecules consisting of hybridized carbon atoms in a hexagonal arrangement	Conceptually formed via the rolling up of a single sheet of graphene[85]	Growth conditions and pore site functionalization
Nanotubes with stackable units	m-PE (0.64 nm)	Hexakis macrocyclic rings that are held by inter-ring hydrogen bonding	Palladium (Pd)-catalysed coupling reaction of trimers, followed by concentration and purification[70]	Side chains and functionalities of the macrocycles as well as host–guest chemistry[86]
	CPNs (0.47 nm)	Rings of amino acids (stackable units) that assemble into tubular structures	Solid phase peptide synthesis followed by coupling reactions[87]	Building blocks and functional groups of the pore lumen
Synthetic 2D channels				
Graphene	Nanofluidic graphene channel (0.34–10 nm)[8,18]	Atomically thin monolayer of sp^2 carbon atoms tightly bound in a hexagonal honeycomb array	Chemical vapour deposition, reduction of graphene oxide (GO) through heating or mechanical exfoliation from graphite	Channel size
Graphene oxide (GO) and derivatives	GO (0.8–7 nm, depending on the hydration extent)[88]	Monolayer of graphite with various oxygen-containing functionalities (e.g. carboxyl and hydroxyl groups)	Hummers' method (via the oxidation of graphite)	Nanosheet size, interlayer functionalization, oxidation degree
MXenes	$Ti_3C_2T_x$ (0.38–0.64 nm, depending on the hydration extent)[32]	Inorganic compounds that are made of transition metal carbides, nitrides, or carbonitrides (~thicknesses of a few atoms)	Top-down selective chemical etching process (e.g. removing the A layers from the parent MAX phases)	Nanosheet size, interlayer functionalization, combination of different MXenes, lateral dimension (flake size)
Others	MoS_2 (0.62–1.2 nm, depending on the hydration extent)[89]	Inorganic, transition metal dichalcogenide compound that is made up of molybdenum and sulfur	Top-down (mechanical exfoliation) or bottom-up synthesis approaches (solvothermal or hydrothermal)	Nanosheet size and interlayer functionalization
Synthetic sub-nanopores				
Zeolites	Zeolite A/Linde Type A (0.3–0.8 nm) and MFI zeolite (0.5–0.6 nm)	Aluminosilicate and microporous minerals that consist of alkali and alkaline-earth metals[10,90–92]	Hydrothermal, microwave and sol–gel methods	Cations, temperature, reaction time and pH
MOFs	ZIF series (0.3–0.35 nm), copper-based series (0.52–0.9 nm) and UiO-66 series (0.6 nm)	Compounds consisting of metal ions/clusters coordinated to organic ligands	Solvothermal/hydrothermal growth, slow diffusion, electrochemical, microwave assisted heating and ultrasound[93–95]	Secondary building units, organic linkers for the desired functional groups, pore shapes and sizes
Microporous organic polymers and cages	COFs (0.5–5.8 nm)[96,97]	Porous organic polymers that are assembled by the linking of organic building units via covalent bonds	Solvothermal, bottom-up reticular synthesis, interfacial synthesis, top-down mechanical exfoliation[98–102]	Building blocks and their symmetries, monomer design, reaction temperature and pressure

Table 2 (continued)

Channel type and classification	Specific examples (pore size range)[a]	Structural characteristics and constituents	Typical synthesis method(s)	Synthesis parameters that control its structural tunability
	Porous organic cages (0.4–1.07 nm)[35]	Porous material that consists of discrete molecules with intrinsic, guest accessible cavities that are connected by a pore network	Reversible routes such as imine condensation, boronic ester condensation and alkyne metathesis[103,104]	Building blocks, cage precursors, bond angles in the precursors, reaction conditions (concentration, temperature, choice of solvent and catalyst)

[a] The pore size refers to the pore diameter, interlayer spacing or pore window depending on the type of nanochannel unless otherwise mentioned. For example, the pore diameter is used for tubular structures or sub-nanopores, whereas the interlayer spacing or distance is used for 2D nanochannels. For some nanochannels such porous organic cages, the pore size can also refer to the pore window.

was created by modifying the peptide-arms of pillar[5]arenes with amino acid residues, with the aim of enhancing the incorporation efficiency into the lipid bilayer as well as modulating the transport properties of cations (e.g. by conferring charge-repulsion properties to the nanochannel).[114]

There are three main characteristics of peptide-attached pillar[5]arenes that mimic the ultrafast water transport of biological AQPs: (1) a hydrophobic interior that provides slip-flow conditions, (2) the ability to support single-file transport of water molecules because of its small pore diameter and (3) the presence of a constriction zone that tapers down from the peptide-appended arms, thereby allowing it to reject some solutes.[20,53,54] Overall, peptide-attached pillar[5]arenes are relatively more stable than AQPs because of hydrogen bonding between the peptide-appended arms, granting the former the necessary stability to be functionalized into tubular nanostructures. In addition, peptide-attached pillar[5]arenes have an outer hydrophobic surface that is compatible with lipid environments. The channel pore packing density can also be increased dramatically when assembled into dense clusters of parallel channels.[69]

While peptide-appended pillar[5]arene nanochannels can attain high permeability comparable to those of AQPs, their inability to exclude monovalent ions because of their high molecular weight cut-off (MWCO) of ~420 Da renders them inadequate for desalination applications (see Table 1).[69] This necessitates the need for pillar[5]arenes that are suitable for desalination applications, either by designing a tighter constriction zone (i.e., smaller diameter) or by functionalizing the appended peptides to restrict salt passage. It is important to highlight that pillar[5]arenes have a fascinating trait of planar chirality that arises from the rotation of benzene rings around the methylene bridges. The rotation can be restrained by the attachment of bulky and rigid substituents into the pillar[5]arene backbone such that two stable isomers (pR and pS type) are formed and subsequently isolated. Li et al. successfully showed that the two diastereomers (pR- and pS-type) exhibit different chemical and physical properties, which subsequently resulted in different water permeation rates.[53] Stopped-flow tests indicated that the peptide-attached pillar[5]arene (pR-PH) type channel showed very high water transport rates in the order of 10^{-14} cm^3 s^{-1} (refer to Table 1). Molecular dynamics simulations further revealed that for a similar insertion

efficiency, the rotation of the phenylalanine side chain in the pS-PH channel blocked the nanochannel pore, thereby inhibiting water transport.[53] In short, the planar chirality and chiral inversion of pillar[5]arenes can lead to the synthesis of pillar[5]arene derivatives with distinct characteristics by manipulating the reaction temperature, achiral guest and solvents used.[106] This added another degree of freedom in the synthesis of nanochannels with the desired properties, and we believe that continuing research can unlock further application prospects of pillar[5]arene derivatives with the desired chemical properties.

It is also worth noting that some pillar[5]arene derivatives can reject protons (like AQPs) because of the disruption of the water wire within their cavity due to the inherent channel geometry.[115] Another creative way to alter the properties of pillar[5]arenes would involve the use of multiple pillar[5]arene units. Fa et al. recently outlined the possibility of synthesizing pillar[n]arene 'chains' consisting of individual pillararene tubes that are stacked and assembled through dimerization and trimerization (i.e., pillar[5]arenes are piled up to made a longer pillar[5]arene tube) (Fig. 5b).[110] The peralkylamino-substituted and rim-differentiated pillar[5]arenes are stepwise-bound via hydrogen bonds and salt bridges to form an overall tube that has a fivefold helical structure. Eventually, this technique of rim-to-rim assembly can form longer nanotubes with two open ends and different properties compared to the pillar[5]arene macrocycle. As an another example, peralkyl-carboxylate-pillar[5]-arene dimers are known to have a smaller pore diameter of 0.28 nm (as compared to 0.5 nm for pillar[5]arenes) due to the superimposition of pillar[5]arene pores with narrowly twisted carboxy-phenyl pores.[116] The much smaller pore size makes them suitable for desalination applications because of their ability to exclude salt ions. The study also outlined that the pillar[5]arene nanochannels with the shortest alkyl chains showed the highest permeability because longer chains have the propensity to aggregate, leading to lower membrane permeability.

When compared with pillar[5]arenes, the peptide-appended hybrid[4]arene (PAH[4]) channel is capable of achieving high permeability and salt rejection because of its tighter constriction zone.[34] PAH[4] has a 1D tubular structure that is synthesized by the attachment of eight peptide subunits on the hybrid[4]arene macrocycle (refer to Table 2), in which the former consists of an arene of alternating resorcinol and catechol subunits (Fig. 5c). Although the central constriction

4548 | Chem. Soc. Rev., 2022, 51, 4537–4582

This journal is © The Royal Society of Chemistry 2022
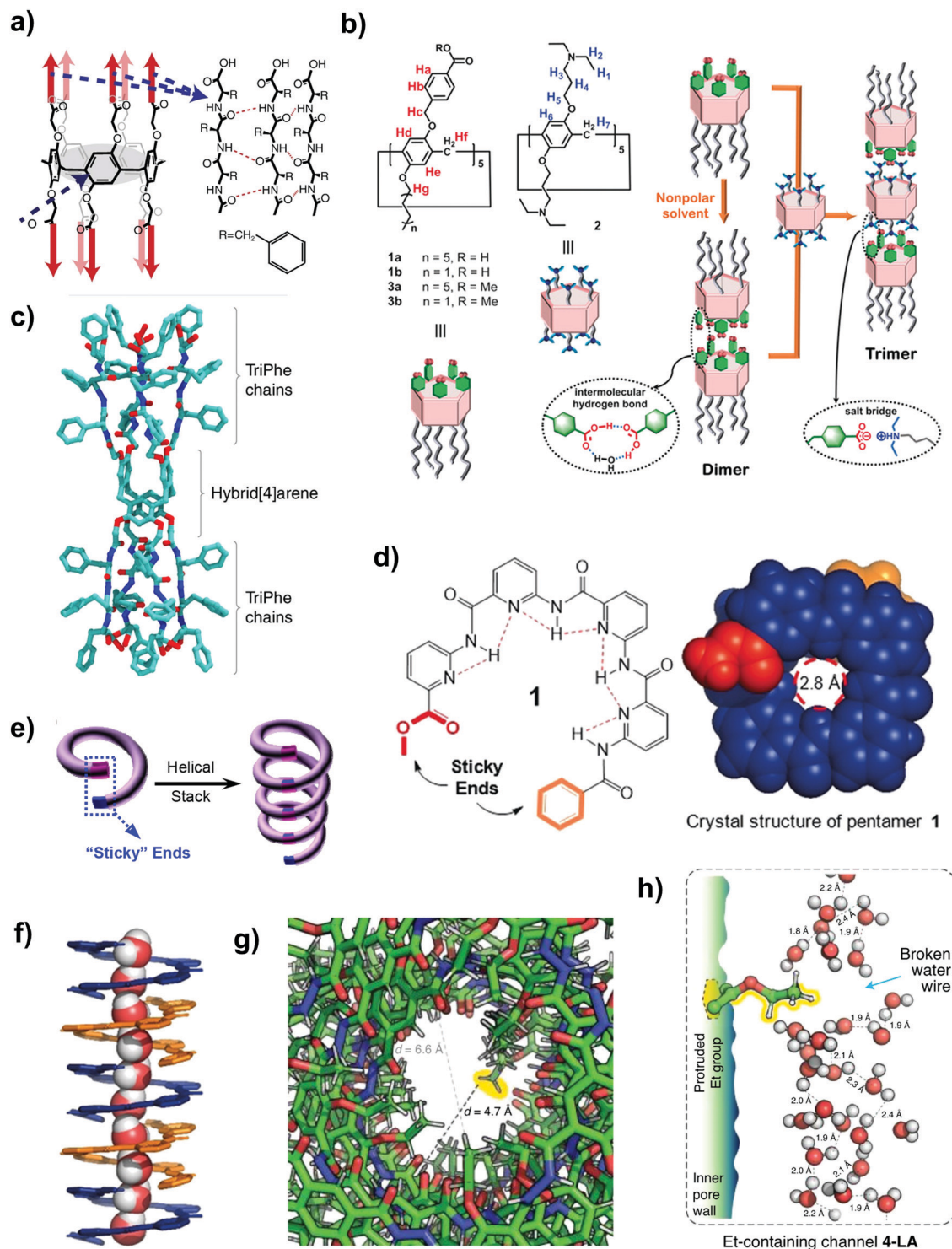
Fig. 5 (a) The chemical structure of the peptide-appended pillar[5]arene nanochannel. The intermolecular hydrogen bonding between the adjoining alternating D–L–D phenylalanine chains results in the formation of the observed pentameric tubular structure. Reproduced from ref. 109 with permission from Springer Nature, copyright 2018. (b) A schematic illustration of the design of discrete tubular water nanochannels that are formed by the dimerization and trimerization of pillar[5]arene compounds. Reproduced from ref. 110 with permission from Wiley-VCH, copyright 2020. (c) The molecular model of the PAH[4] nanochannel (side view) outlining its cylinder-like structure. Reproduced from ref. 34 with permission from Springer Nature Limited, copyright 2020. (d) The chemical (left) and crystal (right) structures of a helically folded pentamer (denoted 1) that contains two sticky ends marked in red and orange. The pore size of the eventual nanochannels is 0.28 nm. (e) A schematic illustration of the 'sticky end' methodology used to create aquafoldamer (Aqf) water nanochannels. Reproduced from ref. 55 with permission from American Chemical Society, copyright 2020. (f) The single-file transport of water molecules in an Aqf nanochannel. The latter was created using the sticky-end methodology. Panels (d) and (f) reproduced from ref. 23 with permission from Wiley-VCH, copyright 2020. (g) The reduction in local cross-section of the nanochannels (denoted by local pore size, *d*) due to the inward protrusions of the interior methyl and ethyl groups. (h) An illustration of the breaking of proton water wire due to the protrusion of the interior ethyl group. Panels (g) and (h) reproduced from ref. 7 with permission from Springer Nature Limited, copyright 2021.

This journal is © The Royal Society of Chemistry 2022

Chem. Soc. Rev., 2022, **51**, 4537–4582 | **4549**

of PAH[4] is impermeable to water, it can laterally aggregate to form dense clusters within amphiphilic matrices. The interesting point to note is that such self-assembled clusters lead to the emergence of lateral void windows (dimensions of ~0.5–0.7 nm) that are sterically more favourable for water permeation as compared to the central pore, thereby allowing interconnected water-wire pathways to 'jump' between the channels.[34] At high channel densities, the single channel permeability of PAH[4] is ~11×10^{-14} cm^3 s^{-1} (refer to Table 1), which is comparable to that of AQP-1 discussed in Section 2.1.1.

The third class of unimolecular channels that has the ability to mimic AQPs and gA is aquafoldamers (Fig. 5d and e), in which oligomers with sticky ends are continuously linked through intermolecular hydrogen bonds to form 1D tubular structures (length ~3 nm).[23,55] In simple terms, the helical and crescent-shaped oligomer sub-units have chain-end functionalities that allow them to be assembled through stacking and the eventual structure is stabilized by intermolecular hydrogen bonding, with the inner cavity acting as an aquapore for molecular transport (refer to Fig. 5f and Table 2). Because of their bottom-up construction, the properties of aquafoldamer nanochannels can be fine-tuned by manipulating their chemical and physical properties. Shen et al. showed that two types of aquafoldamer channels (Aqf-1 and Aqf-2), both of which consisted of pyridine-based aromatic polyamide chains starting with an ester moiety and ending with a benzene ring, could have profoundly different transport rates.[55] The primary difference between Aqf-1 and Aqf-2 is that the former has an additional oxygen and methylene group before its terminal benzene ring, which forces the benzene ring in Aqf-1 to point away from the central pore to a larger extent. Consequently, Aqf-1 has a rounded aquapore (diameter ~0.28 nm), whereas Aqf-2 has a more cuboidal structure (~0.21 nm × 0.27 nm).[55] Because of their small pore diameters, water transport across both nanochannels is single-file in nature and small ions can be rejected. Experimental stopped-flow results revealed that the single channel water permeability of Aqf-1 was 14 times higher than that of Aqf-2 (refer to Table 1). With the aid of molecular dynamics simulations, it was postulated that the 14-fold higher water permeability of Aqf-1 was attributed to its enlarged pore such that water molecules had higher degrees of translational and rotational freedom as well as its lower degree of surface wettability which reduced the frictional resistance to water permeation.[55] At the current stage, aquafoldamer channels have only been incorporated in lipid bilayers. Future work should also elucidate the self-assembly and stability of these channels in block copolymer matrices.

To further advance the boundaries of unimolecular biomimetic channels beyond what is achievable in AQPs, Roy et al. recently explored the possibility of synthesizing a new type of aquafoldamer channel by precisely designing its internal chemistry.[7] The aquafoldamer channel with a hydrazide backbone was synthesized using the one-pot polymerization technique (refer to Table 2)[7,23] and was reported to achieve 2.5 times higher permeability than AQP-1 while having the ability to exclude monovalent salts (KCl and NaCl) and even protons

(refer to Table 1). To achieve such a superb performance, the surface of the inner cavity was first decorated with the desired functional groups such that the hydrophobicity imparted by the non-polar C–H bonds induces a slightly positive electrostatic surface that blocks cation passage. Next, carboxylic acid-based lipid anchors are secured onto the terminal ends of the channels, which will ionize into a negatively charged anion at neutral pH, thereby repelling anions at the entrance. This work also outlined an interesting idea of using proton breakers to inhibit salt passage (Fig. 5g and h). According to the Grotthuss mechanism (that is, a process by which an excess proton diffuses through the hydrogen bond network of water molecules through the generation and associated splitting of covalent bonds involving adjacent molecules), a water chain can form a proton wire whereby protons can "hop on and off" the water molecules. The presence of inward facing groups in the foldamer channels was found to protrude up to 0.28 nm (from the pore wall to the centre of the filled pore), causing ~40% fluctuations in the local pore size (~0.5 nm to 0.7 nm) and water chain breakages (Fig. 5h).[7] It was reported that 36% of the positively charged residues lining the channels were proton wire breakers and the single file water chain can be reduced by 63% from 2.9 nm to 1.1 nm. Our key message here is that the selection of an appropriate interior group or the attachment of lipid anchors can be a way to inhibit proton transport (by minimizing proton jumping according to the Grotthuss mechanism) while maintaining a pore size that may not exclude protons inherently based on the size exclusion principle.

2.2.2 **Self-assembled channels.** The second class of biomimetic nanochannels is the supramolecular type that consists of self-assembled monomer units held together by non-covalent interactions. These nanochannels are structurally simpler as compared to unimolecular nanochannels, with the earliest types of self-assembled biomimetic channels being the zwitterionic coordination polymer (Fig. 6a) and dendritic dipeptides (Fig. 6b). For the former, the helical macrostructure was created from ZnBr(H$_2$O) constituents linked by bridging dicarboxylate anions, and it was surmised that the weak π–π stacking interactions (between the imidazolium moieties as well as by the intra-helical hydrogen bond) played a role in the assembly of the macrostructure. The pore size of the zwitterionic polymer channel was estimated to be 0.26 nm, with a full cycle within the helix consisting of two polymer units that are spaced 0.623 nm apart (Fig. 6a).[31] Dipeptides are known to form 1D straight structures in which the side chains constitute the inner hydrophobic surface and that 1D hydrogen bonding and side chain packing maintain their straight structures.[117] Dendritic dipeptides are touted as primitive mimics of AQPs because of their ability to transport water and reject some monovalent ions (but not protons). However, no water permeability tests were conducted for both biomimetic channels at that time.

Since then, researchers have attempted to synthesize other types of self-assembled channels that could mimic AQPs to a greater extent. The first example is the imidazole-quartet (I-quartet) nanochannel derived from the supramolecular arrangement of alkylureido-ethylimidazole compounds (refer to Fig. 6c and d).

4550 | Chem. Soc. Rev., 2022, 51, 4537–4582

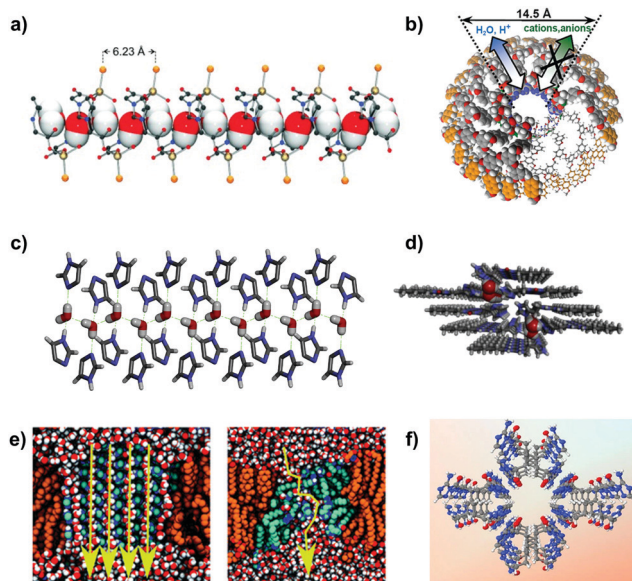This journal is © The Royal Society of Chemistry 2022

Fig. 6 (a) The illustration of encapsulated water (sketched with van der Waals radii) in the zwitterionic polymer channels. Reproduced from ref. 31 with permission from Wiley-VCH, copyright 2005. (b) An illustration of the selective transport of water and protons over cations and anions in the porous dendritic dipeptide channel (pore size estimated to be 1.45 nm). Reproduced from ref. 21 with permission from American Chemical Society, copyright 2007. (c) Side view of the tetrameric tubular architectures of the self-assembled I-quartet water channels that are capable of confining dipolar oriented water wires. Reproduced from ref. 84 with permission from American Chemical Society, copyright 2016. (d) A top view of I-quartet nanochannels. Reproduced from ref. 22 with permission from American Chemical Society, copyright 2021. (e) An illustration of two contrasting views of water transport across self-assembled channels: ordered water wires (left) and porous sponges (right). Reproduced from ref. 118 with permission from Royal Society of Chemistry, copyright 2018. (f) The pore structure of the TCT channel. The colours of the ellipsoids represent the following atoms: red (oxygen), blue (nitrogen), grey (carbon) and white (hydrogen). Reproduced from ref. 119 with permission from Springer Nature, copyright 2014.

Hydrophilic I-quartets are widely studied as water nanochannels because of their ability to form planar matrices with regularly spaced pores and can exclude ions due to their small pore diameter of ~ 0.26 nm (see Table 2).[84] They were able to mimic AQPs because of their confined chiral conduit that encapsulated oriented dipolar water wires in a single file manner and that the interaction between I-quartets and water wires within the lipid bilayer acted as a form of stabilization to the channel, resulting in the formation of highly ordered nanostructures containing structured water wires.[120] I-quartet channels can achieve a water permeability of $\sim 10^6$ H_2O molecules per s while rejecting all ions except for protons.[84] Analogous to the pR-PH channels discussed earlier in Section 2.2.1, the transport properties of the I-quartet channels can also be fine-tuned by optimizing their chirality, the size of their alkyl tail and the number of hydrogen bonds which are formed by the inner cavity with the water wire.[22,84,120] Overall, I-quartets present the concept of generating cluster water pathways through the lipid bilayer (either ordered or disordered, as shown in Fig. 6e), with this approach showing success for

newer types of biomimetic water channels such as the hydroxy channels made from octyl-ureido-polyol compounds.[24]

Conceptually similar to I-quartet channels, triazole channels are created from self-assembled columnar aggregates in bilayer membranes and their chemical properties can be fine-tuned for specific purposes such as water and selective ion transport.[121] For example, a bola-amphiphile-triazole compound (TCT) has successfully mimicked the characteristics and transport properties of a natural gA channel. TCT channels (Fig. 6f) are known to self-assemble into bilayers *via* hydrogen bonding to form an interior void (~ 0.5 nm) that is similar to the dimensional behaviours of the gA channel,[119] with the former displaying diastereoisomeric chiral internal surfaces that support the water wire array. TCT channels consist of twisting monomeric strands in a double-helix configuration and the carbonyl moieties lining the channel are solvated by water. Their robustness arises from the synergistic effect of hydrogen bonding between the triazole substructure and the hydrophobic bonds between the central chain of $-(CH_2)_6-$ groups. The X-ray structure of TCT channels reveals their hour-glass shape consisting of staggering tight and large openings, with free pore opening sizes of 0.25 nm and 0.4 nm, respectively.[119]

For all the above mentioned biomimetic channels, it is evident that the desired traits for all channels are high water permeability and the ability to selectively exclude ions. We note that another crucial challenge is to develop solution-phase methods that can be scaled-up to assemble and align these biomimetic channels in robust selective layers. This means that another critical aspect would be the synthesis of ideal structural features that can aid the alignment of biomimetic channels, which will be discussed in detail in Section 4.

2.3 Synthetic water channels

2.3.1 Nanotubes and their derivatives. Carbon nanotubes (CNTs) are one of the most studied nanomaterials ever since their discovery almost 30 years ago,[122] and have been widely explored for membrane separation because of their ability to conduct water and gas much higher (~ 3–4 times) than predicted by the Hagen–Poiseuille theory. Being an inorganic material, CNTs have a uniquely 1D cylinder-like tubular structure that spans up to a few micrometers in length and is conceptually known to be formed by the rolling up of graphene sheets, with the eventual internal cavity (pore sizes of ~ 0.8–2 nm for single-walled CNTs) acting as a nanochannel for water transport (refer to Table 2).[17,85] The smooth hydrophobic surface in the internal cavity provides high slip length and low frictional resistance for water transport, thereby granting CNTs the characteristic trait of ultrafast water transport. The exterior properties of CNTs as well as their openings can be chemically redesigned to fine-tune for particular applications, but there are currently no methods to functionalize the inner walls. Measuring the pressure-driven flow through a single CNT is yet another huge challenge. There has always been a lack of direct empirical results showing ultrafast water transport through the inner diameter of CNTs, despite the massive amount of simulation evidence.

In 2016, Secchi *et al.* provided an empirical showcase of flow slippage through a single CNT by using a nanojet setup to quantify the fluid jet entraining from the CNT (Fig. 7a and b).[123] They reported that the high hydrodynamic slip length was strongly dependent on the radius of the CNT. Interestingly, the impact made by the electronic properties of the nanotube was also observed for the first time. Comparing with an insulating boron nitride nanotube of similar radius, the authors realized a vastly different behavior in the slip length – one that was significantly higher for the semi-metallic CNT than the insulating boron nitride nanotube (Fig. 7c). This result opens up another avenue for controlling water transport *via* friction engineering at the water/carbon interface by tuning the electronic properties of nanotubes in contrast to the usual nanoconfinement effect.[124] In this regard, Velioğlu *et al.* followed up with a study on the effect of CNTs' metallicity on water transport and found that semi-conducting CNTs offered several fold higher water conductance as compared to other metallic CNTs and boron nitride nanotubes.[125] Results of their molecular dynamics simulation suggested that the metallicity of CNTs has a strong effect on the number of water files along the nanotube channel, the water–carbon interaction energy and the energy barrier at the entrance and exit of the nanotubes for water passage. Collectively, these factors drive an ultrafast in-channel water conductance for semi-conducting CNTs.

Carbon nanotube porins (CNTPs) are short segments of CNTs capable of self-inserting into a lipid bilayer. Recent experimental studies have outlined the success of preparing carbon nanotube porins (CNTPs) by the use of ultrasonication to cleave CNTs.[2] CNTPs differ from CNTs in that the length is much shorter ($\sim$10 nm) and can self-align within amphiphilic matrices (Fig. 7d) due to their predominantly hydrophobic exterior with hydrophilic oxygen functionalities at the ends. There are two types of CNTPs currently, the narrow type ($\sim$0.7 nm internal diameter, Fig. 7e) and the wider type (1.4 nm internal diameter), both of which have fairly similar lengths.[2,126] Narrow CNTPs exhibit $\sim$12-fold higher water permeability than the wider version (see Table 1) because of the reduction in water–water hydrogen bonding, even though the pore diameters of both types of CNTPs are higher than those of hydrated water molecules. Because of their short length and small size, CNTPs are typically encapsulated into liposomes or block copolymers (polymersomes) before use.[128] Activation energy measurements revealed the single-file transport of water molecules across narrow CNTPs when encapsulated in liposomes.[129] Using measured water and NaCl permeabilities, narrow CNTPs are calculated to have a water–salt selectivity (P_w/P_{NaCl}) of about 10^5, which translates to salt rejections exceeding 99%. The advantage of CNTPs as compared to biological channels is their stability and processability. However, the grand challenge facing CNTPs is the ability to produce large amounts of narrow CNTPs with uniform pore diameter, which is currently difficult to achieve.

Besides CNTs, there are two other types of nanotubes that have shown promise as water nanochannels; they are: *m*-phenylene ethynylene (*m*-PE) nanotubes[27,70,86] and cyclic peptide nanotubes (CPNs),[87] both of which are high aspect ratio and solvent stable nanotubes formed using macrocyclic rings with interior walls that are chemically modified to tune the permselectivity of the channel (refer to Table 2). Molecular level design has outlined the possibility of forming small pore widths for both nanotubes (narrowest diameters down to $\sim$0.47 nm and $\sim$0.64 nm for CPNs and *m*-PE, respectively).[5,70] First, *m*-PE nanotubes are formed through the self-assembly of rings *via* π–π stacking interactions and hydrogen bonding (Fig. 7f and g). The former are the principal driving force for the macrocyclic rings to self-associate, whereas the latter helps in aligning and stabilizing the resultant assemblies.[70,86] Different types of rings could be stacked up to form a diverse range of nanotubes (different chemistries, lengths or diameters), including hybrid tubes that have inner pores with varying functional groups.[27] Because the functional groups within the inner pores dictate the channel pore size and its corresponding transport properties, our key message here is that the heteroassociation of different macrocycles can be optimized to synthesize *m*-PE nanotubes with the desired properties.

Another intriguing trait of *m*-PE nanotubes is that their hydrophobic interior can serve as supramolecular hosts for binding hydrophobic guests in aqueous systems. Experimental studies have indicated that the nanotubes could further assemble into a pseudorotaxane that comprises a pair of axles (guests) that are threaded to the lumen (host) of the nanotube, thereby controlling the length of the nanotube by limiting the extent of macrocycle stacking (Fig. 7h).[86] At the current stage, some *m*-PE nanotubes can reject K^+, Na^+ and Cl^1 ions, while maintaining high water permeability in the hydrated state (refer to Table 1).[70] Overall, we believe that there is still a lot of potential for developing ideal *m*-PE nanotubes for water purification and desalination applications because supramolecular chemistry offers plentiful opportunities to tune their length, pore size and internal chemistry, all of which are crucial factors that dictate the transport properties of the nanochannels and their compatibility in the membrane matrix (discussed in Section 3).

Cyclic peptide nanotubes (CPNs) are nanochannels that consist of rings of amino acids assembled into stackable flat units that have the propensity to crystallize into nanotubes that are $\sim$2–100 nm long (see Table 2 and Fig. 7i). The number (typically 6–12) and side chain of the amino acid monomers can be modified to control the nanotube diameter (Fig. 7j) or the chemistry of the internal cavity of the CPN channels, respectively.[87,127] Molecular dynamics simulations have shown that the channel performance is dependent on the behaviour of water molecules under nanoconfinement inside the CPN cavity, which includes factors such as the stability and number of hydrogen bonds the peptides form with water as well as the extent of nanotube filling.[130] Empirical evidence has shown that CPN units can self-assemble *in situ* into a nanochannel within an amphiphilic matrix *via* β-type hydrogen bonds between the backbone atoms of adjacent rings (Fig. 7j).[130] During the stacking of CPN units, two of the methylenes of each cyclohexyl functional group are pointed towards the internal cavity, thereby granting its hydrophobic character.[130] From a bottom-up point of view, this type of assembly into a channel has one benefit in that physical mismatches with the
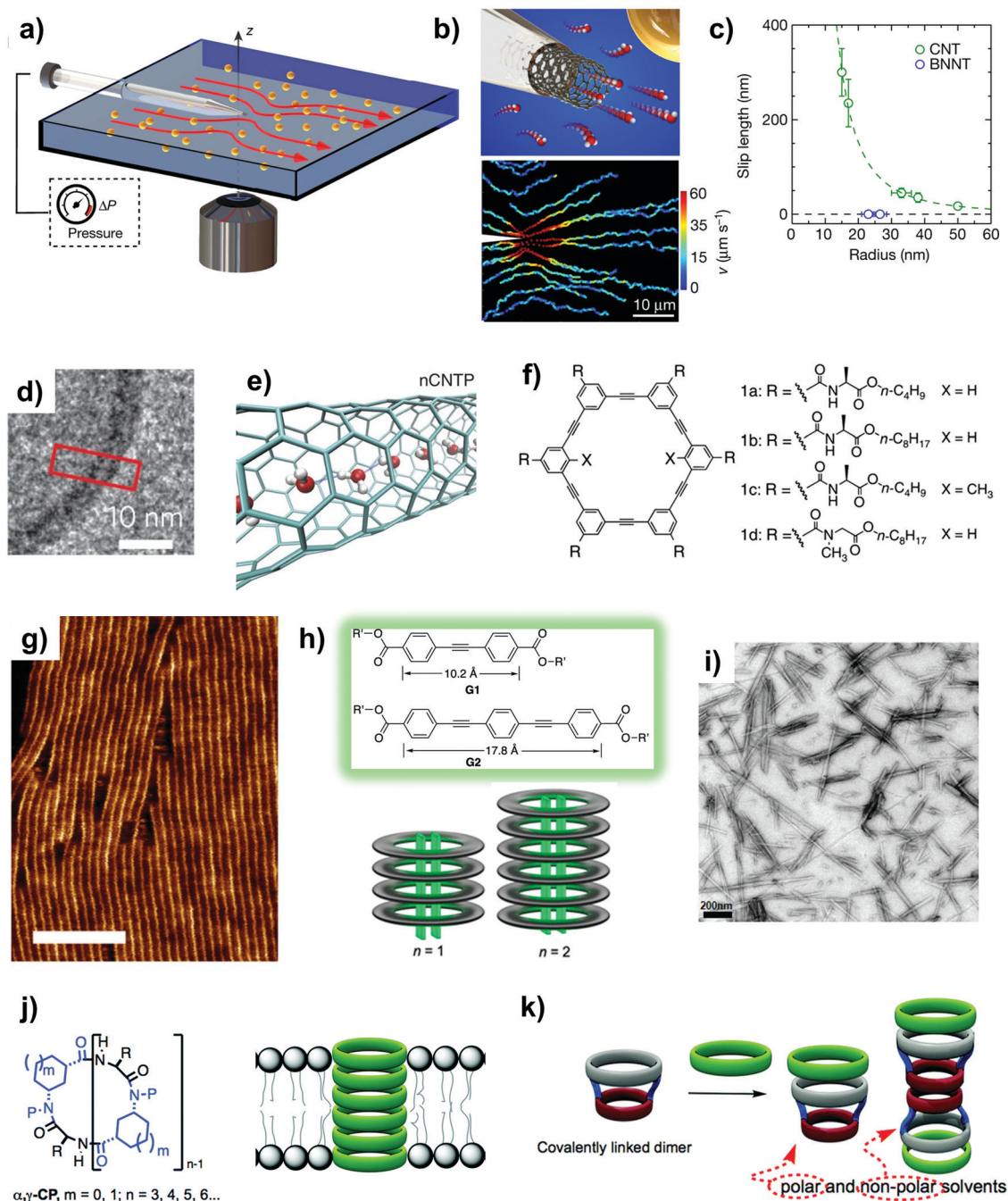
4552 | *Chem. Soc. Rev.*, 2022, **51**, 4537–4582

This journal is © The Royal Society of Chemistry 2022

Fig. 7 (a) A schematic sketch of the fluidic cell that is used to image the Landau–Squire flow set-up by nanojets coming out from discrete nanotubes. (b) Top: A schematic sketch of a nanotube protruding from a nanocapillary tip. Bottom: Trajectories of discrete colloidal tracers in a Landau–Squire flow field in the exterior reservoir. (c) The dependence of the experimentally determined slip length inside CNTs and BNNTs on radius. Panels (a–c) reproduced from ref. 123 with permission from Springer Nature, copyright 2016. (d) A cryogenic transmission electron microscopy (TEM) image outlining a CNTP (denoted by the red frame) inserted into a liposome. Reproduced from ref. 126 with permission from Springer Nature, copyright 2016. (e) Molecular dynamics simulations outlining the single file transport of water molecules across narrow CNTPs. Reproduced from ref. 2 with permission from AAAS, copyright 2017. (f) The chemical structure of self-assembling macrocycles that has the potential to be assembled into hydrogen-bonded nanotubes. (g) High magnification atomic force microscopy (AFM) image showing uniform nanofilaments packed into parallel clusters (scale bar: 40 nm). Panels (f) and (g) reproduced from ref. 70 with permission from Springer Nature, copyright 2012. (h) An illustration of the combination of tubular stacking and guest-templated discrete assembly of water-soluble *m*-phenylene ethynylene (*m*-PE) macrocycles. Reproduced from ref. 86 with permission from American Chemical Society, copyright 2020. (i) A TEM image of CPNs that aggregated into bundles. Reproduced from ref. 87 with permission from American Chemical Society, copyright 2011. (j) Left: A generic chemical structure of the α,γ-cyclic peptide (CP); right: a CPN held within a lipid bilayer. (k) A schematic illustration of the formation of Venturi-like peptide nanotubes that are formed *via* the stacking of CPN units with different diameters. Panels (j) and (k) reproduced from ref. 127 with permission from Royal Society of Chemistry, copyright 2017.

This journal is © The Royal Society of Chemistry 2022

Chem. Soc. Rev., 2022, **51**, 4537–4582 | **4553**

matrix can be avoided. Here, the physical mismatch refers to the scenario when the overall channel length and the hydrophobic/hydrophilic regions do not align well with the length of the surrounding matrix.

Typical CPNs can transport water and ions because of their pore diameters ranging from 0.47 to 1 nm (refer to Table 1).[73,87] For CPNs to achieve a solute exclusion ability, the pore size could be reduced using a synthetic aromatic amino acid. Simulation studies have outlined the possibility of tuning the single-channel water permeability by modifying the interior-facing functional groups,[71] with the highest single-channel permeability estimated to be 18×10^{-14} cm^3 s^{-1} (refer to Table 1). Molecular dynamics simulation revealed that the functionalization of the internal cavity of CPNs could lead to the disruption of the symmetry because of the change in channel morphology, but in general the enhanced internal hydrophobicity and enlarged channel volume are methods to synthesize CPNs with higher permeability.[131] The transport behaviours of water molecules inside the CPNs are controlled by molecular diffusion and sorption characteristics,[131] which means that optimizing both parameters is essential to synthesize CPNs with the desired permeabilities. On top of the possibility of fine-tuning the pore size and interior chemistry of CPNs, some researchers proposed the creative idea of stacking up various cyclic peptides with different diameters (Fig. 7k), which eventually could be assembled to form CPNs with various lengths and shapes.[37,127] The click reaction was adopted in this approach whereby one tetrapeptide was first functionalized, while the other octapeptide was modified with the propargyl moiety such that they were attached *via* covalent bonding.[37] Our key

message here is that various types of CPNs with different nanoarchitectures and precise length can be synthesized by manipulating the reaction conditions as well as the monomers and solvents used.

2.3.2 Graphene-based materials. Unlike nanotubes which are 1D in nature, graphene-based materials are a family of two-dimensional (2D) materials that can serve as synthetic water channels in their own right. Pristine graphene is a one-atom thick sheet, comprising sp^2-hybridized carbon atoms bonded in a hexagonal honey-combed lattice (see Table 2).[132] Derivatives of graphene that form the entire family are mostly chemically derived, which include the widely used graphene oxide (GO) and reduced graphene oxide (rGO) amidst the huge number of different possibilities that can be obtained through various chemical modifications by using GO as the building block.[85,132–134] Apart from their high-aspect-ratio, the most appealing attribute of graphene-based materials would be the monoatomic thickness that endows the lowest theoretical transport resistance that can be ever achieved by any materials discovered thus far.[135] Hence, graphene-based materials are hitherto one of the most well-studied 2D synthetic water nanochannels for nanofiltration (NF) and desalination.

Typically, there are two routes for graphene-based materials to act as synthetic channels – one is through nanopores on the basal planes of the single-layer graphene, while the other is through the 2D channels formed by the interlayer spacing or gallery between two graphene nanosheets (Fig. 8a and b). A defect-free single-crystalline graphene layer is intrinsically impermeable to any solutes as the electron density on the aromatic rings exerts an exceedingly large energy barrier that
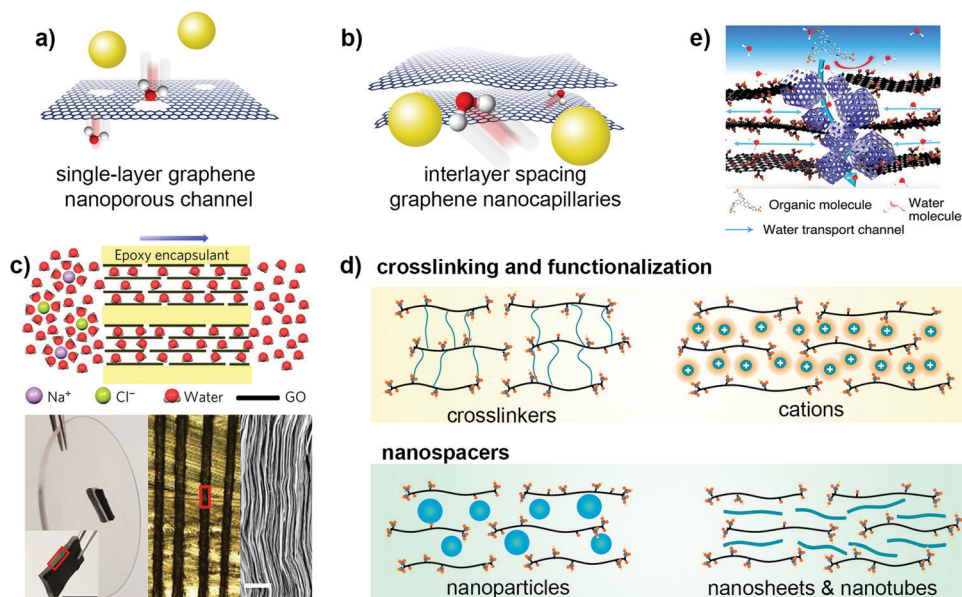
Fig. 8 The two typical routes where graphene can serve as water channels, showing (a) single-layer graphene with nanopores on the basal plane, and (b) interlayer spacing between graphene nanosheets with 2D nanocapillaries. (c) Physically confined GO nanosheets using well-defined interlayer spacings as 2D water channels. Reproduced from ref. 144 with permission from Springer Nature, copyright 2017. (d) Different strategies to tune the interlayer spacing and widen the channel to enhance water permeance. Reproduced from ref. 145 with permission from Springer Nature, copyright 2021. (e) A new route that leverages percolating pores of ZIF-8 nanocrystals as water channels to facilitate water transport in a GO laminate. Reproduced from ref. 146 with permission from Springer Nature, copyright 2021.

4554 | *Chem. Soc. Rev.*, 2022, **51**, 4537–4582

This journal is © The Royal Society of Chemistry 2022

can repel any atoms and molecules passing through it.[136] As such, sub-nanometer pores must first be created on the single-layer graphene to initiate selective transport. In general, creating nanopores on graphene is commonly carried out *via* nanofabrication or chemical etching techniques such as high-energy electron or ion bombardment,[137–139] O_2/O_3 plasma[140,141] and oxidative etching methods.[142] Most of these methods produced nanopores with edges decorated with oxygen-containing functional groups, rendering the pore channels suitable for water separation. For example, Surwade *et al.* produced nanopores of size 0.5–1 nm using O_2 plasma and obtained an extremely high water permeability of ~ 250 L m^{-2} h^{-1} bar^{-1} at $> 99\%$ rejection rate of 1 M KCl solution.[143] They attributed the high water flux to the nanoporous channel with oxygen-containing groups, which makes water entrance into the nanopores energetically favourable. While this proof-of-concept demonstrates the potential of nanoporous single-layer graphene for high-performance water desalination, the current consensus is that there remain critical challenges such as uniform nanopore production with high-density narrow pore size distribution and scaling-up issues.[132]

To address these technical problems, the second route, where water transport occurs within the interlayer spacing between two graphene nanosheets, is deemed a better option (Fig. 8b). Nair *et al.* first demonstrated that a freestanding 1 μm-thick GO laminated film was able to allow water vapor permeation but impeded the transport of other organic solvents such as ethanol and hexane, and even helium gas.[147] They reasoned that the nonoxidized region between the GO nanosheets formed a network of pristine-graphene nanocapillaries, which enabled only a monolayer of water molecules to carry out low-friction flow through these 2D nanocapillaries. Many years later, this proposition was corroborated by Keerthi *et al.*, where they found that water exhibited strong physisorption with the surface of boron nitride, resulting in high friction inside boron nitride nanochannels. However, in graphene nanochannels, such strong interaction of water molecules within nanoconfining walls was missing, and thus high slip length across the nonoxidized region of the graphene nanochannel resulted in low-friction and ultrafast water flow.[148] This provides direct evidence of the use of interlayer spacing between graphene-based materials as 2D channels for selective water permeation.

Another study by Abraham *et al.* embedded GO laminates into epoxy and oriented the channels parallel to the direction of water transport (Fig. 8c).[144] The physically confined GO laminate exhibited a well-defined interlayer spacing ranging between ~ 9.8 and 6.4 Å. Results showed that the water permeance decreased linearly, whereas the ion permeance decreased exponentially with decreasing interlayer spacing, suggesting a low water entry barrier into the 2D channel and a high slip length as the water flowed across the graphene nanocapillaries. With no physical confinement, GO laminates offered synthetic channels that had a sharp MWCO of ~ 9 Å with an interlayer spacing that could increase from 7–8 Å up to ~ 13.5 Å when accommodated by two to three layers of water molecules during swelling.[88,149,150] An interlayer spacing in this regime would be too large for sieving of any common hydrated salts, rendering the channels nonselective. As a

result, swelling of the interlayer spacing between GO nanosheets by intercalated water molecules has always been a recurring issue for such GO-type 2D channels. To address this issue, different strategies have been developed to mitigate swelling, which include partial reduction of GO to rGO,[151] crosslinking and functionalization of GO laminates[145] and intercalation of nanospacers to induce stronger interaction.[152,153] With the exception of partial reduction where the interlayer spacing actually decreases, the remaining strategies increase the interlayer spacing by either introducing sterically demanding functional groups onto the basal planes or intercalating crosslinkers or bulky nanospacers that widen the channel (Fig. 8d). This opens up an entirely new area of research, where different crosslinkers, polyelectrolytes and nanomaterials have been reported as nanospacers to engineer the interlayer spacing for achieving ultrafast water permeance, precise cutoff for molecular sieving, and other value-adding properties such as mechanical strength and stability[85] – a detailed discussion of which is available in Section 3.3.

Recently, Zhang *et al.* unveiled a new route of transport using GO as the building block and zeolitic imidazolate framework-8 (ZIF-8) nanocrystals to build a stable porous architecture (Fig. 8e).[146] The ZIF-8 nanocrystals were *in situ* crystallized at the edges of the GO nanosheets, widening the interlayer spacing and imparting mechanical stability to the laminated framework. More importantly, from the perspective of water channels, the selective growth of ZIF-8 created additional water transport channels by leveraging the percolating pores of ZIF-8 at the edges to form a network where water can penetrate rapidly but not solutes with sizes larger than the pore size of ZIF-8 nanocrystals (Fig. 8e). Hence, the use of porous materials provides new opportunity to rationally design selective GO water channels beyond that of interlayer spacing and this leads us to the next section where we discuss how porous materials can serve as synthetic water channels with different natures.

2.3.3 Metal– and covalent–organic frameworks. Porous framework materials such as metal–organic frameworks (MOFs) and covalent–organic frameworks (COFs) possess well-defined pore structures that can serve as synthetic channels for water transport (refer to Table 2). MOFs are crystalline frameworks that form an extended network *via* strong coordination bonds between the metallic nodes (single- or multi-ions) and organic bridging linkers (such as multidentate ligands). Apart from their extraordinarily high surface areas and void volumes,[154] some of the most important attributes as selective water channels are their well-defined and highly tailorable pore windows as well as their rich organic and inorganic chemistries which allow versatile functionalization and modification of pores to facilitate the transport of water.[155,156] Nevertheless, due to their kinetically labile metal–ligand coordination bonds, many of the currently available MOFs are hydrolytically unstable, limiting their use as synthetic water channels.

Only a handful of MOFs have shown good water stability and these MOFs are generally categorized into three main groups: (1) those which form stronger bonds and more rigid framework structures by coordinating hard metal ions of high valency and

This journal is © The Royal Society of Chemistry 2022

Chem. Soc. Rev., 2022, **51**, 4537–4582 | 4555

high charge density to hard ligands such as carboxylate ligands; (2) those which utilize azolate ligands (such as imidazolates, pyrazolates, triazolates and tetrazolates) that contain soft nitrogen-donor groups to coordinate to soft divalent ions; and (3) those that are functionalized with hydrophobic pore surfaces or sterically hindered metal ions.[157,158] In principle, the first two groups of water stable MOFs capitalize on the HSAB (hard and soft acids and bases) theory to bolster the metal–ligand bond strength, while the third group focuses on preventing water from penetrating the pores and weakening the frameworks.[155,156] MOFs reported to date that are robust towards water include the MIL-series, UiO-series, ZIF-series, CAU-series, PCN-series and MOF-800-series.[159] Examples of commonly used water stable MOFs that can serve as synthetic channels are MIL-53(Al), MIL-53(Cr), MIL-100(Al), MIL-101(Cr), UiO-66, ZIF-7 and ZIF-8 (Fig. 9a).[160]

Most of these water stable MOFs have three-dimensional (3D) pore windows that can serve as water channels (refer to Table 2). The pore size of the MOFs plays a crucial role. Guest water molecules must first enter through the pore before populating the cavities by forming new hydrogen bonds at the active binding sites. In the presence of a driving force such as temperature or concentration gradient, bound water molecules can then be desorbed and released. Solutes such as hydrated salt ions that have sizes larger than the pores will not be able to gain entry into the channel, rendering the pores as selective water channels. Also, coupled with their rich chemistry and versatility for chemical functionalization, it is possible to modify the pore cavities to facilitate water transport. For example, Reinsch et al. discovered a new CAU-10-H MOF, alongside its derivatives that were functionalized with –CH_3, –OCH_3, –NO_2, –NH_2, and –OH.[161] Water uptake results at low relative pressure showed pronounced uptakes by CAU-10-NH_2 and CAU-10-OH over the others, which they attributed to the higher water affinity given the ability to form strong hydrogen bonds by the polar functional groups (Fig. 9b). In addition, Akiyama et al. studied the water uptake of MIL-101-H and found that by substituting –H for the more hydrophilic –NH_2 and –SO_3H groups, the more hydrophilic environment within the pores induced a stronger interaction between the binding sites and water molecules, resulting in MIL-101-NH_2 and -SO_3H starting to adsorb water in a lower pressure region than the pristine MIL-101-H.[162]

The MIL-series of MOFs are an interesting one as, unlike other water stable MOFs that have rigid water channels, some of the MIL-series MOFs offer unique dynamic water channels.[167] For example, MIL-53(Al) demonstrates a "breathing effect" where the structure undergoes reversible flexibility during hydration and dehydration. Upon adsorbing one water molecule per aluminium, the MIL-53(Al) pore can collapse from the originally wide 8.5×8.5 Å^2 window to a narrow channel with dimensions of 2.6×13.6 Å^2 (Fig. 9c).[164] Hydrogen bonding between water and the hydrophilic moiety of the framework is deemed at work here to stabilize the narrow pore form. Apart from hydration, the dynamic pore size and flexible framework can also be induced by pressure and temperature,[167] and

suggesting the high possibility for "smart" water channels to be responsive to external stimuli and fine-tuned.

Covalent–organic frameworks (COFs), on the other hand, are a newer class of crystalline frameworks that are made up of light elements such as H, B, C, N and O to form higher-order well-defined porous structures via strong covalent bonds (refer to Table 2).[154,168] Similar to MOFs, COFs have orderly aligned pores of high density and uniform sizes, large surface areas and the capacity to fine-tune the pore sizes and tailor the chemical functionalities via molecular level design.[97] The pore sizes of currently available COFs typically range between 5 and 58 Å, making them ideal as selective water channels to discriminate water molecules from hydrated salt ions or even larger solutes.[96,97] To enable fine-tuning of pore sizes, the most direct strategy is to exploit reticular engineering by adjusting the strut length of organic monomers.[154] For example, Dey et al. synthesized – from the monomer of 1,3,5-triformylphloroglucinol (**Tp**) and [2,2'-bipyridine]-5,5'-diamine (**Bpy**) – a freestanding COF film (**Tp-Bpy**) with a pore size of 25 Å. By replacing the monomer with 4,4',4''-(1,3,5-triazine-2,4,6-triyl)trianiline (**Tta**), [4,4',4''-(1,3,5-triazine-2,4,6-triyl)tris(1,1'-biphenyl)trianiline (**Ttba**) and 4,4'-azodianiline (**Azo**), other COF films, namely **Tp-Tta**, **Tp-Ttba** and **Tp-Azo**, were formed with different pore sizes (Fig. 9d).[166] It was also evident from this study that the pore sizes of COFs can be fine-tuned to a resolution down to <5 Å, suggesting the high precision that reticular engineering can offer. Alternatively, post-synthesis modification of pore cavities is another compelling strategy for fine-tuning pore sizes. Nagai et al. used click chemistry to couple alkynes onto an azide-appended COF's wall to create triazole-linked moieties that narrowed the pore size of COF-5 from 3.0 to 1.2 nm (Fig. 9e).[165] All in all, reticular engineering and pore surface engineering are the current mainstream strategies, which can be employed for tuning the pore size, shape and microenvironment of COFs to realize tailored selectivity and enhanced hydrophilicity for elevating water transport through the synthetic channels.

Interestingly, most of the COFs studied to date are 2D in structure. While 3D COFs are also reported, they still remain a minority. Here, from the perspective of synthetic water channels, 2D COFs are attractive over their 3D counterparts given the relative ease of aligning nanosheets to enable vertical 1D nanochannels for unidirectional water permeation parallel to the transport pathway (Fig. 9f). Unlike graphene-based materials which are intrinsically impermeable (or otherwise nanopores must first be created to induce water permeation, see Section 2.3.2), the pores of 2D COFs are inherent, highly ordered and high in density. Coupled with their correct pore sizes, synthetic channels can expedite water permeance through the nanosheets, resulting in enhanced water transport, all the while being selective towards targeted solutes that are larger in size. On this note, MOFs are also available in 2D structures though less common. But, contrary to MOFs, there is a bigger pool of 2D COFs, especially those that are imine-, hydrazine- and ketoenamine-linked COFs, which demonstrate greater chemical and hydrolytic stability, owing to the stronger covalent bonds formed.[96,169] In this respect, 2D COFs as water

4556 | Chem. Soc. Rev., 2022, 51, 4537–4582

This journal is © The Royal Society of Chemistry 2022
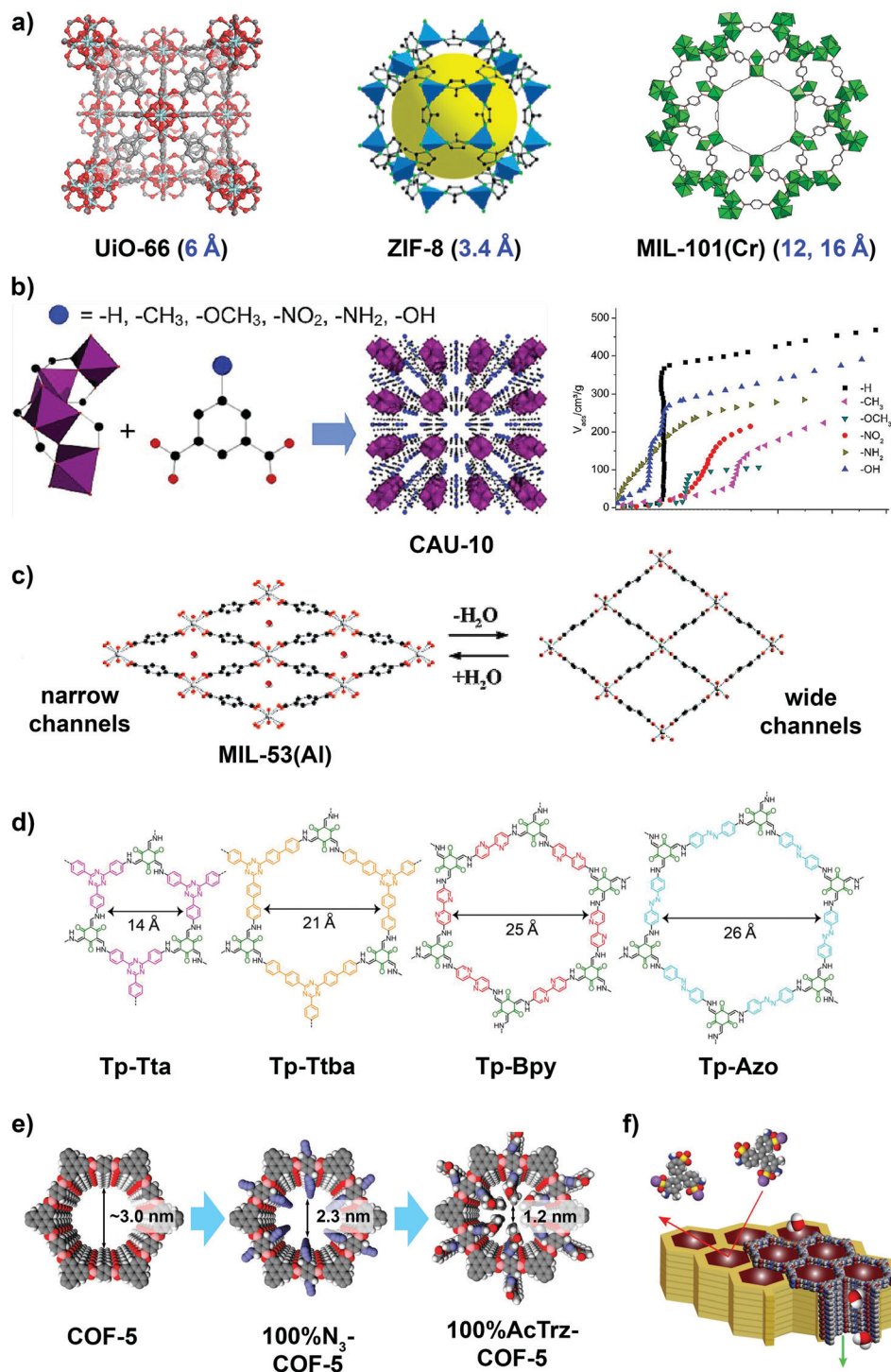
Fig. 9 (a) Chemical structures of representative water stable MOFs including UiO-66, ZIF-8 and MIL-101(Cr) and their window sizes (color-coded in blue). Reproduced from ref. 26, 36 and 163 with permissions from American Chemical Society, Royal Society of Chemistry and Springer Nature, copyright 2010, 2016 and 2019, respectively. (b) Chemical structure of CAU-10 and its derivatives, showing the effect of pore functionalization on water uptake capacity. Reproduced from ref. 161 with permission from American Chemical Society, copyright 2013. (c) Chemical structure of MIL-53(Al), showing the narrow and wide pore channels of the reversible ''breathing effect'' during hydration and dehydration. Reproduced from ref. 164 with permission from American Chemical Society, copyright 2002. (d) Fine-tuning of the pore size of COFs *via* reticular engineering. (e) Pore surface engineering to change the size and microenvironment of the walls of COF-5. Reproduced from ref. 165 with permission from Springer Nature, copyright 2011. (f) Schematic illustration showing a 2D COF nanosheet aligned in an orientation that was vertical to the transport direction such that smaller water molecules could permeate through its 1D nanochannel while discriminating the larger solute molecules. Panels (d) and (f) reproduced from ref. 166 with permission from American Chemical Society, copyright 2017.

channels seem to have a slight edge over 2D MOFs. However, there are critical drawbacks of COFs that certainly need to be addressed, such as their complex synthesis protocols, moderate to low product yields that result in poor scalability, and low solubility in many solvents leading to poor solution processability.[170] These drawbacks will be further discussed in Section 3.

2.3.4 Others. Our discussion thus far has revolved around some of the most exciting 1D nanotubes, 2D graphene-based materials and 2D/3D MOF and COF nanomaterials that have attracted the attention of researchers and how their unique psychochemical properties have helped in enabling them as synthetic water channels. In this section, we will be presenting other emerging water channels that are beyond the aforementioned and are of potential interest to readers to complement what have been shared.

In an effort to increase water–solute selectivity and to eliminate the orientation-dependency that exists in 1D, 2D and 3D channels, Yuan *et al.* synthesized zero-dimensional (0D) porous organic cages (POCs) as synthetic water channels.[35] POC molecules are purely organic in construct and have window openings that are synthetically tunable (refer to Table 2 and Fig. 10a).[103] In this work, POCs with a tetrahedral-shape were aligned window-to-window such that an extended 3D pore network, comprising internal (intrinsic to POC) and external (between POC) cavities, was formed as synthetic water channels (Fig. 10b). The POC water channels were inserted into bilayer systems and found to have a high water permeability of 146 μm s^{-1} under liposome shrinkage test conditions (Fig. 10c), which was far more superior to most of the synthetic channels already discussed in Section 2.2 such as peptide-appended pillar[5]arenes (1 μm s^{-1}) and I-quartets (3–4 μm s^{-1}).[69,84] Various cation and anion permeations through the channels were also found to be negligible, which was attributed to the high dehydration energy penalty needed to enter the channels.[35]

Contrary to POCs but similar to graphene-based materials, there are other emerging 2D nanomaterials that are nonporous – and thus intrinsically impermeable – but able to serve as synthetic water channels, owing to their ability to be assembled into nanolaminated microstructures to offer interlayer spacing for water transport. 2D molybdenum disulfide (MoS$_2$) is one such example. However, different from GO nanosheets, MoS$_2$ has much stronger van der Waals forces between nanosheets such that the water channels are hydrolytically more stable and less likely to swell.[171] In addition, MoS$_2$ nanosheets are more rigid given their three-atomic-layered structure.[29] This renders the water channels less susceptible to mechanical compaction under the high transmembrane pressure applied during membrane operation. And most importantly, MoS$_2$ does not have any hydrophilic groups oriented into the surfaces of the water channels. Coupled with the high surface smoothness which leads to low hydraulic resistance, MoS$_2$ laminated membranes were reportedly having water permeance that was $\geq$5 times higher than GO membranes. Furthermore, due to the well-defined interlayer spacing – 12 Å when fully hydrated and 6 Å when dry (Fig. 10d), MoS$_2$ water channels were able to perform effective ionic and molecular sieving with a MWCO of $\sim$500 Da (equivalent to a Stokes radius of $\sim$11–12 Å).[89] As for single-layered MoS$_2$ nanopores, their potential as synthetic water channels is evidenced by a 70% higher water permeation rate as compared to graphene nanopores, owing to the special hourglass architecture of the Mo-only pore with a hydrophobic edge and a hydrophilic centre.[172]

Lately, a new family of transition metal carbides, nitrides and carbonitrides (termed MXenes in short) are also emerging rapidly as novel nonporous 2D nanomaterials with strong potential as synthetic water channels.[176,177] Similar to MoS$_2$, 2D MXenes can serve as synthetic channels by leveraging their tunable interlayer spacing for water transport when assembled into laminated membranes (refer to Table 2). Thus far, the most commonly studied member of the 2D MXene family is titanium carbide (Ti$_3$C$_2$T$_x$) nanosheets, where T represents terminating functional groups, such as –O, –OH and/or –F, and x represents the number of terminating groups present.[32] The interlayer spacing of Ti$_3$C$_2$T$_x$ in the wet state is smaller than those of GO and MoS$_2$ – $\sim$6 Å.[178] As such, the as-assembled MXene nanochannels demonstrated a Na$^+$/Mg^{2+} selectivity of $\sim$10, which is 5-fold higher than that of GO nanochannels.

Furthermore, being electrically conductive is probably one of the greatest advantages of the MXene water channel. Ti$_3$C$_2$T$_x$ films have one of the highest metallic conductivities, as high as 10 000 S cm^{-1},[179] and hence MXene water channels show strong promise for modulating ion transport under an externally applied potential. Ren *et al.* was the first to present a voltage-gating ion transport through Ti$_3$C$_2$T$_x$ nanochannels.[174] The permeation rates of mono- and divalent cations like Na$^+$ and Mg^{2+} were reported to slow down at a negative potential of –0.6 V due to the shrinkage in interlayer spacing but increased backup as the potential was switched to positive at +0.4 V (Fig. 10e). The same observation was further corroborated by other studies.[175,180] Notably, Wang *et al.* demonstrated the high on–off voltage-gating ratio using sub-nanometer (7 Å) interlayer Ti$_3$C$_2$T$_x$ nanochannels.[175] By switching between the "on- and off-states", an order of magnitude difference in ionic conductivity was reported (Fig. 10f), suggesting that a positive voltage facilitated ion transport, while a negative voltage suppressed it. The authors attributed this to the sub-nanometer MXene channel, which resulted in stronger repulsion towards the permeating cations as more cations were intercalated under a negative applied voltage of –1.0 V. When the voltage was switched positive to +1.0 V, the negative charge of the channel was neutralized, resulting in a weakened ion–channel interaction that facilitated the higher ion conductivity (Fig. 10g).[175] Nevertheless, despite the appeal of moderating ion transport *via* an external stimulus, MXene water channels are in general less chemically stable as compared to graphene-based materials and MoS$_2$,[32] owing to the susceptibility of the surface-exposed metal atoms to spontaneous oxidation. Hence, there is a need to address the long-term chemical stability issue in order to enable MXenes as synthetic water channels.

4558 | *Chem. Soc. Rev.*, 2022, **51**, 4537–4582

This journal is © The Royal Society of Chemistry 2022
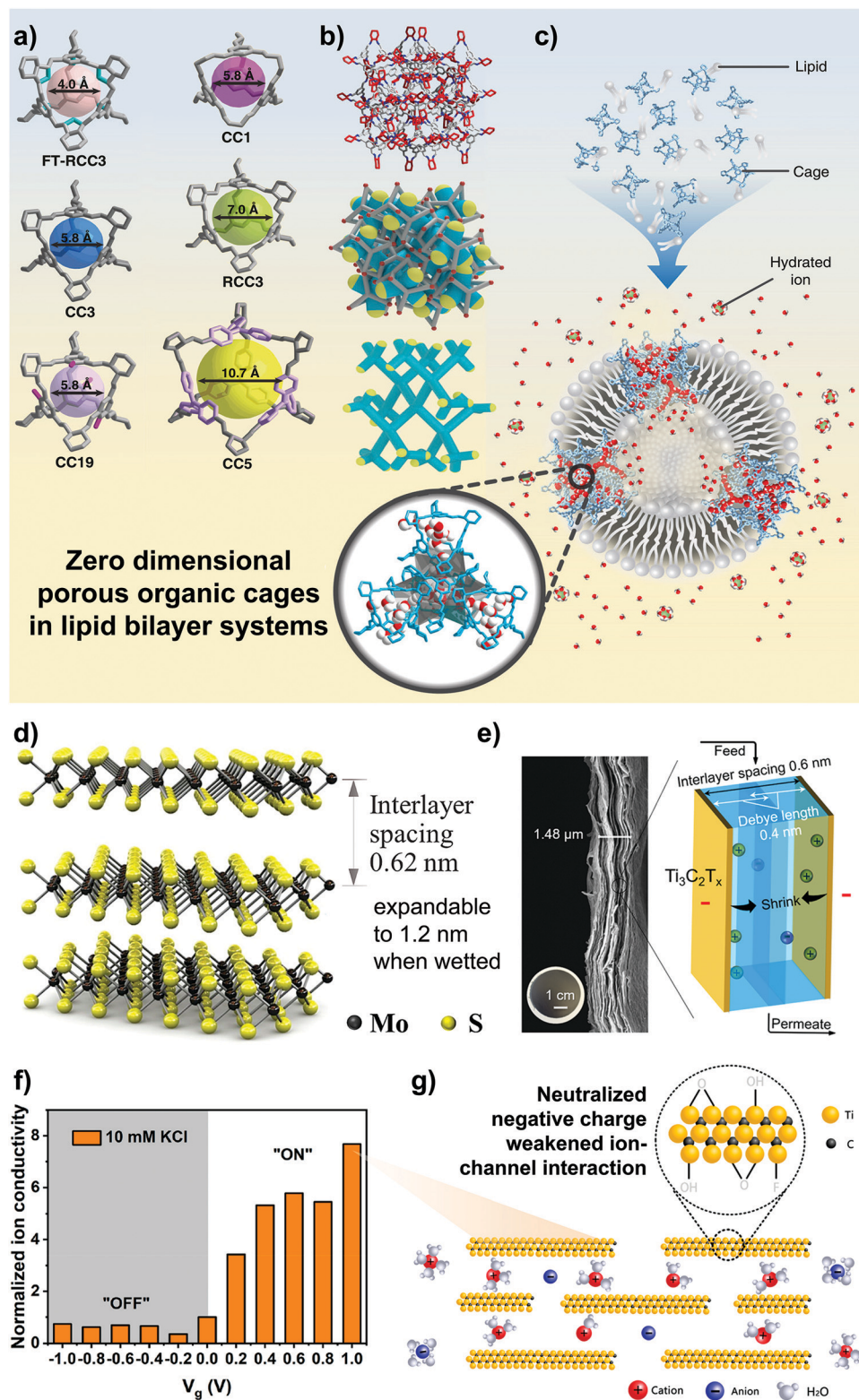
Fig. 10 (a) POC crystal structures showing tunable window sizes; (b) structures of the window-to-window packing of tetrahedral POCs (top), with the channel network shown in blue and the end of the channel network shown in yellow (middle) as possible entry points for water molecules, and the extended channel network without the tetrahedral POC shell (bottom); and (c) schematic illustration showing a CC3 POC embedded within a lipid bilayer, showing how chains of water pass into the synthetic water channels. Reproduced and modified from ref. 35 with permission from Springer Nature, copyright 2020. (d) Schematic illustration showing 2D MoS_2 and the interlayer spacing acting as synthetic water channels. Reproduced from ref. 173 with permission from Springer Nature, copyright 2011. (e) $Ti_3C_2T_x$ MXene nanolaminated membrane, showing the shrinkage of the interlayer spacing under a negative applied voltage. Reproduced from ref. 174 with permission from American Chemical Society, copyright 2018. (f) The on–off voltage gating effect with (g) a positive "on-state" neutralizing the negative charges of the oxygen-containing groups on the surfaces of the MXene channels, resulting in weakened ion–channel interaction and a higher cation conductivity. Reproduced and modified from ref. 175 with permission from American Chemical Society, copyright 2019.

This journal is © The Royal Society of Chemistry 2022

Chem. Soc. Rev., 2022, **51**, 4537–4582 | **4559**

3. Membrane nanoarchitectonics incorporating water nanochannels

In this section, approaches for incorporating water channels into membranes are discussed with respect to the design and engineering of the membrane structures. To facilitate easy referencing for readers, we briefly discuss the various fabrication methods and associated separation mechanisms before going into the details of membrane designs. There are three main membrane designs that are of interest to nanochannels: freestanding membranes, supported membranes, which consist of multilayered, lipid bilayered and block copolymer membranes, and thin-film nanocomposite (TFN) membranes (Fig. 11a). In particular, we will touch on the various methods to incorporate

nanochannels to fit into these membrane designs, the location of the nanochannels in the membrane and the advantages and inherent limitations.

3.1 Fabrication methods

One of the most important applications of nanomaterial research is membrane design. Owing to the difference in the physicochemical and morphological properties of different nanochannels, not all membrane designs are suitable for all nanochannels (Fig. 11a). For example, the TFN design is widely suitable for most nanochannels as the polyamide matrix forms the basis of the selective layer with nanochannels embedded within, but freestanding membranes are mainly suited for 2D materials only, given the capacity to form continuous defect-free films.
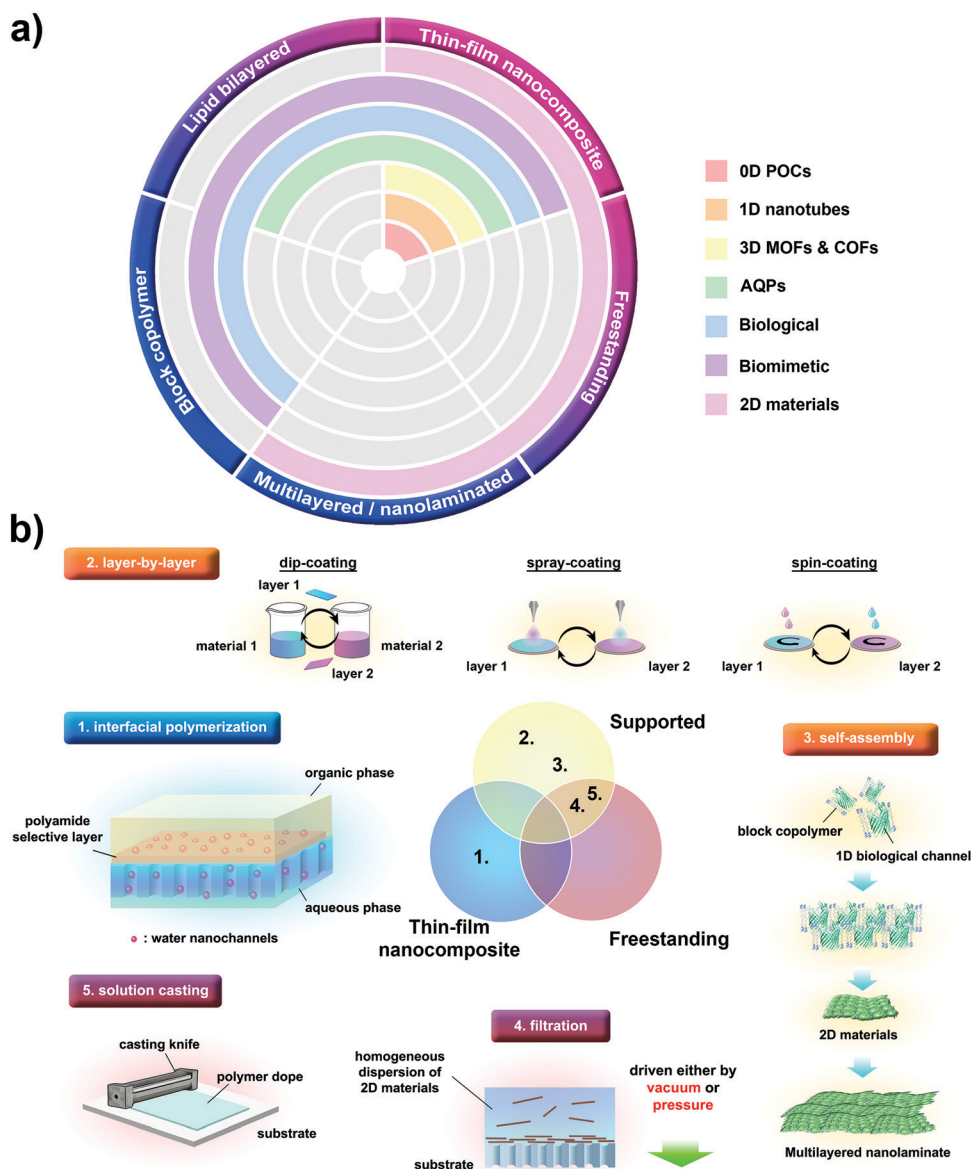
Fig. 11 (a) The versatility of various nanochannels that is manifested by their potential use in various membrane designs. (b) Five mainstream techniques for the fabrication of water separation membranes incorporating nanochannels. The illustrations in the self-assembly section were reproduced and modified from ref. 81 with permission from Springer Nature, copyright 2020.

4560 | Chem. Soc. Rev., 2022, 51, 4537–4582

This journal is © The Royal Society of Chemistry 2022

Hence, to fabricate membranes or devices incorporating water channels, we need to evaluate the mainstream fabrication methods used to date (Fig. 11b). The first method is interfacial growth at the liquid–liquid interface, which typically involves the use of a porous support membrane that functions as micro-pores controlling the diffusion of reactants. One of the most common examples is interfacial polymerization (IP),[39] which involves polymerization at an interface between two immiscible phases (e.g. aqueous and organic), thereby constraining the membrane formation at the interface. As compared to the relatively controllable process of interfacial growth, Layer-by-Layer (LbL) assembly involves exposure of the membrane substrate to different solutions of materials in a cyclic manner to deposit channels or channel-containing nanosheets. Instead of immersing the substrate into different solutions, LbL assembly can also involve the use of spray-coating or spin-coating methods to deposit channel materials as multilayered membranes on the membrane substrate.[181,182] More often than not, the purpose is to fabricate membranes with a more homogeneous distribution of materials as well as to obtain the desired alignment onto the membrane substrate. The third and fourth methods are mostly interconnected, and involve the use of pressure- or vacuum-filtration to deposit channel-containing solutions onto the membrane substrate.[183,184] Prior to filtration, water nanochannels, especially those of biological and unimolecular biomimetics, are at times required to undergo self-assembly to form channel-containing nanosheets with greater capacity to form defect-free continuous films. It is also noteworthy to mention that self-assembly as described in the third method can also be used alongside LbL assembly to produce multilayered membranes. The fifth method is solution casting, which traditionally involves direct blending of nanochannels into polymeric dope solutions before casting and phase inversing the nascent films to obtain mixed matrix membranes.[185,186] By and large, mixed matrix membranes prepared by solution casting have stronger relevance as dense membranes for gas separation – where nanochannels serve as performance-enhancing filler materials – or as porous substrate membranes with strengthened mechanical or surface properties for fabrication of composite membranes. In this context of nanochannel-enabled membranes, solution casting is more aptly applied to form freestanding or nanolaminated membranes of 2D materials, which will be further discussed in Sections 3.3.1 and 3.3.2.

3.2 Separation mechanisms

Membrane separation of water from solutes is dominated by a variety of mechanisms at the micro- to nanoscale (Fig. 12). Because the mechanism dictates the separation performance (e.g. permeability and selectivity) of the membrane, it is imperative to have an understanding of the mass transport and associated mechanisms. As the channel sizes decrease to the molecular scale (the size ranges of ions, gases and liquids), the mass transport behaviour changes drastically due to nano-confinement effects, which results in the breaking down of the commonly known no-slip condition in classical fluid mechanics. At the sub-micron scale, hydrodynamic filtration occurs when solutes in the liquid are removed based on the size exclusion principle. As the pore size decreases to the nano or sub-nano scale, interface effects and molecular sieving mechanisms become dominant.[40,187] As shown in Fig. 12, molecular sieving occurs when water molecules and dissolved solutes are separated based on the sheer size differentiation effect, whereas interface effects that arise from the electrostatic properties can occur for a wider window of pore sizes (e.g. Donnan exclusion effect). Subsequently, as the pore size decreases further to the sub-nano or near ångström scale, mass transport is then governed by the solution-diffusion mechanism in which the more permeable solute of interest is one that dissolves better and diffuses faster across the polymer matrix than the less permeable retentate.[40,187]

Currently, the solution-diffusion theory is the most widely accepted separation mechanism for polymeric membranes with dense selective layers such as that of TFC-RO and TFC-forward osmosis (TFC-FO) membranes because of the sub-nanometre pore size of the polyamide matrix (e.g. ~0.25 nm for RO membranes).[10] NF membranes, on the other hand, work on the combination of hydrodynamic filtration, the solution-diffusion mechanism and the Donnan exclusion principle.[188,189] Upon

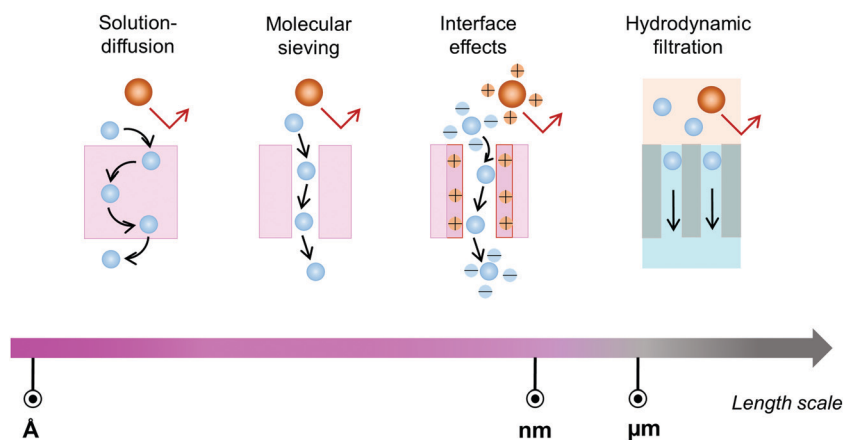

Fig. 12 Schematic illustration of the mass transport mechanisms in water separation with increasing length scale (from left to right).

This journal is © The Royal Society of Chemistry 2022

Chem. Soc. Rev., 2022, 51, 4537–4582 | 4561

incorporation of nanochannels into the membrane matrix, molecular sieving, interface effects and solution-diffusion mechanisms are probable mechanisms that govern the separation of water and solutes. For transport through the nanochannel, surface friction as well as the interactions between the channel cavity and permeation species will affect the transport rates of the permeating species (this will be elaborated in the subsequent subsections).[9,190]

3.3 Different membrane designs

Water nanochannels offer interesting transport properties that are well-aligned with the efforts aimed at fabricating next-generation membranes. As introduced above, various methods may or may not be suitable for a particular type of membrane design. Accordingly, the three types of water nanochannels have so far been nanoarchitectured into various membrane designs for water separation (*i.e.*, water purification and desalination) and their incorporation *via* different techniques as introduced in Section 3.1. Herein, we probe deeper into the five main types of membrane designs together with their associated fabrication methods and resultant membrane performances.

3.3.1 Freestanding membranes. Freestanding membranes, in this context, refer to continuous membranes that are made up entirely of water channels without any support layers and/or polymer matrices. In order for water channels to stand alone as freestanding membranes, they must be able to assemble into a mechanically robust and self-supporting structure. For that, biological channels, which rely on lipid bilayers to be effective, and low molecular weight biomimetic channels, which lack the ability to form long-range ordered structures, cannot be made into defect-free continuous freestanding membranes. Hence, in this section, we focus mainly on synthetic water channels, in particular 1D nanotubes and 2D materials, which have demonstrated high capacity to assemble into freestanding membranes.

One of the most compelling freestanding membranes is vertically aligned CNT membranes. This type of membrane is prepared by first growing vertically-aligned CNT forests *via* a chemical vapour deposition (CVD) method before a densification process by mechanical compaction to close up the interstitial gaps between the CNTs. There are many membrane designs that can spin off thereafter, with the most common being composite membranes made by implanting polymer matrices to seal up the interstitial gaps for inducing selectivity and mechanical strength.[191,192] It is also possible to fabricate purely freestanding membranes without polymer matrix, in which case, the interstitial gaps can also double up as water channels. Lee *et al.* exploited this design and synthesized a freestanding vertically-aligned CNT membrane with a small densified interstitial gap size of 7 nm and the water permeability reaching up to 5800 L m^{-2} h^{-1} bar^{-1}.[193] When the capped ends of the CNTs were opened *via* O$_2$ plasma, supplementary water channels comprising CNTs with an inner diameter of 6 nm were made available, which increased the water permeability close to 30 000 L m^{-2} h^{-1} bar^{-1}, and reached one of the highest permeabilities known so far for UF membranes.

Despite this huge water permeability, the membrane selectivity was not compromised at >98% rejection of Dextran of 12 kDa molecular weight.[193]

Compared to freestanding vertically aligned CNT membranes, it is much easier to fabricate freestanding 2D material membranes. As highlighted in Section 3.1, these membranes are mostly prepared *via* vacuum- or pressure-assisted filtration methods, where 2D materials are filtered directly on membrane substrates before delaminating to afford freestanding laminated membranes. To date, freestanding membranes from 2D materials such as rGO and COFs have been reported.[194,195] For instance, an ultrathin freestanding rGO membrane with 100 nm thickness was demonstrated to have a water flux of 57.0 L m^{-2} h^{-1} when evaluated under FO conditions using deionized water as feed solution and 2.0 M NaCl as draw solution.[194] This water flux was ~5 times higher than that of commercial FO membranes with a low reverse salt flux of 1.3 g m^{-2} h^{-1}. Interestingly, internal concentration polarization, which is the Achilles heel of all FO membranes, was notably missing, owing to the unique freestanding and ultra-thin design of the rGO membrane.[194]

Other examples of freestanding membranes include highly crystalline freestanding 2D COF membranes. But, unlike their rGO counterparts, these freestanding membranes are fabricated *via* an interfacial crystallization method. Typically, in interfacial crystallization, the interface at the aqueous and organic phases serves as the site of crystallization, where the free amine building block diffuses and reacts with the aldehyde to form a highly crystalline porous 2D network of COFs. Dey *et al.* was the first to demonstrate this *via* a salt-mediated interfacial crystallization method. Amine-*p*-toluene sulfonic acid (PTSA) salt was added to slow down the diffusion rate of the building blocks, resulting in thermodynamically-controlled crystallization.[166] As a result, COF fiber-like crystallites were first formed and self-assembled laterally into sheet-like layers before extending into a large thin film connected entirely by covalent bonds. Recently, Li *et al.* used the same method to form freestanding 2D COF laminated membranes with sub-nanopores *via* AB stacking of 2D COF nanosheets.[195] Owing to the AB stacking as opposed to AA stacking, the pores of the freestanding membranes shrunk from >1 to ~0.6 nm. Correspondingly, the water permeability was found to decrease from ~10 to ~4 L m^{-2} h^{-1} bar^{-1} with high Na$_2$SO$_4$ or K$_2$SO$_4$ rejection rates between 90 and 95%.

Being the most straightforward design for utilizing synthetic water channels – with some even showing unprecedentedly high separation performances as a result, freestanding membranes comprising water channels are not without drawbacks. One of the most critical issues is the lack of mechanical robustness to handle high transmembrane pressure.[196] Examples discussed so far tend to circumvent this problem by demonstrating only UF/NF or FO performances under low or no applied pressure. However, to better manage the much higher transmembrane pressure required by some pressure-driven processes such as NF and RO, freestanding membranes have to be made much thicker, and this would see a drastic tradeoff in water

4562 | *Chem. Soc. Rev.*, 2022, **51**, 4537–4582

This journal is © The Royal Society of Chemistry 2022

permeability, undermining the ultrafast water transport promised by the water channels. Hence, we believe that it is important to derive the required mechanical support from a separate substrate layer so that the selective layer can be made ultrathin to unlock the full potential of the water channels. For this reason, the following sections are geared towards discussion on supported and TFN membranes.

3.3.2 Supported membranes

3.3.2.1 Multilayered or nanolaminated supported membranes. Similar to the freestanding membrane design, synthetic water channels, especially those put together by 2D materials, are best demonstrated as multilayered and/or nanolaminated supported membranes, owing to their high aspect ratio and good solution processability into defect-free continuous thin films. A multitude of synthesis methods as discussed in Section 3.1 can be employed for this purpose, which include LbL, vacuum- or pressure-assisted filtration, inkjet printing, LB film formation and various casting and coating methods such as drop-casting, solution-casting, spin-coating, slot-die coating, and spray-coating.[197–199] The wide selection of methods also entails that the multilayered and/or nanolaminated membrane design is easily adaptable to almost all kinds of 2D water channels given the right physicochemical properties of the materials used.

To date, the most commonly used method is vacuum- or pressure-assisted filtration, where 2D materials are first dispersed in suitable solvents to form solutions before filtering through support membranes, where the 2D materials are deposited and assembled into highly ordered lamellar microstructures. This method is the easiest to implement among all methods and has hitherto been applied to almost all 2D materials, including graphene-based materials, 2D MOFs and COFs, MoS_2, MXenes and others.[19,200–204] The key towards a uniform and intact nanolaminated membrane is the duration of filtration and use of good solvents to create well-exfoliated and well-dispersed suspensions of 2D materials.[205] Water is by far the most preferred solvent for graphene-based materials, especially GO, owing to its cost-effectiveness, polar nature and low volatility, which leads to a high degree of exfoliation, stable and homogeneous aqueous solutions and slow drying that promotes uniform assembly of laminated films. Recently, Zhang et al. also showed that other organic solvent systems are suitable. Specifically, the study revealed that polar aprotic solvents such as dimethyl sulfoxide and dimethylformamide are also good solvents for exfoliating and dispersing GO nanosheets to yield nanolaminated membranes with good integrity.[206] The sizes of the synthetic channels formed by the interlayer spacing were tunable to endow the GO nanolaminate with varying water permeability from 30 to 70 L m^{-2} h^{-1} bar^{-1} based on the solvent used.

Beyond GO-based materials, other 2D materials that can exploit an aqueous system include MXenes and MoS_2 nanosheets.[32,89] Owing to their high hydrophilicity and negative charges, MXenes and MoS_2 can be easily dispersed in water to afford stable colloidal suspensions. For this reason, nanolaminated membranes of MXenes and MoS_2 are generally prepared *via* vacuum- or pressure-assisted filtration. Apart from that, being able to suspend homogeneously in aqueous systems means that MXenes and MoS_2 can leverage LbL assembly for producing multilayered membranes. For example, Li et al. first reported an LbL assembly of MoS_2 by first dipping a polyethersulfone (PES) substrate into a positively charged polyethyleneimine (PEI) solution, before moving to the negatively charged MoS_2 dispersion, and finally back to a positively charged poly(acrylic acid) (PAA) solution to prepare a trilayer selective layer for FO application.[207] Because of the enhanced surface hydrophilicity and surface smoothness brought about by the incorporation of MoS_2, the FO water flux was able to see a 35% increase from 20 to 27 L m^{-2} h^{-1}, while reducing the reverse NaCl salt flux by 28% to 17 g m^{-2} h^{-1}.

Further to filtration and LbL methods, 2D materials that are well-dispersed in water can exhibit viscoelastic properties that render them suitable for solution-casting and various coating methods. GO dispersion is one of the best examples as it shows non-Newtonian shear-thinning behaviour with large viscosity changes occurring at concentrations beyond 5 mg mL^{-1}. This behaviour allows the GO dispersion to exhibit high viscosity at zero shear rate, while inducing a thinning effect at high shear rates that enables uniform casting of the dispersion. Generally, solution casting of 2D nanochannels has stronger up-scaling potential than filtration and LbL methods. As an attestation to this claim, Yang et al. utilized different crosslinking agents, such as calcium ions (Ca^{2+}), ferric ions (Fe^{3+}), polyethylene oxide (PEO) and PEI, on lower concentration GO dispersions ranging between 1 and 5 mg mL^{-1}.[208] It was observed that, with crosslinking agents added, low viscosity GO dispersions were able to turn into hydrogel-like slurries with higher zero-shear viscosity that warrants the casting of nanolaminated GO-based membranes feasible. In particular, at 3 mg mL^{-1} GO concentration, the viscoelasticity of the Fe^{3+}-crosslinked GO dispersion was considered to be befitting for casting such that an intact membrane with a large area of >1000 cm^2 could be fabricated on a commercial UF substrate. Also, the interlayer spacing between the GO nanosheets was found to be between 8.0 and 9.4 Å, depending on the intercalating crosslinkers added. Accordingly, the as-prepared Fe^{3+}-crosslinked GO nanolaminated membrane with a narrow interlayer spacing of 8.2 Å showed >99% rejection rates towards various organic dyes of different molecular weights and charges.[208]

The discussion so far is focused on a top-down approach, where 2D nanochannels are first synthesized and exfoliated before nanoarchitecturing into multilayered and/or nanolaminated membranes. While this approach is generally more facile and scalable, finding a good solvent system to do so may not always be easy. For example, not all MOFs and COFs exfoliate well in water and would require other solvent systems such as ethanol and chloroform to induce favorable exfoliation. In this regard, supported membranes of ultrathin MOFs and COFs are often fabricated *via* a bottom-up approach such as *in situ* growth.[209] Notwithstanding the issues of dispersion and exfoliation, the biggest merit of *in situ* growth lies in the formation of a continuous defect-free polycrystalline layered membrane,

This journal is © The Royal Society of Chemistry 2022

Chem. Soc. Rev., 2022, **51**, 4537–4582 | 4563

which allows high permselectivity to be derived directly from the intrinsic porosity of the crystalline MOF/COF layers. For example, Shen *et al.* demonstrated a polydopamine (PDA)-modulated *in situ* growth approach, where PDA was first deposited onto a polyacrylonitrile (PAN) support to serve as a molecular linker for building units like 1,3,5-triformyl-phloroglucinol (TFP) and 2,5-diaminobenzenesulfonic acid (DABA) to bind and promote heterogeneous nucleation on the surface of the support.[210] As a result, a sulfonated imine-linked COF nanolaminate with a pore size of 1.4 nm and a submicron thickness of $\sim$42 nm was formed. More importantly, due to the modulating effect of the uniform PDA layer, the polycrystalline COF nanolaminate was defect-free as evidenced by high rejection rates of >99% towards Congo red and Eriochrome black T. The pure water permeance of up to 135 L m^{-2} h^{-1} bar^{-1} was attributed to the ultrathin COF layer that offered water nanochannels with low hydrodynamic resistance.

Despite their high performances, one of the drawbacks of multilayered or nanolaminated membranes is the poor stability brought about by water swelling into the interlayer spacing, which eventually enlarges the interlayer spacing to a point that disintegrates the nanochannels. To date, chemical crosslinking using cations, and low-molecular-weight crosslinkers or polyelectrolytes with specific functional groups, is one of the most common strategies in alleviating swelling and stabilizing 2D nanochannels.[85] The crosslinkers can also serve as spacers to tune the interlayer spacing for well-defined molecular cutoffs by the nanochannels. In recent years, an emerging strategy – focusing on amalgamating mixed-dimensional nanochannels – has been considered as promising in creating synergistic effects for delivering enhanced performances and membrane stability.[211] Notably, by intercalating 1D CNTs and cellulose nanofibers (CNFs) into graphene-based and COF nanosheets, the composite nanolaminates exhibited NF performances that were several times higher than those of commercial membranes. Furthermore, driven by the exertion of strong interlamellar interactions, which include electrostatic interaction, van der Waals forces of attraction and π–π stacking, the 1D nanospacers endowed the nanolaminates with the necessary robustness for handling the compressive and flow-induced shear stress encountered during pressure-driven separation processes.[196,203,212] In contrast, studies on amalgamating unidimensional nanochannels were shown to produce complementary effects. Intercalating rigid 2D COFs into GO nanosheets could increase the self-supporting capacity of the nanolaminates to alleviate the poor mechanical stability of GO-based membranes, leading to stronger resistance towards compressive deformation.[152] Alongside the presence of in-plane pores, 2D COFs were capable of providing transport "shortcuts" for reducing the tortuous pathway through the GO nanosheets to achieve an overall performance enhancement.[213] Intercalating Ti$_3$C$_2$T$_x$ into GO nanosheets, on the other hand, was able to prevent the formation of nonselective channels and/or pinholes in MXene-based nanolaminates, resulting in higher rejection rates towards organic dye and salt solutions.[214]

3.3.2.2 Supported lipid bilayer membranes. To demonstrate the superb transport properties of biological nanochannels, many research studies have attempted to incorporate biological and biomimetic channels into supported lipid bilayer membranes (SLBMs). This type of membrane structure originated from the conceptual design in biological cellular membranes whereby lipid bilayers encapsulating biological channels regulate the selective transport of water over solutes. First, the nanochannels are encapsulated into synthetic lipid bilayers *via* self-assembly, and thereafter the channel-embedded liposomes are then ruptured on the top of a support membrane (Fig. 13a). The underneath support membrane is typically functionalized with a desired charge to anchor the lipid bilayer *via* electrostatic attraction, and subsequently a hydraulic pressure is applied to ensure a complete rupturing process and liposome fusion (Fig. 13a).[53,72] Synthetic lipids are typically used to encapsulate the water channels, whereas the underlying support membranes are typically of ultrafiltration (UF) or NF type (Fig. 13b and c). Besides the vesicle rupture method, other methods to fabricate SLBMs include: (1) spin-coating of the lipid bilayers onto NF membranes and (2) engineering of the lipid and support membrane's surface chemistries such that the channel-containing bilayers can be spontaneously fused onto the support membrane *via* attractive forces.[67,215,216] However, the thickness and chemistry of the coating need to be carefully fine-tuned because the additional coating usually decreases the overall permeability of the membrane.

In the fabrication of SLBMs, it is fundamental that the chemistry of the nanochannel outer surface is compatible with that of the lipid environment such that it can readily insert and self-align within the lipid bilayer. Furthermore, the nanochannel length must be fairly similar to the thickness of the lipid bilayer. As illustrated in Fig. 13d, the nanochannel cannot be shorter than the thickness of the hydrophobic part of the lipid bilayer ($\sim$3.0–3.5 nm), else the channel end will not be opened to the feed solution.[115] For some biomimetic channels such as pillar[5]arenes, researchers have outlined the possibility of attaching side chains to the macrocycle backbones to ensure that the channel spans the bilayer or to modulate ion transport *via* charge effects (Fig. 13e).[114,217] An intriguing point to note for SLBMs incorporating dimeric channels is that the membrane structure might be different from the ideal scenario where channels are aligned parallel to the bilayer, assuming that hydrogen bonding is strong enough to hold the dimers in a stable state.[110] There is a possibility that the adjacent dimers might stack up to form a toroidal structure (Fig. 13f), which can provide an additional water transport pathway through the membrane, on top of the water wire in the dimeric pillar[5]arene channel.[116] Another study has also hypothesized that the permeability of biomimetic dipeptide channels can be affected by the lateral stress and strain forces on the lipid membrane.[117] It is obvious that the assimilation of water channels into membranes can induce structural changes in the lipid bilayer and the consequential water transport pathway through the latter. We recommend future studies to resolve the intricate interplay between channels and the lipid bilayer because the

4564 | Chem. Soc. Rev., 2022, 51, 4537–4582

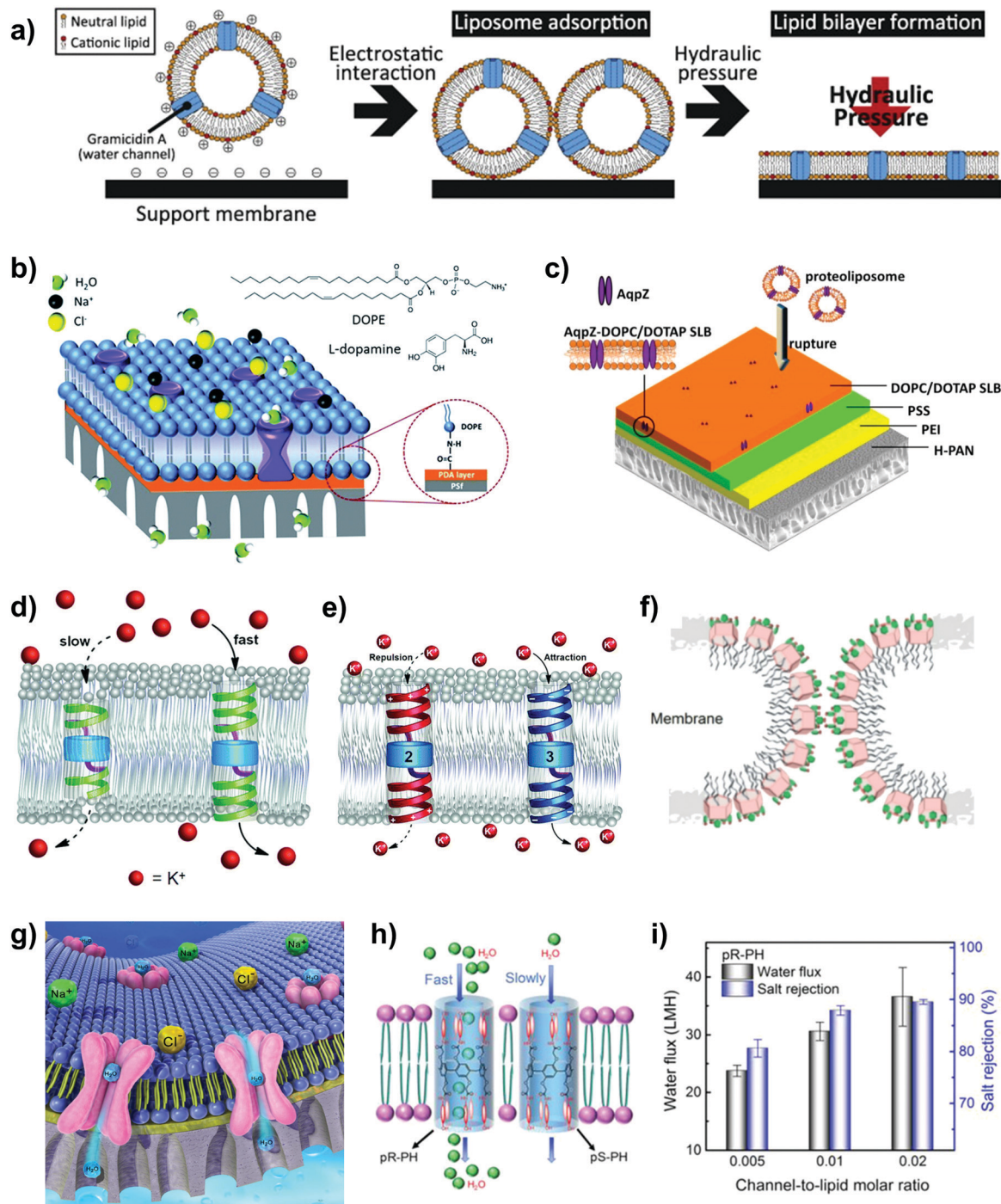This journal is © The Royal Society of Chemistry 2022

Fig. 13 (a) The schematic illustration of an SLBM incorporating gA water channels. Electrostatic attractions are needed to anchor the liposomes and a hydraulic pressure is applied in the liposome rupturing process. Reproduced from ref. 72 with permission from Elsevier, copyright 2015. (b) An illustration of an SLBM incorporating AQP-Z channels. The SLBM is formed on top of the polysulfone membrane coated with a polydopamine layer. Reproduced from ref. 215 with permission from Royal Society of Chemistry, copyright 2015. (c) The different layers of an SLBM membrane formed via layer-by-layer deposition of AQP proteoliposomes. Reproduced from ref. 216 with permission from American Chemical Society, copyright 2015. (d) A schematic illustration of water channels with different lengths in the lipid bilayer. Reproduced from ref. 217 with permission from Royal Society of Chemistry, copyright 2017. (e) A schematic illustration of water channels with different end-group charges in the lipid bilayer. Reproduced from ref. 114 with permission from Royal Society of Chemistry, copyright 2020. (f) The ideal schematic illustration of a toroidal pore in a bilayer membrane. Reproduced from ref. 116 with permission from Wiley-VCH, copyright 2020. (g) An illustration of the selective transport of water over monovalent ions in an AQP-based SLBM membrane. Reproduced from ref. 215 with permission from Royal Society of Chemistry, copyright 2015. (h) A schematic comparison between the fast and slow water transport across the pR-PH and the pS-PH channels, respectively, in a pillar[5]arene-based SLBM. (i) The water flux and salt rejection of SLBMs with the pR-PH at different channel-to-lipid molar ratios (tested with 100 ppm Na_2SO_4 as feed, under 1 bar applied pressure). Panels (h) and (i) reproduced from ref. 53 with permission from Wiley-VCH, copyright 2019.

permselectivity of such unique membrane designs remains to be resolved by experimental studies.

Overall, the most prominent advantage of the SLBM design is the ability to exploit the transport properties of the nano-channels because water is directly funnelled through the nano-channels in the bilayer (Fig. 13g and h). To date, various types of SLBMs incorporating biological and biomimetic channels (e.g. AQPs,[215,216] gA,[72] pillar[5]arenes[53]) have shown success in fabricating next-generation membranes with enhanced perme-ability (∼3–5 times higher than that of the control membrane) at a fairly similar selectivity (Fig. 13i). However, the funda-mental downside of the SLBM design is the inability to achieve complete coverage and the subsequent salt leakages through the nanoscale defects will compromise the membrane selectivity. The active area of membranes fabricated in the SLBM design is also typically very small (0.07–0.096 cm^2)[67] and the testing conditions are very mild for the purpose of proof-of-concept (applied pressures ∼1–4 bar, salt concentrations of ∼100–1000 ppm).[53,216] Thus, the SLBM design is mainly for pre-liminary investigations but its inherent structure lacks the mechanical robustness and practicality for large-scale indus-trial fabrication. Also, the chemical stability of lipid bilayers is another issue because while they maintain their functionality well, they are known to be not stable in non-aqueous environ-ments, given their tendency to undergo oxidative degradation within hours.

3.3.2.3 Supported block copolymer membranes. As an alterna-tive to the SLBM design, biological and biomimetic nano-channels can be incorporated into polymer matrices and the latter subsequently deposited onto an underlying substrate to form supported block copolymer membranes (SBCMs).[218,219] First, the nanochannels are reconstituted into 2D amphiphilic block copolymer sheets *via* self-assembly using the dialysis approach. In this method, the nanochannels, block copolymers and detergents are mixed (Fig. 14a), and thereafter high concentration detergents are slowly removed from the ternary mixture in order to initiate self-assembly and control the assembly kinetics of the nanochannels and block copolymers.[109] The second step would involve the stacking of the crystalline planar sheets (Fig. 14b) onto porous support membranes *via* layer-by-layer (LbL) deposition to synthesize the membrane selective layer (Fig. 14c–e). The fundamental idea here is to lay down layers of alternately charged sheets and polyelectrolytes that attach *via* electrostatic attractions (Fig. 14f). Thus, the underlying support membrane and block copolymer are usually first ionized or functionalized to a desired charge prior to the LbL and pressure-assisted filtration process. A total of 3–5 cycles of deposition are typically needed to ensure complete coverage of the support, and thereafter the membranes are incubated for ∼12 h to ensure that the 2D nanosheets are chemically cross-linked.[109]

The SBCM design can fully capitalize on the nanochannel properties by forming uniform sub-nanometer sized pores, which is manifested by a precise molecular weight cutoff (MWCO) or sharp rejection profile of the membrane (Fig. 14g and h).[109]

Besides being more mechanically stable than lipids, the use of block copolymers offers the possibility of customizing the polymer, terminal functional groups and membrane thickness, thereby adding another degree of freedom to the membrane fabrication process. The ideal membrane must be thin and defect-free with flows directed through the pores of the nano-channels. However, empirical evidence suggests that defects can be present (due to insufficient coverage) such that the feed solution can flow laterally through the interlayers of the membrane selective layer as well as the gaps between the block copolymer and nanochannels.[73,81] To minimize the presence of defects, a typical strategy is to deposit more layers or perform post-treatment (e.g. chemical cross-linking) to seal the defects and enhance the integrity of the selective layer. This will increase the robustness and stability of the membranes for filtration and also protect the nanochannels from the harsh conditions under filtration. However, this is done at the expense of membrane permeability because of the additional resistance posed by the auxiliary layers.

The main drawback of the dialysis approach is its time consuming nature (i.e., it takes about 5–7 days to complete), rendering the SBCM design unfeasible from an industrial scale-up point of view. As an alternative to the dialysis method, Tu et al. explored the feasibility of a rapid 2 h organic solvent extraction method to optimize the packing density of protein channels into the polymeric matrix, whereby the nanochannels and block copolymers are mixed in a solvent mixture and thereafter the solvents are evaporated to form ultrathin films on a glass surface.[81] The films are then rehydrated using buffer solutions and deposited onto the support membrane to synthe-size a membrane selective layer (Fig. 14e). This method has shown preliminary success in fabricating SBCMs with tunable pore sizes through the proper selection of nanochannels, but its applicability for desalination applications remains to be elucidated (because the nanochannels used cannot reject monovalent salts).[81] Therefore, future studies should explore the feasibility of the solvent extraction approach to fabri-cate SBCMs incorporating nanochannels that are of different chemistries and pore sizes for various types of molecular separation.

In short, the purpose of incorporating water nanochannels in the form of SLBM or SBCM designs demonstrated the possibility of fabricating next-generation membranes with enhanced per-meability and narrower pore size distribution, of which the latter can lead to higher membrane selectivity using nanochannels with sub-nanometer sized pores. One important consideration is the chemical compatibility between the nanochannel and lipid bilayer/block copolymer matrix, because the latter determines the channel insertion efficiency and defect formation propensity. The presence of nanoscale defects and gaps in and between the selective layers would likely remain a persistent challenge, which necessitates methods to minimize interfacial defects such as the use of compatibilizers that are commonly employed in gas separation membranes.[154]

3.3.3 Thin-film nanocomposite membranes. While the SLBM and SBCM designs have shown promise in the development of

4566 | *Chem. Soc. Rev.*, 2022, **51**, 4537–4582

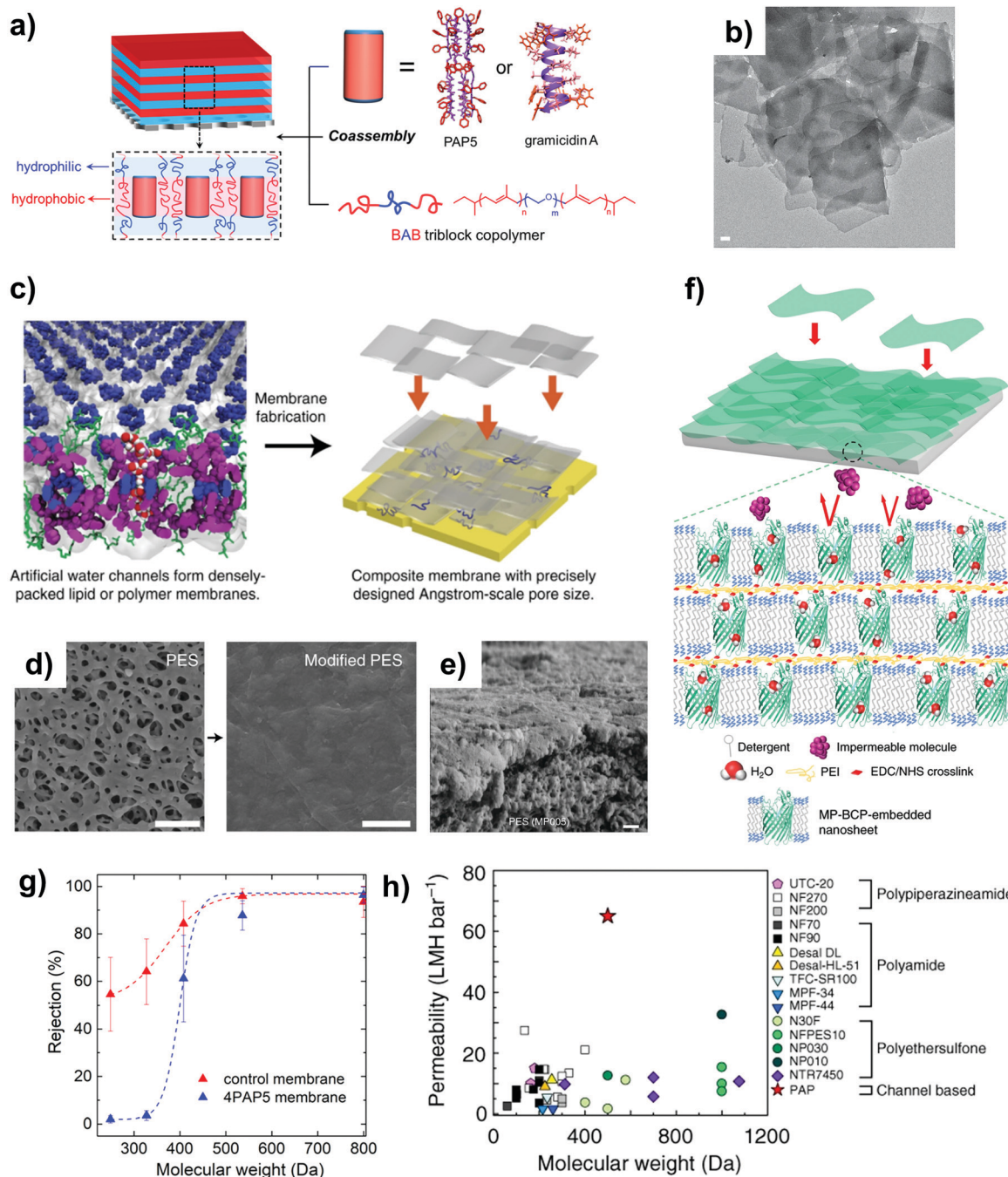This journal is © The Royal Society of Chemistry 2022

Fig. 14 (a) A schematic summary of the formation of BCMs incorporating block copolymers and water channels *via* the self-assembly process. (b) A negative-stain TEM image of OmpF nanosheets prepared *via* the dialysis approach. Scale bar: 100 nm. (c) The formation of SBCMs *via* two steps: (1) the self-assembly of water channels into polymer membrane sheets and (2) the deposition of the sheets onto a support membrane to form SBCMs with designed pore sizes. (d) SEM images outlining the complete deposition of 2D nanosheets onto a support membrane after 3–4 cycles of LbL deposition. Scale bar: 1 μm. (e) A cross-sectional TEM image showcasing an OmpF nanosheet deposited onto a membrane substrate (the thickness is ~232 nm). (f) Schematic illustration of the layer-by-layer to form SBCMs incorporating membrane protein channels. (g) The rejection profile of a lamellar membrane incorporating peptide-appended pillar[5]arene water channels, determined by a range of small molecular weight dyes. The control membrane does not contain any water channels. (h) A comparison of the performance of membranes incorporating peptide-appended pillar[5]arene water channels with commercial NF membranes in terms of the permeability and molecular weight cutoff. Panels (a) and (g) reproduced from ref. 218 with permission from American Chemical Society, copyright 2019. Panels (b), (e) and (f) reproduced from ref. 81 with permission from Springer Nature, copyright 2020. Panels (c), (d) and (h) reproduced from ref. 109 with permission from Springer Nature, copyright 2018.

next-generation membranes, they are mostly tested under mild and ideal lab-scale conditions to demonstrate the nanochannel transport properties as well as for proof-of-concept. For water desalination and purification purposes, the conditions are much

This journal is © The Royal Society of Chemistry 2022

Chem. Soc. Rev., 2022, **51**, 4537–4582 | **4567**

harsher and thus three additional criteria need to be considered for the membrane design: (1) mechanical robustness to endure high pressures (up to 80 bar) and high velocity crossflow rates, (2) ability to demonstrate scalable defect-free selective layers and (3) ability to withstand biological and chemical degradation.[10,220] The TFC design is currently the gold standard for NF and RO membranes, in which the polyamide selective layer is synthesized *via* an IP reaction on the top of a porous support membrane.[221,222] IP is based on a Schotten–Baumann reaction mechanism that capitalizes on the fast and irreversible reaction between an amine and acyl chloride dissolved in aqueous and organic phases, respectively, to produce a thin polyamide film as the selective layer (150–300 nm).[39] As an extension of the TFC design, the TFN design is adopted for enhancing membrane performances, owing to its relatively easy implementation and, most importantly, its ability to fulfil the three aforementioned criteria. In this design, a small amount of nanochannel is added into the polyamide matrix to confer additional characteristics to the selective layer. In general, there are three overarching methods to incorporate nanochannels into the selective layer of TFN membranes: (1) vesicle- or polymersome-based, (2) direct dispersion into IP monomeric solutions and (3) coating of an interlayer prior to IP.

The first method is adopted when incorporating biological channels (*e.g.* AQPs),[63,64,66,223] or unimolecular channels (*e.g.* pillar[5]arenes),[54] or when the channels are extremely small (<5 nm) and thus unstable when standalone (*i.e.*, this method can preserve the structure and functionality of the nanochannels). In this method, the nanochannels are first reconstituted into amphiphilic liposomes or polymersomes, and the eventual solutions are subsequently blended in the aqueous amine phase. During IP, the reaction between the amine and acyl chloride will encapsulate the channel-containing liposomes or polymersomes into the membrane's selective layer. This approach has led to the development of membranes with enhanced permeability (∼10–50% increase) for a wide range of applications, including NF, FO and brackish water RO (BWRO) and SWRO (refer to Table 3 for details). The enhanced

permeability (at a similar salt rejection) is postulated to arise from the preferential water transport pathway through the channel-containing liposomes (Fig. 15a), but no work has so far provided direct evidence of water transport through these nanochannels. The nanochannels are also rarely observed in cross-sectional transmission electron microscopy (TEM) images due to their small size (∼3 nm). To date, only a recent study has provided stronger confirmation of the presence of liposomes in the TFN's selective layer (Fig. 15b) using scanning transmission electron microscopy-energy dispersive X-ray spectroscopy (STEM-EDX) characterization.[54]

In the second approach, nanochannels are incorporated directly into the polyamide selective layer as filler materials without the use of any lipid vesicles (Fig. 15(c–g)). This method has been used to incorporate a multitude of synthetic channels such as carbon nanomaterials, COFs, cucurbit[6]urils, MOFs and MXenes and zeolites (refer to Table 4 for specific examples). Prior to the IP process, the nanochannels are sonicated to ensure complete dispersion and/or exfoliation in the IP monomeric solution (in either an aqueous or organic phase), which is a prerequisite for achieving a homogeneous distribution of fillers in the polyamide layer for minimizing defect formation.[22] The concentration is usually low (0.005–0.02 wt/v%) to minimize material agglomeration, which can cause serious defect formation in the selective layer.[230,231] The direct dispersion method is also more straightforward when compared with the vesicle method and has shown promising results both in academia and in industrial settings. For example, some industrial patents have reported the development of TFN seawater desalination membranes (incorporating CNTs, GO, MOFs or zeolites), showing positive enhancement in permeability (∼15–30%).[10] More importantly, this approach has shown success in enhancing permeability while achieving high salt rejections (99.0–99.9%) even under harsh SWRO conditions (feed salinity ∼32 000 ppm NaCl with an applied pressure of 55 bar). Some studies have provided imaging evidence of nanochannels embedded in the polyamide layer using TEM

Table 3 Summary of recent studies on the fabrication of TFN membranes incorporating water nanochannels in the form of lipid vesicles (liposomes) or polymersomes. The separation performances are reported in the form of water flux (J) and solute rejection for pressure-driven membranes (RO and NF). For osmotically driven membranes (*e.g.* FO), the performance is reported in terms of J and the specific reverse solute flux, *i.e.*, the ratio of salt reverse flux (J_s) to J. The testing conditions are reported in terms of the feed solution characteristics and applied pressure (ΔP)

Water channel	Membrane application	Separation performance: flux (L m^{-2} h^{-1}); selectivity[a]	Testing conditions: feed (ΔP)	Ref. (year)
Biological nanochannels				
AQPs	BWRO	39.4; 97.2% NaCl rejection	584 ppm NaCl (10 bar)	64 (2016)
AQPs	BWRO	31.9; 93.5% NaCl rejection	500 ppm NaCl (5 bar)	223 (2020)
AQPs	BWRO	17; 94.7% NaCl rejection	500 ppm NaCl (2 bar)	224 (2022)
AQPs	SWRO	20; 99% NaCl rejection	32 000 ppm NaCl (55 bar)	63 (2019)
AQPs	SWRO	47; 99.5% salt rejection	Real seawater (50 bar)	225 (2022)
AQPs	FO (AL-FS)[b]	49.1; J_s/J: 0.1 g L^{-1}	Draw solution: 1 M NaCl	226 (2017)
AQPs	FO (AL-FS)[b]	9.4; J_s/J: 0.16 g L^{-1}	Draw solution: 0.5 M NaCl	66 (2021)
Biomimetic nanochannels				
(pR)-pillar[5]arenes	BWRO	85; 98.2% NaCl rejection	2000 ppm NaCl (15.5 bar)	54 (2021)

[a] Some BWRO and NF experimental studies reported the permeability or pure water permeability (normalized flux per pressure) instead. For standardization purposes, they were converted to (J) by multiplying with ΔP, assuming a relatively low osmotic pressure. [b] FO operation can be achieved in two orientations: the active layer (AL) facing the feed solution (FS) or draw solution (DS), *i.e.*, AL-FS or AL-DS modes, respectively, depending on the operational requirements. Readers are referred to the literature for discussions on this topic.[227]
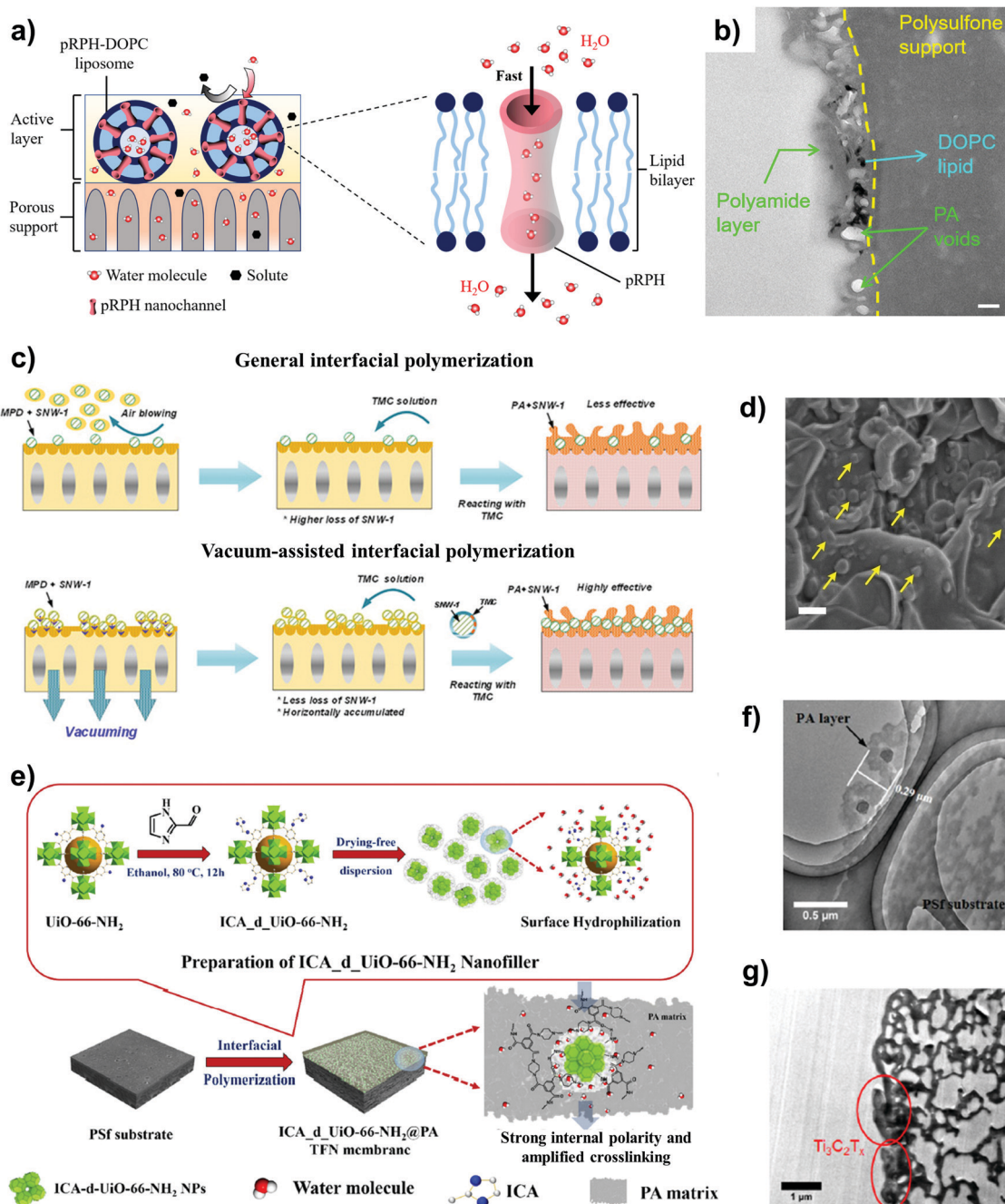
4568 | *Chem. Soc. Rev.*, 2022, **51**, 4537–4582

This journal is © The Royal Society of Chemistry 2022

Fig. 15 (a) The schematic illustration of the selective transport of water molecules over solutes across the RO membranes embedded with pRPH channel-containing liposomes. (b) Cross-sectional TEM image of the polyamide layer containing liposomes. The yellow dotted line corresponds to the boundary between the polyamide and support layers. Scale bar: 100 nm. Panels (a) and (b) reproduced from ref. 54 with permission from Elsevier, copyright 2021. (c) An illustrative comparison of the normal IP and vacuum-assisted IP, as well as the eventual location of the nanomaterials in the polyamide selective layer. (d) High magnification SEM image of nanoparticles (denoted by the yellow arrows) embedded in the leaf and valley structure of the polyamide layer (scale bar: 100 nm). Panels (c) and (d) reproduced from ref. 228 with permission from Elsevier, copyright 2020. (e) A schematic illustration of the formation of TFN membranes embedded with ICA_d_UiO-66-NH$_2$, as well as the latter's influence on the polyamide chemical structure. (f) TEM cross-sectional image outlining the successful embedment of ICA_d_UiO-66-NH$_2$ fillers onto the membrane selective layer. Panels (e) and (f) reproduced from ref. 229 with permission from Elsevier, copyright 2020. (g) TEM cross-sectional image outlining the location of MXenes in the membrane selective layer. Reproduced from ref. 230 with permission from Elsevier, copyright 2021.

cross-sectional analysis (Fig. 15f and g), and the enhanced permeability is typically hypothesized to arise from the supplementary transport pathway through the nanochannel pores.

Besides enhancing the membrane permeability, some fillers such as CNTs, MOFs and MXenes have also demonstrated success in decreasing fouling propensity, and enhancing boron

Table 4 Summary of recent studies on the fabrication of TFN membranes incorporating water nanochannels whereby the latter are dispersed into the IP monomeric solutions. The brackets (AQ) and (O) denote that the additive is incorporated in the aqueous and organic phases of the IP monomeric solutions, respectively. The separation performances are reported in the form of water flux (J), solute rejection or specific reverse solute flux depending on the membrane application (refer to Table 3 for details)

Water channel	Membrane application	Separation performance: flux (L m^{-2} h^{-1}); selectivity	Testing conditions: feed (ΔP)	Ref. (year)
Synthetic nanochannels				
Carbon dots (AQ)	NF	60; 96.4–99.0% Na$_2$SO$_4$ rejection	2000 ppm salts (6 bar)	188 (2020)
CNTs (AQ)	SWRO	29.2; 99.9% NaCl rejection	32,000 ppm NaCl (50 bar)	232 (2022)
COFs (AQ)	FO (AL-FS)	31.5; J_s/J: 0.18 g L^{-1}	Draw solution: 1 M NaCl	228 (2020)
COFs (AQ)	FO (AL-FS)	64.2; J_s/J: 0.1 g L^{-1}	Draw solution: 1 M NaCl	234 (2020)
Cucurbit[6]urils (AQ)	BWRO	62.2; 98.8% NaCl rejection	2000 ppm NaCl (15.5 bar)	235 (2020)
Graphene quantum dots (AQ)	NF	98.2; 97.4% Na$_2$SO$_4$ rejection	1000 ppm salts (10 bar)	236 (2021)
MXenes (AQ)	BWRO	40.5; 98.5% NaCl rejection	2000 ppm NaCl (16 bar)	231 (2020)
MXenes (AQ)	NF	14.1; 97.6% Na$_2$SO$_4$ rejection	2000 ppm salts (3 bar)	230 (2021)
MXenes (AQ)	NF	83.6; 65.7% Na$_2$SO$_4$ rejection	1000 ppm salts (4 bar)	237 (2022)
Zwitterionic MOFs (O)	BWRO	40.2; 98.6% Na$_2$SO$_4$ rejection	2000 ppm NaCl (15 bar)	233 (2021)
MOFs (AQ)	NF	94; 97.4% Na$_2$SO$_4$ rejection	1000 ppm salts (10 bar)	229 (2020)
MOFs (O)	SWRO	38; 98.8% NaCl rejection	32 000 ppm NaCl (50 bar)	238 (2021)
MOFs (O)	SWRO	61.3; 99.3% NaCl rejection	32 000 ppm NaCl (55 bar)	239 (2019)

selectivity and chlorine resistance, all of which are crucial traits needed for RO membranes.[10,229,232,233]

For some synthetic nanochannels like MXenes or CNTs, nanomaterials can be created as an interlayer between the support and polyamide layer (Fig. 16a and b). For this third approach, the nanochannels are first deposited on the support membrane (typically in the form of nanosheets) prior to the IP process.[221,240] It is typically used to incorporate biomimetic and synthetic nanochannels such as I-quartets, CNTs (Fig. 16c and 16d), COFs, GO, MOFs, MoS$_2$ and MXenes for NF, RO and FO membranes (refer to Table 5 for specific examples). Vacuum filtration is the most common method used thus far to deposit nanochannels onto support membranes, but a major drawback is that the vacuum filtration unit often limits the scalability of this method of IP with the membrane size typically found to be <20 cm^2.[241] In short, vacuum filtration is a viable approach for the proof-of-concept of uniform nanochannel deposition, but, from an industrial perspective, it lacks the scalable potential to initiate large-area TFN membrane fabrication.

In the past five years, newer approaches for channel deposition have emerged, such as brush-coating, spray-coating and inkjet printing (Fig. 16c).[242–244] Overall, as compared to the second approach, of which the channels are blended in the IP solutions, the third approach of creating an interlayer has two major advantages: (1) the ability to achieve a uniform distribution of nanochannels and (2) the ability to achieve high channel loadings without any severe aggregation of nanochannels. Overall, empirical evidence suggests that the interlayer method can indeed enhance permselectivity with the strong potential of overcoming the upper-bound limit of TFC membranes (Fig. 16e and f).[240] Also, instead of functioning as water nanochannels, it is worth highlighting that some nanomaterials are embedded as sacrificial layers prior to IP, with the end goal of modulating the IP reaction for altering the nanoscale morphology of the eventual polyamide layer.[245] In this case, the nanomaterial is removed after the IP process *via* dissolution in water (Fig. 16d).

In the TFN membrane design, the polyamide layer acts as the primary selective layer responsible for salt rejection and protects the nanochannels from direct exposure to chemical and physical degrading elements (Fig. 16g). Hence, defect formation and stability issues can be minimized if the nanochannels are fully sandwiched in the polyamide layer without any protrusions (Fig. 16h), which is the reason why TFN membranes are suitable for desalination applications. However, it must be highlighted that the TFN design cannot lead to ground-breaking performance enhancement because the overall membrane permeability is still dictated by the dense polyamide matrix, and that there is a limit on the amount of nanochannels that can be encapsulated in the polyamide layer to ensure that the latter is defect-free.[10] In a bid to elucidate the potential of the membranes for practical desalination operation, recent studies have examined the stability of these nanochannel-embedded membranes to typical cleaning agents such as acids, bases, solvents and chlorinated oxidants. The nanochannels studied include AQPs,[64,256,257] CNTs,[258] COFs,[248,259] GO[260–262] and MOFs.[263] For example, a study outlined the stability of AQP-based RO membranes by subjecting them to 5 cycles of chemical cleaning and it was shown that the water flux and salt rejection of the biomimetic membrane remained fairly consistent throughout the long-term test (duration of 100 days).[64]

Also, empirical evidence suggests that some nanochannels can also take part in the IP reaction and alter the free volume, cross-linking degree and height of the selective layer, thereby indirectly affecting the membrane permeability.[264] Our key message here is that the permeability enhancement of TFN membranes might not be solely attributed to the water transport across nanochannels (that is the ideal scenario), because the nanochannel itself might have affected the physicochemical and structural properties of the polyamide selective layer formed. We recommend that future studies examine in greater detail the interplay between IP and nanochannels' chemistry to elucidate other possibilities for permeability enhancement. Lastly, although TFN membranes incorporating channel-containing
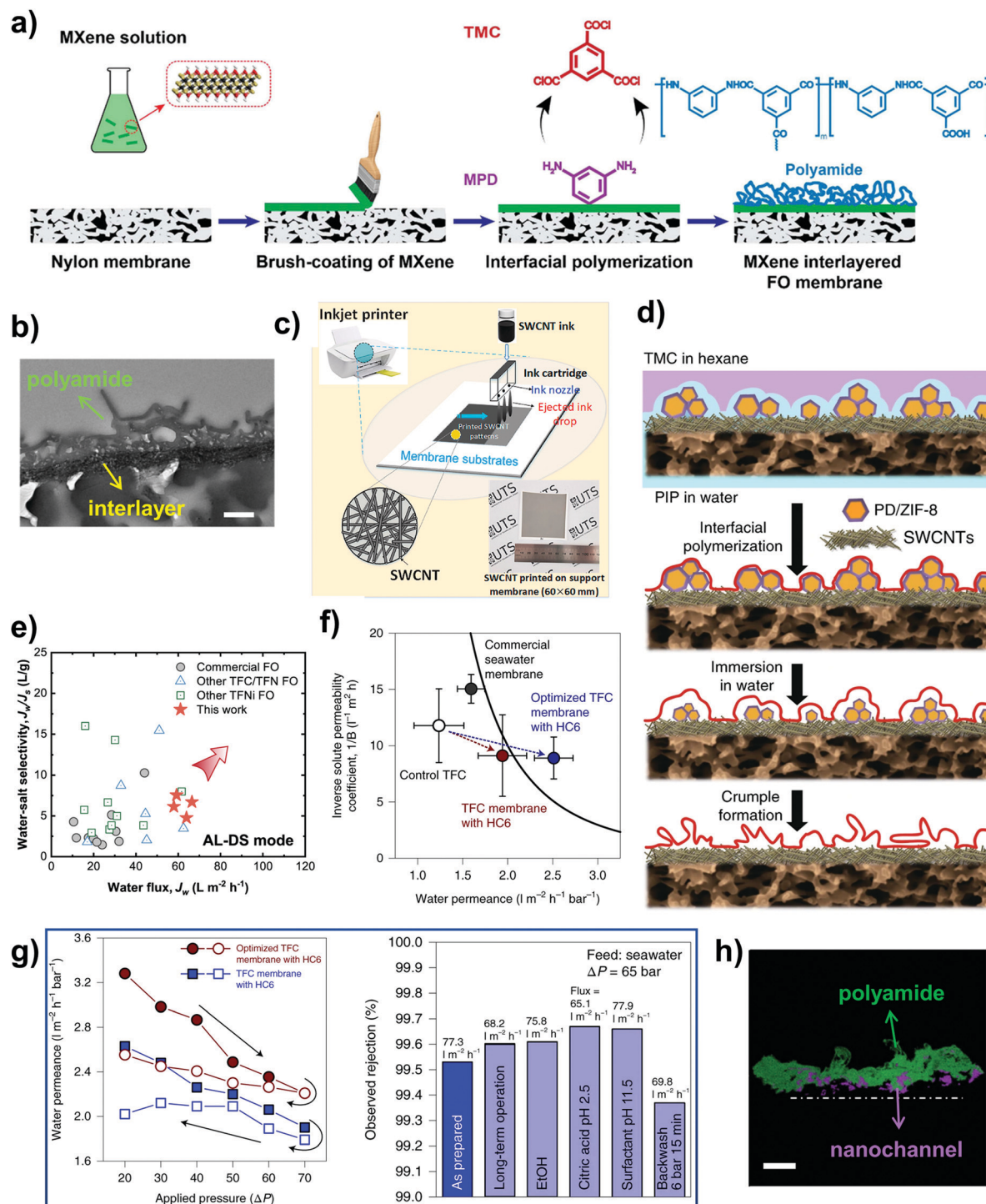
4570 | *Chem. Soc. Rev.*, 2022, **51**, 4537–4582

This journal is © The Royal Society of Chemistry 2022

Fig. 16 (a) A schematic illustration of a MXene interlayered membrane using the brush-coating methodology to deposit MXene sheets prior to IP. Reproduced from ref. 242 with permission from American Chemical Society, copyright 2020. (b) Cross-sectional TEM image of the TFN membrane outlining the polyamide selective layer that sits on top on the interlayer. Scale bar: 200 nm. (c) A schematic summary of deposition of CNTs onto a support membrane *via* an inkjet printing methodology. Reproduced from ref. 243 with permission from Elsevier, copyright 2021. (d) The evolution process outlining the fabrication of a nanomaterial-induced crumpled polyamide selective layer. Reproduced from ref. 245 with permission from Springer Nature, copyright 2018. (e) A comparison of the water flux and selectivity of TFN membranes with interlayers (TFNi) with commercial and other TFN FO membranes in AL-DS mode, with the red arrow outlining better performance. Panels (b) and (e) reproduced from ref. 241 with permission from American Chemical Society, copyright 2021. (f) A comparison of the permeability and selectivity of an optimized biomimetic membrane with respect to control the TFC membrane and commercial SWRO membrane. The black solid curve denotes the upper bound curve of TFC membranes. (g) Left: An example of the inability of membranes to regain their original permeability values after being subjected to high pressure compaction tests in SWRO, right: biomimetic desalination membrane performances when subjected to various chemical and physical tests (testing conditions: ΔP = 65 bar and 35 000 ppm NaCl as feed solution). (h) Screenshot of the biomimetic membrane tomography at a fixed angle in which the polyamide layer and I-quartet channels are marked in green and purple, respectively. Scale bar: 200 nm. Panels (f)–(h) reproduced from ref. 246 with permission from Springer Nature, copyright 2020.

This journal is © The Royal Society of Chemistry 2022

Chem. Soc. Rev., 2022, **51**, 4537–4582 | **4571**

Table 5 Summary of recent studies on the fabrication of TFN membranes incorporating water nanochannels whereby the latter are pre-deposited onto the membrane prior to IP. The separation performances are reported in the form of water flux (J), solute rejection or specific reverse solute flux depending on the membrane application (refer to Table 3 for details)

Water channel	Channel deposition method	Membrane application	Separation performance: flux (L m^{-2} h^{-1}); selectivity	Testing conditions: feed (ΔP)	Ref. (year)
Biomimetic nanochannels					
I-quartets	Pouring	BWRO	35; 97.5–99.3% observed rejection	Real tap water (6 bar)	247 (2021)
I-quartets	Pouring	BWRO	59.7; 99.5% observed rejection	5844 ppm NaCl (15.5 bar)	22 (2021)
I-quartets	Pouring	SWRO	75; 99.5% NaCl rejection	35 000 ppm NaCl (65 bar)	246 (2020)
Synthetic nanochannels					
CNTs	Inkjet printing	NF	72.8; 97.9% Na$_2$SO$_4$ rejection	1000 ppm salts (4 bar)	243 (2021)
CNTs and MOFs	Vacuum filtration	NF	214; >95% Na$_2$SO$_4$ rejection	1000 ppm Na$_2$SO$_4$ (4 bar)	245 (2018)
COFs	Immersion	NF	43.3; 96.6% Na$_2$SO$_4$ rejection	2000 ppm salts (5 bar)	248 (2021)
COFs	Coating	BWRO	25.2; 99.2% NaCl rejection	2000 ppm NaCl (15 bar)	249 (2020)
GO	Immersion	NF	158; 99.7% Na$_2$SO$_4$ rejection	2000 ppm Na$_2$SO$_4$ (10 bar)	250 (2021)
GO and CNTs	Vacuum filtration	FO (AL-DS)	26.7; J_s/J: 0.14 g L^{-1}	Draw solution: 0.5–1.5 M NaCl	251 (2018)
MXenes	Brush-coating	FO (AL-DS)	31.8; J_s/J: 0.27 g L^{-1}	Draw solution: 2 M NaCl	242 (2020)
MXenes	Brush-coating	NF	111.2; 99.9% Na$_2$SO$_4$ rejection	1000 ppm salts (4 bar)	252 (2021)
MXenes and CNTs	Vacuum filtration	FO (AL-DS)	63.9; J_s/J: 0.21 g L^{-1}	Draw solution: 1 M NaCl	241 (2021)
MOFs	Spray-coating	SWRO	40; 99.2% NaCl rejection	32,000 ppm NaCl (50 bar)	253 (2020)
MOFs	Immersion	NF	48; 91% SO$_4$$^{2-}$ rejection	500 ppm salts (5 bar)	254 (2021)
MoS$_2$	Vacuum filtration	NF	120; 98.8% Na$_2$SO$_4$ rejection	10 mM salts (8 bar)	255 (2021)

vesicles have shown success in fabricating membranes with better permselectivity, we would like to point out that the insertion efficiency (that is, the actual amount of channels reconstituted into the vesicle divided by the theoretical insertion number) of channels as well as the alignment in the polyamide layer are crucial factors that still cannot be precisely controlled.

4. Challenges and future perspectives: the way forward

4.1 Biological, biomimetic *versus* synthetic channels for next-generation membranes

In this section, we seek to discuss the strengths and weaknesses of the three overarching types of nanochannels using seven criteria, which are shortlisted *via* a comparison of their structural characteristics, synthesis, easy functionalization (see Table 2 for some representative examples) and the fabrication methods that support specific nanochannels. Namely, the seven criteria are processability, tunability, versatility, stability, scalability, performance and cost, which are further explained in the caption to Fig. 17. At present, only a few biomimetic or synthetic channels have the ability to attain the high water permeability observed in biological channel AQPs.[7] However, the major downside of biological channels is their low structural stability, as well as the need to use detergent during the self-assembly process, which makes it difficult to realize on a large industrial scale. The purity of membrane proteins is another issue that has yet to be considered. From a membrane fabrication point of view, there is also the fundamental challenge of limited protein insertion into lipid bilayers or block copolymer matrices, which in turn results in inconsistent or lower than expected performance enhancement.
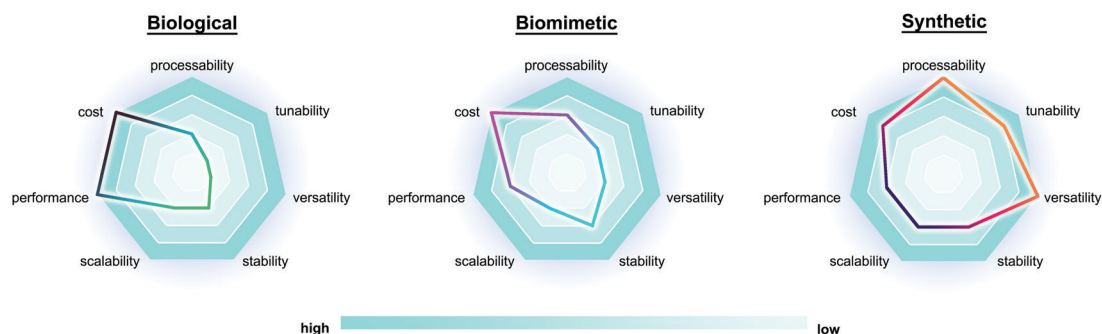

Fig. 17 A comparison of the strengths and weaknesses of the three overarching types of water nanochannels presented in the form of a spider diagram. The criteria for comparison are as follows. (1) Processability, which refers to the ease of being processed during synthesis (*e.g.* duration of synthesis, as well as the chemicals and energy needed).[265] (2) Tunability, which refers to the ability to be adjusted or adapted for target applications. (3) Versatility, which is manifested by the channels' adaptability and use in different membrane designs. (4) Stability, which refers to the chemical and mechanical steadiness of the channel itself as well as within the membrane matrix in the long-term.[266] (5) Scalability, which refers to the ability to be scaled up for practical use (*e.g.* mass production). (6) Performance, which refers to the channel performance (*e.g.* water permeability) as well as the eventual nanochannel-enabled membrane separation properties (water flux and selectivity). (7) Production costs.

On the other hand, the major advantages of biomimetic and synthetic channels are their higher processability and tunability as evidenced by their richer chemistries, which allow them to attune to a wider choice of solvent systems and an array of chemical functionalizations. High versatility is demonstrated in the ability of the nanochannels to adopt other membrane designs such as nanolaminated and freestanding membranes, apart from the more practical TFN design, which has the widest applicability to almost all nanochannels reviewed thus far.[10] In particular, we would like to emphasize 2D materials and their versatility to take on different membrane designs as already highlighted in Fig. 11(a). The 2D materials, owing to their high-aspect-ratios and lateral dimensions, are well-suited to form nanochannels with a strong continuity required for defect-free film formation. Furthermore, as nanosheets of 2D materials restack together, the interlayer spacings between nanosheets are also well-defined and tunable down to ångström-scale precision. For these reasons, 2D materials can be processed into nearly every design used by membranes for desalination and water purification and thus are deemed to have the greatest versatility.

Next, lowering the barrier for implementing a particular nanochannel-enabled membrane design is directly tied to its scalability potential. We have to stress that the TFN design again has the highest scaled-up potential as the fabrication process is conceptually similar to the already mature IP technology. In this regard, biological channels are not as ready to be scaled-up for real-world application, owing to the yet-to-be-resolved channel/polymer incompatibility that leads to the formation of a detrimental non-ideal interfacial morphology. On this note, the rich chemistry of synthetic channels can enable a multitude of functionalizations to optimize compatibility with the polyamide matrix of the selective layer, thereby minimizing defect formation. For the TFN design, this is crucial because a small amount of defects can drastically increase and enlarge the solute passage, which subsequently compromise the membrane selectivity.[5,10,267] In addition, some synthetic nanochannels exhibit inherent properties that increase the anti-fouling properties of nanochannel-enabled membranes by altering the chemistry of the membrane surface to weaken membrane–foulant interactions (discussed in Section 4.3). Thus far, one example of nanochannel-embedded membranes that have been commercialized is Aquaporin Inside® membrane products.[268] However, the mainstream RO membranes are still dominated by the TFC membranes manufactured by mature key players such as DuPont FilmTec (USA), Hydranautics (USA) and Toray Industries (Japan).[10]

With respect to stability and cost, synthetic nanochannels have a slight edge over the biological and biomimetic counterparts, considering that CNTs and a bulk of graphene-based materials are chemically inert as driven by the sp^2 hybridized carbon atoms that form strongly conjugated systems. Hence, nanochannels of carbon nanomaterials are mostly stable under acidic and alkaline conditions.[269] And, owing to their good mechanical properties,[270] these channels have higher capacity to maintain mechanical stability under the high transmembrane pressures required for the RO and NF processes. Also, carbon nanomaterials have a stronger presence in today's commercial market.[85] As such, in terms of cost, they show more competitive advantages over other nanochannels as discussed in this review.

4.2 Rational design of water nanochannels down to the molecular level

For the sole purpose of desalination, where drinking water is the expected final outcome, near absolute solute rejection is more often than not unnecessary as remineralization at downstream would be needed to produce drinking water and it is not cost-effective – and certainly does not make sense – for saline water to undergo expensive water treatment only to be remineralized again. Recently, there has been a new thrust in developing selective membranes with the capacity to carry out single solute rejection from saline water.[271–273] The rationale is to realize high discrimination between different solutes such that membranes can selectively separate undesired solutes, while allowing essential solutes to pass through, so as to avoid generating a huge osmotic gradient across membranes. In this way, membrane separation can occur at lower transmembrane pressures and can be carried out more sustainably. From the perspective of water nanochannels, there is certainly huge potential for compelling nanochannels to contribute towards this demand for solute–solute (or ion–ion) selectivity. To do so, it is essential to first understand the mechanism of solute or ion transport through the nanochannels. According to the transition state theory, a solute will need to pass through a series of barriers at the pore entrance and within the channel pore during the transportation process.[274,275] As illustrated in Fig. 18a, when an ion enters the channel pore that is smaller than its hydrated ion, the hydrated shell needs to be removed or rearranged.[276] This phenomenon, known as the dehydration of ions, will impose the first energy barrier to the permeation of the solute, which will in turn control the ion selectivity of the water nanochannel. This means that we must acquire the technical acumen to precisely control the pore size of nanochannels such that the pores are tunable to be larger than the dehydrated ion size, while being smaller than the hydrated ion size to induce dehydration for the solute of interest.

As the ion transverses across the nanochannel, different forms of interactions such as frictional and viscous forces will further present the second energy barrier to the permeation of solute (Fig. 18b).[277] It is worth noting that these interactions are not only applicable to ions, because uncharged permeating species might exert van der Waals interaction with the nanochannel interior that is polarizable.[278] Hence, techniques that allow localized engineering of nanochannels will then enable us to exploit the difference in energy barriers for achieving specific ion–ion selectivity. For instance, decorating the opening of the nanochannel will create a gating effect, which will increase the energy barrier for the entry of undesired ions (likewise, we can also decrease the energy barrier of the desired ion).[279,280] In this sense, the rich chemistry and wide morphological structure that are intrinsic to synthetic nanochannels can offer lots of
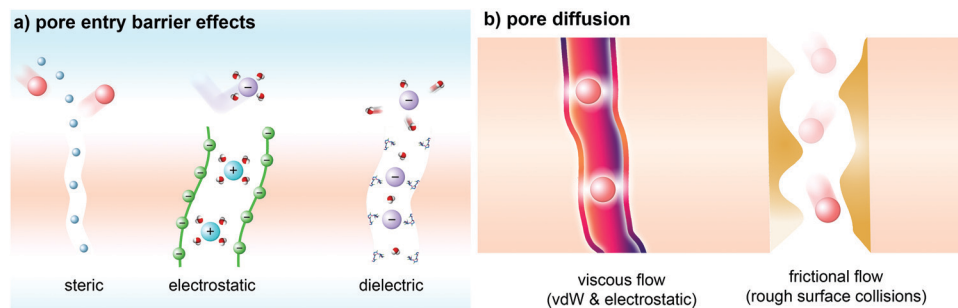
Fig. 18 Schematic illustrations of (a) pore entry barrier effects of water and ions in a water nanochannel and (b) pore diffusion mechanisms inside the water nanochannel.

opportunities to induce solute–solute selectivity. Recently, some researchers have outlined the possibility of tuning the physical dimensions (*e.g.* interlayer spacing in GO membranes as well as the diameter of CNTPs),[2,12,281,282] and the internal chemistry of nanochannels by manipulating synthesis conditions.[7,283] Leveraging atomic layer deposition (ALD) of tiny precursors (*e.g.* MoS_2 and metal oxides) to engineer and regulate the pore interior of nanochannels is one good example that has achieved preliminary success in the fields of chemical sensing, catalysis and biomolecule fractionation.[284–286] Adopting coordination chemistry to bind specific species in a host–guest complex is another example where engineering the internal of sub-nanometre channels could be initiated to induce facilitated transport of specific solutes.[287–290] We reckon these techniques can be exploited for membrane separation.

With this understanding, we now examine in greater detail how nanochannels can fit into the current landscape of developing solute-selective membranes. The main challenges in incorporating nanochannels with solute–solute selectivity are mostly similar to those already discussed in Section 3.3. However, owing to the fact that solute-selective nanochannels perform under ångström-scale precision,[18,291,292] designs such as TFN membranes with inherent chemical heterogeneity and surface roughness on the microscale are unlikely of practical use.[293] It is possible that the ångström-level effect brought about by the nanochannels be made infinitesimal against the microscale morphology of the polyamide selective layer. In this regard, membranes that exhibit atomic level tunability and homogeneously smooth surfaces such as those of freestanding and/or nanolaminated membranes (as discussed in Sections 3.3.1 and 3.3.2) have stronger potential for harnessing solute-selective nanochannels. Furthermore, there is currently a lack of understanding of solute–solute selectivity in synthetic membranes from both molecular level and spatial and temporal resolution level standpoints. This calls for stronger emphasis on molecular simulations to gain mechanistic understanding of the effectiveness of nanochannels on solute transport in polymer matrices. Only when knowledge gaps like these are closed can we put ourselves in a better position to design more compelling nanochannel-enabled membranes that can make desalination and water reuse more competitive and sustainable.

4.3 Balancing material innovation and membrane engineering

In this sub-section, our intention is to draw the critical link between nanochannel-enabled membranes and process design. From a big picture perspective, we examine the impact and actual significance of the benefits which nanochannel-enabled membranes can bring about from a system level. First and foremost, it is crucial to understand the uniqueness of membranes used for water separation. Currently, state-of-the-art TFC membranes (for NF/RO) are plagued by two major Achilles heels: permeability–selectivity tradeoff and membrane fouling.[10,294] For RO-based membranes, insufficient boron rejection and chlorine resistance further necessitate the development of nanochannel-enabled membranes to overcome these limitations. While achieving high water permeability may not seem as critical as before, membranes incorporating water nanochannels should aim to address the permeability–selectivity tradeoff by focusing on improving selectivity, especially at the far end spectrum of high permeability, to mellow the slope of the current upper-bound limit in TFC membrane performances. In particular, nanochannel-enabled membranes that show promise of outperforming TFC membranes should be scaled beyond lab-scale studies for more accurate evaluation of the potential and to identify possible translational challenges for early intervention during the membrane design stage. Otherwise, the ability of these membranes to outperform TFC "gold standard" membranes remains elusive.[5,10]

Suppose that nanochannel-enabled membranes can indeed outperform TFC membranes in terms of separation performance; it is also crucial to review what they can and cannot achieve in terms of reforming desalination technologies. For RO membrane desalination, some modelling studies have argued that the water permeability achievable by current membranes is sufficiently high because the energy consumption is already within the limits imposed by the system's thermodynamics and mass transfer. According to RO system-level modelling studies, the upper limits for the water permeability of spiral-wound SWRO and BWRO membranes currently stand at ~ 3 and 8–12 L m^{-2} h^{-1} bar^{-1}, respectively (at a salt rejection $> 99.0\%$ for SWRO).[295,296] The incentive for increasing the water permeability above these upper limits, assuming similar selectivity, would be a reduction in the required membrane

surface area, which potentially entails lowering the footprint of the membrane unit and downsizing the system to supply the same throughput. In this way, the energy consumption can be decreased, but further efforts have to be carried out, including process optimization as well as techno-economic review to evaluate the cost advantages offered by nanochannel-enabled membranes.

Another crucial point to consider when designing nanochannel-enabled membranes with high water permeability is the flux-driven nature of membrane fouling – meaning that the membranes are more prone to fouling as the water permeability increases. Technically, fouling is inevitable in all membrane processes.[297,298] Despite the high intrinsic water permeability coefficients exhibited by nanochannel-enabled membranes, the initial high water flux will not stay constant throughout operation but decreases quickly once membrane fouling comes into effect. This will nullify the as-promised high water permeability advantage of nanochannel-enabled membranes, rendering little difference between their final water flux and that of TFC membranes. Hence, to unlock the potential of nanochannel-enabled membranes, we argue that it is necessary to accentuate the anti-fouling properties of nanochannel-enabled membranes as we continue along the quest for improved water permeability in separation membranes. Interestingly, among the nanochannels discussed thus far, only synthetic channels, such as carbon nanotubes, graphene-based materials, and MOFs, have demonstrated anti-fouling properties when incorporated onto membrane surfaces.[85,167] And fortunately, for RO and NF processes, flux-driven fouling is not as severe as that of microfiltration (MF) and UF, owing to the relatively lower flux exhibited by the two processes. Hence, we should see more future efforts put in place for fouling studies on nanochannel-enabled membranes, especially for newer nanochannels such as POCs and MXenes.

Beyond maximizing permeability and selectivity as well as mitigating the flux-driven fouling phenomenon, nanochannels that can enhance boron rejection and chlorine resistance are also needed for RO processes.[5,40] To date, some channels such as GO, MOFs and CNTs have shown the capability to achieve this because of their tighter pore constrictions as well as the ability to restrain the conformational change in the structure of the membrane selective layer upon attack by chlorine.[10,239,299,300] However, it remains unknown if other nanochannels are similarly effective and/or chemically stable towards real operating conditions used in desalination. On this note, many of the TFN membranes (see Tables 3–5) that have shown promise for seawater desalination were evaluated under lab-scale conditions. It is therefore necessary to subject nanochannel-enabled membranes to real seawater feed and operating conditions to better understand the stability of the nanochannels when exposed to foulants and chlorine as well as evaluate their long-term separation performances when compressed under high transmembrane pressures, especially for softer biological and biomimetic channels.

Lastly, to see successful translation of nanochannel-enable membranes and put them into real practice, we need to address issues with scalability and module fabrication. Among the five membrane designs discussed in Section 3.3, only the TFN design has the versatility to accommodate different types of nanochannels (see Fig. 11a). Furthermore, TFN appears at this point to be the most scalable design as IP is a mature technology that has been widely used in commercial production of TFC membranes. Hence, modifying the recipe to fit into current IP practice to produce TFN membranes seems to be most technically viable from the industrial perspective. At present, spiral-wound modules that house flat-sheet TFC membranes for RO and NF processes are also well-suited for TFN membranes. However, to better leverage the ångström-scale precision of nanochannels for water–solute and the impending solute–solute selectivity, TFN may not always be the best design, for reasons already discussed in Section 4.2. For that, we contend that there is a need to develop more scalable fabrication methods to close the technological gap for large-scale production of other membrane designs such as those of nanolaminated membranes. And, relooking at module designs that are optimized for such nanolaminated membranes will then be crucial in realizing the real-world applicability of nanochannel-enabled membranes.

5. Concluding remarks

The coming of age of water nanochannels is definitely here for sure. Over the past two decades, we have already seen more than 20 different types of water nanochannels being explored for desalination and water separation membranes. And we foresee this trend will be here to stay with more nanochannels to come in the future. In this review, we have looked at an array of nanochannels that include aquaporins, pillar[5]arenes, I-quartets, different types of nanotubes and their porins, graphene-based materials, metal– and covalent–organic frameworks, porous organic cages, MoS_2, and MXenes, categorizing them into three overarching types: biological, biomimetic and synthetic. Their physicochemical, structural and intrinsic transport properties, fabrication methods to incorporate nanochannels and separation mechanisms governing water–solute transport through these nanochannels are being put into perspective. Five mainstream membrane designs – where nanochannels are best applied – including freestanding membranes, supported membranes such as multilayered/nanolaminated, lipid bilayered and block copolymer membranes and thin-film nanocomposite membranes – are also discussed, together with current strategies adopted to unlock the full potential of each type of nanochannel. As promised, nanochannels indeed demonstrate a strong capacity to enhance the performances of water separation membranes. Despite different studies utilizing different evaluation criteria and conditions, it is clear that, in general, biological channels tend to give the best performance, while synthetic channels are more tunable and versatile, owing to their rich chemistries and structural diversities that can embrace a wider variety of chemical modifications and membrane designs. Also, albeit the distinct advantages,

This journal is © The Royal Society of Chemistry 2022

Chem. Soc. Rev., 2022, **51**, 4537–4582 | **4575**

the challenges facing each type of nanochannel are ubiquitous, which mostly involve fouling, long-term stability and longevity and membrane engineering issues such as module design optimization. Hence, we provide our perspective to help navigate these challenges and highlight future directions where we feel will make the most significant contributions. Looking forward, we believe that research on water nanochannels will slowly move beyond water–solute selectivity to solute–solute selectivity as new demands call for desalination and water purification to shift towards a more sustainable model.

Conflicts of interest

There are no conflicts to declare.

Acknowledgements

References

1 R. Das, C. D. Vecitis, A. Schulze, B. Cao, A. F. Ismail, X. Lu, J. Chen and S. Ramakrishna, *Chem. Soc. Rev.*, 2017, **46**, 6946–7020.

2 R. H. Tunuguntla, R. Y. Henley, Y.-C. Yao, T. A. Pham, M. Wanunu and A. Noy, *Science*, 2017, **357**, 792–796.

3 S. Bolisetty, M. Peydayesh and R. Mezzenga, *Chem. Soc. Rev.*, 2019, **48**, 463–487.

4 S. Marbach and L. Bocquet, *Chem. Soc. Rev.*, 2019, **48**, 3102–3144.

5 J. R. Werber, C. O. Osuji and M. Elimelech, *Nat. Rev. Mater.*, 2016, **1**, 16018.

6 Y.-M. Tu, L. Samineni, T. Ren, A. B. Schantz, W. Song, S. Sharma and M. Kumar, *J. Membr. Sci.*, 2020, **620**, 118968.

7 A. Roy, J. Shen, H. Joshi, W. Song, Y.-M. Tu, R. Chowdhury, R. Ye, N. Li, C. Ren, M. Kumar, A. Aksimentiev and H. Zeng, *Nat. Nanotechnol.*, 2021, **16**, 911–917.

8 K. Gopinadhan, S. Hu, A. Esfandiar, M. Lozada-Hidalgo, F. C. Wang, Q. Yang, A. V. Tyurnina, A. Keerthi, B. Radha and A. K. Geim, *Science*, 2019, **363**, 145–148.

9 Q. Xie, M. A. Alibakhshi, S. Jiao, Z. Xu, M. Hempel, J. Kong, H. G. Park and C. Duan, *Nat. Nanotechnol.*, 2018, **13**, 238–245.

10 Y. J. Lim, K. Goh, M. Kurihara and R. Wang, *J. Membr. Sci.*, 2021, **629**, 119292.

11 H. Li, C. Qiu, S. Ren, Q. Dong, S. Zhang, F. Zhou, X. Liang, J. Wang, S. Li and M. Yu, *Science*, 2020, **367**, 667–671.

12 L. Chen, G. Shi, J. Shen, B. Peng, B. Zhang, Y. Wang, F. Bian, J. Wang, D. Li, Z. Qian, G. Xu, G. Liu, J. Zeng, L. Zhang, Y. Yang, G. Zhou, M. Wu, W. Jin, J. Li and H. Fang, *Nature*, 2017, **550**, 380–383.

13 Y. Zhao, M. Wu, Y. Guo, N. Mamrol, X. Yang, C. Gao and B. Van der Bruggen, *J. Membr. Sci.*, 2021, **634**, 119407.

14 T. Mouterde, A. Keerthi, A. R. Poggioli, S. A. Dar, A. Siria, A. K. Geim, L. Bocquet and B. Radha, *Nature*, 2019, **567**, 87–90.

15 M. Ma, F. Grey, L. Shen, M. Urbakh, S. Wu, J. Z. Liu, Y. Liu and Q. Zheng, *Nat. Nanotechnol.*, 2015, **10**, 692–695.

16 S. Wang, L. Yang, G. He, B. Shi, Y. Li, H. Wu, R. Zhang, S. Nunes and Z. Jiang, *Chem. Soc. Rev.*, 2020, **49**, 1071–1089.

17 Z. Zhang, L. Wen and L. Jiang, *Chem. Soc. Rev.*, 2018, **47**, 322–356.

18 B. Radha, A. Esfandiar, F. C. Wang, A. P. Rooney, K. Gopinadhan, A. Keerthi, A. Mishchenko, A. Janardanan, P. Blake, L. Fumagalli, M. Lozada-Hidalgo, S. Garaj, S. J. Haigh, I. V. Grigorieva, H. A. Wu and A. K. Geim, *Nature*, 2016, **538**, 222–225.

19 J. Gao, Y. Feng, W. Guo and L. Jiang, *Chem. Soc. Rev.*, 2017, **46**, 5400–5424.

20 Z.-J. Yan, D. Wang, Z. Ye, T. Fan, G. Wu, L. Deng, L. Yang, B. Li, J. Liu, T. Ma, C. Dong, Z.-T. Li, L. Xiao, Y. Wang, W. Wang and J.-L. Hou, *J. Am. Chem. Soc.*, 2020, **142**, 15638–15643.

21 M. S. Kaucher, M. Peterca, A. E. Dulcey, A. J. Kim, S. A. Vinogradov, D. A. Hammer, P. A. Heiney and V. Percec, *J. Am. Chem. Soc.*, 2007, **129**, 11698–11699.

22 L.-B. Huang, M. Di Vincenzo, M. G.-K. Ahunbay, A. van der Lee, D. Cot, S. Cerneaux, G. Maurin and M. Barboiu, *J. Am. Chem. Soc.*, 2021, **143**, 14386–14393.

23 J. Shen, J. Fan, R. Ye, N. Li, Y. Mu and H. Zeng, *Angew. Chem., Int. Ed.*, 2020, **59**, 13328–13334.

24 L.-B. Huang, A. Hardiagon, I. Kocsis, C.-A. Jegu, M. Deleanu, A. Gilles, A. van der Lee, F. Sterpone, M. Baaden and M. Barboiu, *J. Am. Chem. Soc.*, 2021, **143**, 4224–4233.

25 J. Winarta, B. Shan, S. M. Mcintyre, L. Ye, C. Wang, J. Liu and B. Mu, *Cryst. Growth Des.*, 2019, **20**, 1347–1362.

26 A. Phan, C. J. Doonan, F. J. Uribe-Romo, C. B. Knobler, M. O'Keeffe and O. M. Yaghi, *Acc. Chem. Res.*, 2010, **43**, 58–67.

27 Y. Zhong, Y. Yang, Y. Shen, W. Xu, Q. Wang, A. L. Connor, X. Zhou, L. He, X. C. Zeng, Z. Shao, Z.-L. Lu and B. Gong, *J. Am. Chem. Soc.*, 2017, **139**, 15950–15957.

28 F. J. Uribe-Romo, J. R. Hunt, H. Furukawa, C. Klock, M. O'Keeffe and O. M. Yaghi, *J. Am. Chem. Soc.*, 2009, **131**, 4570–4571.

29 Z. Wang and B. Mi, *Environ. Sci. Technol.*, 2017, **51**, 8229–8244.

30 S. Faucher, N. Aluru, M. Z. Bazant, D. Blankschtein, A. H. Brozena, J. Cumings, J. Pedro de Souza, M. Elimelech, R. Epsztein, J. T. Fourkas, A. G. Rajan, H. J. Kulik, A. Levy, A. Majumdar, C. Martin, M. McEldrew, R. P. Misra, A. Noy, T. A. Pham, M. Reed, E. Schwegler, Z. Siwy, Y. Wang and M. Strano, *J. Phys. Chem. C*, 2019, **123**, 21309–21326.

31 Z. Fei, D. Zhao, T. J. Geldbach, R. Scopelliti, P. J. Dyson, S. Antonijevic and G. Bodenhausen, *Angew. Chem., Int. Ed.*, 2005, **44**, 5720–5725.

32 H. E. Karahan, K. Goh, C. Zhang, E. Yang, C. Yıldırım, C. Y. Chuah, M. G. Ahunbay, J. Lee, Ş. B. Tantekin-Ersolmaz, Y. Chen and T.-H. Bae, *Adv. Mater.*, 2020, **32**, 1906697.

4576 | *Chem. Soc. Rev.*, 2022, **51**, 4537–4582

This journal is © The Royal Society of Chemistry 2022

33 R. Chowdhury, T. Ren, M. Shankla, K. Decker, M. Grisewood, J. Prabhakar, C. Baker, J. H. Golbeck, A. Aksimentiev, M. Kumar and C. D. Maranas, *Nat. Commun.*, 2018, **9**, 3661.

34 W. Song, H. Joshi, R. Chowdhury, J. S. Najem, Y.-X. Shen, C. Lang, C. B. Henderson, Y.-M. Tu, M. Farell, M. E. Pitz, C. D. Maranas, P. S. Cremer, R. J. Hickey, S. A. Sarles, J.-L. Hou, A. Aksimentiev and M. Kumar, *Nat. Nanotechnol.*, 2020, **15**, 73–79.

35 Y. D. Yuan, J. Dong, J. Liu, D. Zhao, H. Wu, W. Zhou, H. X. Gan, Y. W. Tong, J. Jiang and D. Zhao, *Nat. Commun.*, 2020, **11**, 1–10.

36 S.-H. Lo, D. Senthil Raja, C.-W. Chen, Y.-H. Kang, J.-J. Chen and C.-H. Lin, *Dalton Trans.*, 2016, **45**, 9565–9573.

37 A. Fuertes, H. L. Ozores, M. Amorín and J. R. Granja, *Nanoscale*, 2017, **9**, 748–753.

38 S. K. Patel, C. L. Ritt, A. Deshmukh, Z. Wang, M. Qin, R. Epsztein and M. Elimelech, *Energy Environ. Sci.*, 2020, **13**, 1694–1710.

39 Y. J. Lim, K. Goh, G. S. Lai, Y. Zhao, J. Torres and R. Wang, *J. Membr. Sci.*, 2021, **640**, 119805.

40 J. Shen, G. Liu, Y. Han and W. Jin, *Nat. Rev. Mater.*, 2021, **6**, 294–312.

41 H. Wang, M. Wang, X. Liang, J. Yuan, H. Yang, S. Wang, Y. Ren, H. Wu, F. Pan and Z. Jiang, *Chem. Soc. Rev.*, 2021, **50**, 5468–5516.

42 L. Cao, X. He, Z. Jiang, X. Li, Y. Li, Y. Ren, L. Yang and H. Wu, *Chem. Soc. Rev.*, 2017, **46**, 6725–6745.

43 S. P. Nunes, P. Z. Culfaz-Emecen, G. Z. Ramon, T. Visser, G. H. Koops, W. Jin and M. Ulbricht, *J. Membr. Sci.*, 2020, **598**, 117761.

44 Y. Wu, C.-F. Fu, Q. Huang, P. Zhang, P. Cui, J. Ran, J. Yang and T. Xu, *ACS Nano*, 2021, **15**, 7586–7595.

45 Z. Zhang, L. Wen and L. Jiang, *Nat. Rev. Mater.*, 2021, **6**, 622–639.

46 D. Wang, Y. Tian and L. Jiang, *Small*, 2021, **17**, 2100788.

47 E. Jones, M. Qadir, M. T. van Vliet, V. Smakhtin and S.-M. Kang, *Sci. Total Environ*, 2019, **657**, 1343–1356.

48 Z. Zhu, D. Wang, Y. Tian and L. Jiang, *J. Am. Chem. Soc.*, 2019, **141**, 8658–8669.

49 D. Ding, P. Gao, Q. Ma, D. Wang and F. Xia, *Small*, 2019, **15**, 1804878.

50 E. Abaie, L. Xu and Y.-X. Shen, *Front. Environ. Sci. Eng.*, 2021, **15**, 1–33.

51 J. Jakowiecki, A. Sztyler, S. Filipek, P. Li, K. Raman, N. Barathiraja, S. Ramakrishna, J. R. Eswara, A. Altaee, A. O. Sharif, P. M. Ajayan and V. Renugopalakrishnan, *Interface Focus*, 2018, **8**, 20170066.

52 F. J. Moss, P. Mahinthichaichan, D. T. Lodowski, T. Kowatz, E. Tajkhorshid, A. Engel, W. F. Boron and A. Vahedi-Faridi, *Front. Physiol.*, 2020, **11**, 728.

53 Q. Li, X. Li, L. Ning, C. H. Tan, Y. Mu and R. Wang, *Small*, 2019, **15**, 1804678.

54 Y. J. Lim, K. Goh, G. S. Lai, C. Y. Ng, J. Torres and R. Wang, *J. Membr. Sci.*, 2021, **628**, 119276.

55 J. Shen, R. Ye, A. Romanies, A. Roy, F. Chen, C. Ren, Z. Liu and H. Zeng, *J. Am. Chem. Soc.*, 2020, **142**, 10050–10058.

56 W. J. Koros and C. Zhang, *Nat. Mater.*, 2017, **16**, 289–297.

57 M. Zhao, Y. Huang, Y. Peng, Z. Huang, Q. Ma and H. Zhang, *Chem. Soc. Rev.*, 2018, **47**, 6267–6295.

58 H. Zhang, X. Li, J. Hou, L. Jiang and H. Wang, *Chem. Soc. Rev.*, 2022, **51**, 2224–2254.

59 M. Jaugstetter, N. Blanc, M. Kratz and K. Tschulik, *Chem. Soc. Rev.*, 2022, **51**, 2491–2543.

60 X. Zhang, H. Liu and L. Jiang, *Adv. Mater.*, 2019, **31**, 1804508.

61 E. Sezgin, I. Levental, S. Mayor and C. Eggeling, *Nat. Rev. Mol. Cell Biol.*, 2017, **18**, 361–374.

62 C. G. Palivan, R. Goers, A. Najer, X. Zhang, A. Car and W. Meier, *Chem. Soc. Rev.*, 2016, **45**, 377–411.

63 Y. Li, S. Qi, M. Tian, W. Widjajanti and R. Wang, *Desalination*, 2019, **467**, 103–112.

64 S. Qi, R. Wang, G. K.-M. Chaitra, J. Torres, X. Hu and A. G. Fane, *J. Membr. Sci.*, 2016, **508**, 94–103.

65 A. Horner, F. Zocher, J. Preiner, N. Ollinger, C. Siligan, S. A. Akimov and P. Pohl, *Sci. Adv.*, 2015, **1**, e1400083.

66 N. Akther, V. Sanahuja-Embuena, R. Górecki, S. Phuntsho, C. Helix-Nielsen and H. K. Shon, *Desalination*, 2021, **498**, 114795.

67 Z. Yang, X.-H. Ma and C. Y. Tang, *Desalination*, 2018, **434**, 37–59.

68 S. M. Saparov, J. R. Pfeifer, L. Al-Momani, G. Portella, B. L. de Groot, U. Koert and P. Pohl, *Phys. Rev. Lett.*, 2006, **96**, 148101.

69 Y.-x Shen, W. Si, M. Erbakan, K. Decker, R. De Zorzi, P. O. Saboe, Y. J. Kang, S. Majd, P. J. Butler, T. Walz, A. Aksimentiev, J.-L. Hou and M. Kumar, *Proc. Natl. Acad. Sci. U. S. A.*, 2015, **112**, 9810–9815.

70 X. Zhou, G. Liu, K. Yamato, Y. Shen, R. Cheng, X. Wei, W. Bai, Y. Gao, H. Li, Y. Liu, F. Liu, D. M. Czajkowsky, J. Wang, M. J. Dabney, Z. Cai, J. Hu, F. V. Bright, L. He, X. C. Zeng, Z. Shao and B. Gong, *Nat. Commun.*, 2012, **3**, 949.

71 L. Ruiz, Y. Wu and S. Keten, *Nanoscale*, 2015, **7**, 121–132.

72 D. Saeki, T. Yamashita, A. Fujii and H. Matsuyama, *Desalination*, 2015, **375**, 48–53.

73 C. J. Porter, J. R. Werber, M. Zhong, C. J. Wilson and M. Elimelech, *ACS Nano*, 2020, **14**, 10894–10916.

74 Z.-L. Qiu, L.-F. Fang, Y.-J. Shen, W.-H. Yu, B.-K. Zhu, C. Hélix-Nielsen and W. Zhang, *ACS Nano*, 2021, **15**, 7522–7535.

75 L. Cheng, M. Zhang, C. Fang, W. Feng, L. Zhu and Y. Xu, *J. Membr. Sci.*, 2021, **625**, 118975.

76 Y. Zhao, T. Tong, X. Wang, S. Lin, E. M. Reid and Y. Chen, *Environ. Sci. Technol.*, 2021, **55**, 1359–1376.

77 M. Razmkhah, A. Ahmadpour, M. T.-H. Mosavian and F. Moosavi, *Desalination*, 2017, **407**, 103–115.

78 D. Sun, S. He, W. D. Bennett, C. L. Bilodeau, O. S. Andersen, F. C. Lightstone and H. I. Ingólfsson, *J. Chem. Theory Comput.*, 2020, **17**, 7–12.

79 D. Sun, T. A. Peyear, W. F.-D. Bennett, O. S. Andersen, F. C. Lightstone and H. I. Ingólfsson, *Biophys. J.*, 2019, **117**, 1831–1844.

This journal is © The Royal Society of Chemistry 2022

Chem. Soc. Rev., 2022, **51**, 4537–4582 | 4577

80 J. Paulino, M. Yi, I. Hung, Z. Gan, X. Wang, E. Y. Chekmenev, H.-X. Zhou and T. A. Cross, *Proc. Natl. Acad. Sci. U. S. A.*, 2020, **117**, 11908–11915.

81 Y.-M. Tu, W. Song, T. Ren, Y.-X. Shen, R. Chowdhury, P. Rajapaksha, T. E. Culp, L. Samineni, C. Lang, A. Thokkadam, D. Carson, Y. Dai, A. Mukthar, M. Zhang, A. Parshin, J. N. Sloand, S. H. Medina, M. Grzelakowski, D. Bhattacharya, W. A. Phillip, E. D. Gomez, R. J. Hickey, Y. Wei and M. Kumar, *Nat. Mater.*, 2020, **19**, 347–354.

82 T. Ogoshi, T.-a Yamagishi and Y. Nakamoto, *Chem. Rev.*, 2016, **116**, 7937–8002.

83 Y. Huo and H. Zeng, *Acc. Chem. Res.*, 2016, **49**, 922–930.

84 E. Licsandru, I. Kocsis, Y.-X. Shen, S. Murail, Y.-M. Legrand, A. Van Der Lee, D. Tsai, M. Baaden, M. Kumar and M. Barboiu, *J. Am. Chem. Soc.*, 2016, **138**, 5403–5409.

85 K. Goh, H. E. Karahan, L. Wei, T.-H. Bae, A. G. Fane, R. Wang and Y. Chen, *Carbon*, 2016, **109**, 694–710.

86 Q. Wang, Y. Zhong, D. P. Miller, X. Lu, Q. Tang, Z.-L. Lu, E. Zurek, R. Liu and B. Gong, *J. Am. Chem. Soc.*, 2020, **142**, 2915–2924.

87 R. Hourani, C. Zhang, R. Van Der Weegen, L. Ruiz, C. Li, S. Keten, B. A. Helms and T. Xu, *J. Am. Chem. Soc.*, 2011, **133**, 15296–15299.

88 S. Zheng, Q. Tu, J. J. Urban, S. Li and B. Mi, *ACS Nano*, 2017, **11**, 6440–6450.

89 Z. Wang, Q. Tu, S. Zheng, J. J. Urban, S. Li and B. Mi, *Nano Lett.*, 2017, **17**, 7289–7298.

90 N. Rangnekar, N. Mittal, B. Elyassi, J. Caro and M. Tsapatsis, *Chem. Soc. Rev.*, 2015, **44**, 7128–7154.

91 M. Y. Jeon, D. Kim, P. Kumar, P. S. Lee, N. Rangnekar, P. Bai, M. Shete, B. Elyassi, H. S. Lee, K. Narasimharao, S. N. Basahel, S. Al-Thabaiti, W. Xu, H. J. Cho, E. O. Fetisov, R. Thyagarajan, R. F. DeJaco, W. Fan, K. A. Mkhoyan, J. I. Siepmann and M. Tsapatsis, *Nature*, 2017, **543**, 690–694.

92 H. Dou, M. Xu, B. Wang, Z. Zhang, G. Wen, Y. Zheng, D. Luo, L. Zhao, A. Yu, L. Zhang, Z. Jiang and Z. Chen, *Chem. Soc. Rev.*, 2021, **50**, 986–1029.

93 Y. Cheng, Y. Ying, S. Japip, S. D. Jiang, T. S. Chung, S. Zhang and D. Zhao, *Adv. Mater.*, 2018, **30**, 1802401.

94 M. H. Yap, K. L. Fow and G. Z. Chen, *Green Energy Environ.*, 2017, **2**, 218–245.

95 M. S. Denny, J. C. Moreton, L. Benz and S. M. Cohen, *Nat. Rev. Mater.*, 2016, **1**, 1–17.

96 S. Yuan, X. Li, J. Zhu, G. Zhang, P. Van Puyvelde and B. Van der Bruggen, *Chem. Soc. Rev.*, 2019, **48**, 2665–2681.

97 Z. Wang, S. Zhang, Y. Chen, Z. Zhang and S. Ma, *Chem. Soc. Rev.*, 2020, **49**, 708–735.

98 R.-R. Liang, S.-Y. Jiang, R.-H. A and X. Zhao, *Chem. Soc. Rev.*, 2020, **49**, 3920–3951.

99 P. J. Waller, F. Gándara and O. M. Yaghi, *Acc. Chem. Res.*, 2015, **48**, 3053–3063.

100 D. Rodríguez-San-Miguel, C. Montoro and F. Zamora, *Chem. Soc. Rev.*, 2020, **49**, 2291–2302.

101 H. Wang, Z. Zeng, P. Xu, L. Li, G. Zeng, R. Xiao, Z. Tang, D. Huang, L. Tang, C. Lai, D. Jiang, Y. Liu, H. Yi, L. Qin, S. Ye, X. Ren and W. Tang, *Chem. Soc. Rev.*, 2019, **48**, 488–516.

102 Y. Jin, Y. Hu, M. Ortiz, S. Huang, Y. Ge and W. Zhang, *Chem. Soc. Rev.*, 2020, **49**, 4637–4666.

103 T. Hasell and A. I. Cooper, *Nat. Rev. Mater.*, 2016, **1**, 16053.

104 M. E. Briggs and A. I. Cooper, *Chem. Mater.*, 2017, **29**, 149–157.

105 T. Ogoshi, R. Sueto, M. Yagyu, R. Kojima, T. Kakuta, T.-A. Yamagishi, K. Doitomi, A. K. Tummanapelli, H. Hirao and Y. Sakata, *Nat. Commun.*, 2019, **10**, 1–8.

106 H. Li, K. Quan, X. Yang, Z. Li, L. Zhao and H. Qiu, *TrAC, Trends Anal. Chem.*, 2020, 116026.

107 Z. Liu, S. K.-M. Nalluri and J. F. Stoddart, *Chem. Soc. Rev.*, 2017, **46**, 2459–2478.

108 P. Wei, X. Yan and F. Huang, *Chem. Soc. Rev.*, 2015, **44**, 815–832.

109 Y.-x Shen, W. Song, D. R. Barden, T. Ren, C. Lang, H. Feroz, C. B. Henderson, P. O. Saboe, D. Tsai, H. Yan, P. J. Butler, G. C. Bazan, W. A. Phillip, R. J. Hickey, P. S. Cremer, H. Vashisth and M. Kumar, *Nat. Commun.*, 2018, **9**, 1–11.

110 S. Fa, Y. Sakata, S. Akine and T. Ogoshi, *Angew. Chem., Int. Ed.*, 2020, **59**, 9309–9313.

111 L. E. Khalil-Cruz, P. Liu, F. Huang and N. M. Khashab, *ACS Appl. Mater. Interfaces*, 2021, **13**, 31337–31354.

112 H. Zhang, Z. Liu and Y. Zhao, *Chem. Soc. Rev.*, 2018, **47**, 5491–5528.

113 J. Murray, K. Kim, T. Ogoshi, W. Yao and B. C. Gibb, *Chem. Soc. Rev.*, 2017, **46**, 2479–2496.

114 P. Xin, L. Zhao, L. Mao, L. Xu, S. Hou, H. Kong, H. Fang, H. Zhu, T. Jiang and C.-P. Chen, *Chem. Commun.*, 2020, **56**, 13796–13799.

115 W. Si, P. Xin, Z.-T. Li and J.-L. Hou, *Acc. Chem. Res.*, 2015, **48**, 1612–1619.

116 D. Strilets, S. Fa, A. Hardiagon, M. Baaden, T. Ogoshi and M. Barboiu, *Angew. Chem., Int. Ed.*, 2020, **59**, 23213–23219.

117 X. Kong, Z. Zhao and J. Jiang, *Langmuir*, 2017, **33**, 11490–11495.

118 S. Murail, T. Vasiliu, A. Neamtu, M. Barboiu, F. Sterpone and M. Baaden, *Faraday Discuss.*, 2018, **209**, 125–148.

119 M. Barboiu, Y. Le Duc, A. Gilles, P.-A. Cazade, M. Michau, Y. M. Legrand, A. Van Der Lee, B. Coasne, P. Parvizi and J. Post, *Nat. Commun.*, 2014, **5**, 1–8.

120 I. Kocsis, M. Sorci, H. Vanselous, S. Murail, S. E. Sanders, E. Licsandru, Y.-M. Legrand, A. van der Lee, M. Baaden, P. B. Petersen, G. Belfort and M. Barboiu, *Sci. Adv.*, 2018, **4**, eaao5603.

121 S.-P. Zheng, Y.-H. Li, J.-J. Jiang, A. van der Lee, D. Dumitrescu and M. Barboiu, *Angew. Chem., Int. Ed.*, 2019, **58**, 12037–12042.

122 S. Iijima, *Nature*, 1991, **354**, 56–58.

123 E. Secchi, S. Marbach, A. Niguès, D. Stein, A. Siria and L. Bocquet, *Nature*, 2016, **537**, 210–213.

124 K. Goh and Y. Chen, *Nano Today*, 2017, **14**, 13–15.

125 S. Velioğlu, H. E. Karahan, K. Goh, T.-H. Bae, Y. Chen and J. W. Chew, *Small*, 2020, **16**, 1907575.

126 R. H. Tunuguntla, F. I. Allen, K. Kim, A. Belliveau and A. Noy, *Nat. Nanotechnol.*, 2016, **11**, 639–644.

4578 | *Chem. Soc. Rev.*, 2022, **51**, 4537–4582

This journal is © The Royal Society of Chemistry 2022

127 A. Fuertes, M. Juanes, J. R. Granja and J. Montenegro, *Chem. Commun.*, 2017, **53**, 7861–7871.

128 J. R. Sanborn, X. Chen, Y. C. Yao, J. A. Hammons, R. H. Tunuguntla, Y. Zhang, C. C. Newcomb, J. A. Soltis, J. J. De Yoreo, A. Van Buuren, A. N. Parikh and A. Noy, *Adv. Mater.*, 2018, **30**, 1803355.

129 Y. Li, Z. Li, F. Aydin, J. Quan, X. Chen, Y.-C. Yao, C. Zhan, Y. Chen, T. A. Pham and A. Noy, *Sci. Adv.*, 2020, **6**, eaba9966.

130 M. Calvelo, C. I. Lynch, J. R. Granja, M. S. Sansom and R. Garcia-Fandiño, *ACS Nano*, 2021, **15**, 7053–7064.

131 H.-C. Wu, T. Yoshioka, H. Nagasawa, M. Kanezashi, T. Tsuru, D. Saeki and H. Matsuyama, *J. Membr. Sci.*, 2017, **537**, 101–110.

132 G. Liu, W. Jin and N. Xu, *Chem. Soc. Rev.*, 2015, **44**, 5016–5030.

133 F. Perreault, A. F. De Faria and M. Elimelech, *Chem. Soc. Rev.*, 2015, **44**, 5861–5896.

134 L. Dong, J. Yang, M. Chhowalla and K. P. Loh, *Chem. Soc. Rev.*, 2017, **46**, 7306–7316.

135 K. Celebi, J. Buchheim, R. M. Wyss, A. Droudian, P. Gasser, I. Shorubalko, J.-I. Kye, C. Lee and H. G. Park, *Science*, 2014, **344**, 289–292.

136 P. Z. Sun, Q. Yang, W. J. Kuang, Y. V. Stebunov, W. Q. Xiong, J. Yu, R. R. Nair, M. I. Katsnelson, S. J. Yuan, I. V. Grigorieva, M. Lozada-Hidalgo, F. C. Wang and A. K. Geim, *Nature*, 2020, **579**, 229–232.

137 J. Buchheim, R. M. Wyss, I. Shorubalko and H. G. Park, *Nanoscale*, 2016, **8**, 8345–8354.

138 C. J. Russo and J. A. Golovchenko, *Proc. Natl. Acad. Sci. U. S. A.*, 2012, **109**, 5953.

139 L. Zhang and M. Jaroniec, *Chem. Soc. Rev.*, 2020, **49**, 6039–6055.

140 J. Zhao, G. He, S. Huang, L. Villalobos, M. Dakhchoune, H. Bassas and K. Agrawal, *Sci. Adv.*, 2019, **5**, eaav1851.

141 S. Huang, S. Li, L. F. Villalobos, M. Dakhchoune, M. Micari, D. J. Babu, M. T. Vahdat, M. Mensi, E. Oveisi and K. V. Agrawal, *Sci. Adv.*, 2021, **7**, eabf0116.

142 S. C. O'Hern, M. S.-H. Boutilier, J.-C. Idrobo, Y. Song, J. Kong, T. Laoui, M. Atieh and R. Karnik, *Nano Lett.*, 2014, **14**, 1234–1241.

143 S. P. Surwade, S. N. Smirnov, I. V. Vlassiouk, R. R. Unocic, G. M. Veith, S. Dai and S. M. Mahurin, *Nat. Nanotechnol.*, 2015, **10**, 459–464.

144 J. Abraham, K. S. Vasu, C. D. Williams, K. Gopinadhan, Y. Su, C. T. Cherian, J. Dix, E. Prestat, S. J. Haigh, I. V. Grigorieva, P. Carbone, A. K. Geim and R. R. Nair, *Nat. Nanotechnol.*, 2017, **12**, 546–550.

145 X. Chen and H. Wang, *Nat. Nanotechnol.*, 2021, **16**, 226–227.

146 W.-H. Zhang, M.-J. Yin, Q. Zhao, C.-G. Jin, N. Wang, S. Ji, C. L. Ritt, M. Elimelech and Q.-F. An, *Nat. Nanotechnol.*, 2021, **16**, 337–343.

147 R. R. Nair, H. A. Wu, P. N. Jayaram, I. V. Grigorieva and A. K. Geim, *Science*, 2012, **335**, 442–444.

148 A. Keerthi, S. Goutham, Y. You, P. Iamprasertkun, R. A.-W. Dryfe, A. K. Geim and B. Radha, *Nat. Commun.*, 2021, **12**, 3092.

149 R. K. Joshi, P. Carbone, F. C. Wang, V. G. Kravets, Y. Su, I. V. Grigorieva, H. A. Wu, A. K. Geim and R. R. Nair, *Science*, 2014, **343**, 752–754.

150 P. Sun, K. Wang and H. Zhu, *Adv. Mater.*, 2016, **28**, 2287–2310.

151 E. Yang, M.-H. Ham, H. B. Park, C.-M. Kim, J.-H. Song and I. S. Kim, *J. Membr. Sci.*, 2018, **547**, 73–79.

152 X. Sui, Z. Yuan, C. Liu, L. Wei, M. Xu, F. Liu, A. Montoya, K. Goh and Y. Chen, *J. Mater. Chem. A*, 2020, **8**, 9713–9725.

153 W.-S. Hung, T.-J. Lin, Y.-H. Chiao, A. Sengupta, Y.-C. Hsiao, S. R. Wickramasinghe, C.-C. Hu, K.-R. Lee and J.-Y. Lai, *J. Mater. Chem. A*, 2018, **6**, 19445–19454.

154 C. Y. Chuah, K. Goh, Y. Yang, H. Gong, W. Li, H. E. Karahan, M. D. Guiver, R. Wang and T.-H. Bae, *Chem. Rev.*, 2018, **118**, 8655–8769.

155 Z. Ji, H. Wang, S. Canossa, S. Wuttke and O. M. Yaghi, *Adv. Funct. Mater.*, 2020, **30**, 2000238.

156 M. Ding, R. W. Flaig, H.-L. Jiang and O. M. Yaghi, *Chem. Soc. Rev.*, 2019, **48**, 2783–2828.

157 Z. Hu, Y. Wang and D. Zhao, *Chem. Soc. Rev.*, 2021, **50**, 4629–4683.

158 C. Wang, X. Liu, N. Keser Demir, J. P. Chen and K. Li, *Chem. Soc. Rev.*, 2016, **45**, 5107–5134.

159 X. Wang and C. Lee, in *Advances in Sustainable Energy: Policy, Materials and Devices*, ed. Y.-J. Gao, W. Song, J. L. Liu and S. Bashir, Springer International Publishing, Cham, 2021, DOI: **10.1007/978-3-030-74406-9_14**, pp. 387–416.

160 N. C. Burtch, H. Jasuja and K. S. Walton, *Chem. Rev.*, 2014, **114**, 10575–10612.

161 H. Reinsch, M. A. van der Veen, B. Gil, B. Marszalek, T. Verbiest, D. de Vos and N. Stock, *Chem. Mater.*, 2013, **25**, 17–26.

162 G. Akiyama, R. Matsuda, H. Sato, A. Hori, M. Takata and S. Kitagawa, *Microporous Mesoporous Mater.*, 2012, **157**, 89–93.

163 L. Liu, Z. Chen, J. Wang, D. Zhang, Y. Zhu, S. Ling, K.-W. Huang, Y. Belmabkhout, K. Adil, Y. Zhang, B. Slater, M. Eddaoudi and Y. Han, *Nat. Chem.*, 2019, **11**, 622–628.

164 C. Serre, F. Millange, C. Thouvenot, M. Noguès, G. Marsolier, D. Louër and G. Férey, *J. Am. Chem. Soc.*, 2002, **124**, 13519–13526.

165 A. Nagai, Z. Guo, X. Feng, S. Jin, X. Chen, X. Ding and D. Jiang, *Nat. Commun.*, 2011, **2**, 536.

166 K. Dey, M. Pal, K. C. Rout, S. H. Kunjattu, A. Das, R. Mukherjee, U. K. Kharul and R. Banerjee, *J. Am. Chem. Soc.*, 2017, **139**, 13083–13091.

167 X. Li, Y. Liu, J. Wang, J. Gascon, J. Li and B. Van der Bruggen, *Chem. Soc. Rev.*, 2017, **46**, 7124–7144.

168 R. Liu, K. T. Tan, Y. Gong, Y. Chen, Z. Li, S. Xie, T. He, Z. Lu, H. Yang and D. Jiang, *Chem. Soc. Rev.*, 2021, **50**, 120–242.

169 J. Wang and S. Zhuang, *Coord. Chem. Rev.*, 2019, **400**, 213046.

170 X. Sui, Z. Yuan, Y. Yu, K. Goh and Y. Chen, *Small*, 2020, **16**, 2003400.

This journal is © The Royal Society of Chemistry 2022

Chem. Soc. Rev., 2022, **51**, 4537–4582 | **4579**

171 M. Deng, K. Kwac, M. Li, Y. Jung and H. G. Park, *Nano Lett.*, 2017, **17**, 2342–2348.

172 M. Heiranian, A. B. Farimani and N. R. Aluru, *Nat. Commun.*, 2015, **6**, 8616.

173 B. Radisavljevic, A. Radenovic, J. Brivio, V. Giacometti and A. Kis, *Nat. Nanotechnol.*, 2011, **6**, 147–150.

174 C. E. Ren, M. Alhabeb, B. W. Byles, M.-Q. Zhao, B. Anasori, E. Pomerantseva, K. A. Mahmoud and Y. Gogotsi, *ACS Appl. Nano Mater.*, 2018, **1**, 3644–3652.

175 Y. Wang, H. Zhang, Y. Kang, Y. Zhu, G. P. Simon and H. Wang, *ACS Nano*, 2019, **13**, 11793–11799.

176 R. P. Pandey, K. Rasool, V. E. Madhavan, B. Aïssa, Y. Gogotsi and K. A. Mahmoud, *J. Mater. Chem. A*, 2018, **6**, 3522–3533.

177 J. Li, X. Li and B. Van der Bruggen, *Environ. Sci.: Nano*, 2020, **7**, 1289–1304.

178 C. E. Ren, K. B. Hatzell, M. Alhabeb, Z. Ling, K. A. Mahmoud and Y. Gogotsi, *J. Phys. Chem. Lett.*, 2015, **6**, 4026–4031.

179 B. Anasori, M. R. Lukatskaya and Y. Gogotsi, *Nat. Rev. Mater.*, 2017, **2**, 16098.

180 M. Cheng, W. Zhang, W. Yuan, J. Xue, C. Li and S. Hou, *ACS Sustainable Chem. Eng.*, 2021, **9**, 7206–7210.

181 J. J. Richardson, M. Björnmalm and F. Caruso, *Science*, 2015, **348**, aaa2491.

182 S. Zhang, F. Xia, S. Demoustier-Champagne and A. M. Jonas, *Nanoscale*, 2021, **13**, 7471–7497.

183 J. Zhu, J. Hou, A. Uliana, Y. Zhang, M. Tian and B. Van der Bruggen, *J. Mater. Chem. A*, 2018, **6**, 3773–3792.

184 Y. Liu, M.-O. Coppens and Z. Jiang, *Chem. Soc. Rev.*, 2021, **50**, 11747–11765.

185 W. Lu, Z. Yuan, Y. Zhao, H. Zhang, H. Zhang and X. Li, *Chem. Soc. Rev.*, 2017, **46**, 2199–2236.

186 Y. J. Lim, S. M. Lee, R. Wang and J. Lee, *Membranes*, 2021, **11**, 508.

187 C. Li, S. M. Meckler, Z. P. Smith, J. E. Bachman, L. Maserati, J. R. Long and B. A. Helms, *Adv. Mater.*, 2018, **30**, 1704953.

188 H. Zheng, Z. Mou and K. Zhou, *ACS Appl. Mater. Interfaces*, 2020, **12**, 53215–53229.

189 K. Wang, X. Wang, B. Januszewski, Y. Liu, D. Li, R. Fu, M. Elimelech and X. Huang, *Chem. Soc. Rev.*, 2022, **51**, 672–719.

190 Y.-L. Ji, B.-X. Gu, S.-J. Xie, M.-J. Yin, W.-J. Qian, Q. Zhao, W.-S. Hung, K.-R. Lee, Y. Zhou, Q.-F. An and C.-J. Gao, *Adv. Mater.*, 2021, **33**, 2102292.

191 L. Zhang, B. Zhao, C. Jiang, J. Yang and G. Zheng, *Nanoscale Res. Lett.*, 2015, **10**, 266.

192 K.-J. Lee and H.-D. Park, *J. Membr. Sci.*, 2016, **501**, 144–151.

193 B. Lee, Y. Baek, M. Lee, D. H. Jeong, H. H. Lee, J. Yoon and Y. H. Kim, *Nat. Commun.*, 2015, **6**, 7109.

194 H. Liu, H. Wang and X. Zhang, *Adv. Mater.*, 2015, **27**, 249–254.

195 Y. Li, Q. Wu, X. Guo, M. Zhang, B. Chen, G. Wei, X. Li, X. Li, S. Li and L. Ma, *Nat. Commun.*, 2020, **11**, 599.

196 Y. Yang, X. Yang, L. Liang, Y. Gao, H. Cheng, X. Li, M. Zou, R. Ma, Q. Yuan and X. Duan, *Science*, 2019, **364**, 1057–1062.

197 R. Han and P. Wu, *J. Mater. Chem. A*, 2019, **7**, 6475–6481.

198 M. Fathizadeh, H. N. Tien, K. Khivantsev, J.-T. Chen and M. Yu, *J. Mater. Chem. A*, 2017, **5**, 20860–20866.

199 A. Akbari, P. Sheath, S. T. Martin, D. B. Shinde, M. Shaibani, P. C. Banerjee, R. Tkacz, D. Bhattacharyya and M. Majumder, *Nat. Commun.*, 2016, **7**, 1–12.

200 B. Meng, G. Liu, Y. Mao, F. Liang, G. Liu and W. Jin, *J. Membr. Sci.*, 2021, **623**, 119076.

201 K. G. Zhou, K. S. Vasu, C. T. Cherian, M. Neek-Amal, J. C. Zhang, H. Ghorbanfekr-Kalashami, K. Huang, O. P. Marshall, V. G. Kravets, J. Abraham, Y. Su, A. N. Grigorenko, A. Pratt, A. K. Geim, F. M. Peeters, K. S. Novoselov and R. R. Nair, *Nature*, 2018, **559**, 236–240.

202 L. Ries, E. Petit, T. Michel, C. C. Diogo, C. Gervais, C. Salameh, M. Bechelany, S. Balme, P. Miele, N. Onofrio and D. Voiry, *Nat. Mater.*, 2019, **18**, 1112–1117.

203 H. Yang, L. Yang, H. Wang, Z. Xu, Y. Zhao, Y. Luo, N. Nasir, Y. Song, H. Wu, F. Pan and Z. Jiang, *Nat. Commun.*, 2019, **10**, 2101.

204 X. Tang, Y. Qu, S.-L. Deng, Y.-Z. Tan, Q. Zhang and Q. Liu, *J. Mater. Chem. A*, 2018, **6**, 22590–22598.

205 W. L. Xu, C. Fang, F. Zhou, Z. Song, Q. Liu, R. Qiao and M. Yu, *Nano Lett.*, 2017, **17**, 2928–2933.

206 M. Zhang, P. Li, M. Li, W. Zheng, G. Xie, X. Xu, C. Liu and J. Jia, *J. Membr. Sci.*, 2021, **640**, 119841.

207 M.-N. Li, X.-F. Sun, L. Wang, S.-Y. Wang, M. Z. Afzal, C. Song and S.-G. Wang, *Desalination*, 2018, **436**, 107–113.

208 E. Yang, H. E. Karahan, K. Goh, C. Y. Chuah, R. Wang and T.-H. Bae, *Carbon*, 2019, **155**, 129–137.

209 C. Zhang, B.-H. Wu, M.-Q. Ma, Z. Wang and Z.-K. Xu, *Chem. Soc. Rev.*, 2019, **48**, 3811–3841.

210 J. Shen, R. Zhang, Y. Su, B. Shi, X. You, W. Guo, Y. Ma, J. Yuan, F. Wang and Z. Jiang, *J. Mater. Chem. A*, 2019, **7**, 18063–18071.

211 D. Jariwala, T. J. Marks and M. C. Hersam, *Nat. Mater.*, 2017, **16**, 170–181.

212 K. Goh, W. Jiang, H. E. Karahan, S. Zhai, L. Wei, D. Yu, A. G. Fane, R. Wang and Y. Chen, *Adv. Funct. Mater.*, 2015, **25**, 7348–7359.

213 X. Sui, Y. Wang, F. Liu, Z. Yuan, C. Wang, Y. Yu, K. Zhou, K. Goh and Y. Chen, *Matter*, 2021, **4**, 2953–2969.

214 K. M. Kang, D. W. Kim, C. E. Ren, K. M. Cho, S. J. Kim, J. H. Choi, Y. T. Nam, Y. Gogotsi and H.-T. Jung, *ACS Appl. Mater. Interfaces*, 2017, **9**, 44687–44694.

215 W. Ding, J. Cai, Z. Yu, Q. Wang, Z. Xu, Z. Wang and C. Gao, *J. Mater. Chem. A*, 2015, **3**, 20118–20126.

216 M. Wang, Z. Wang, X. Wang, S. Wang, W. Ding and C. Gao, *Environ. Sci. Technol.*, 2015, **49**, 3761–3768.

217 P. Xin, Y. Sun, H. Kong, Y. Wang, S. Tan, J. Guo, T. Jiang, W. Dong and C.-P. Chen, *Chem. Commun.*, 2017, **53**, 11492–11495.

218 C. Lang, D. Ye, W. Song, C. Yao, Y.-M. Tu, C. Capparelli, J. A. LaNasa, M. A. Hickner, E. W. Gomez, E. D. Gomez, R. J. Hickey and M. Kumar, *ACS Nano*, 2019, **13**, 8292–8302.

219 L. Guo, Y. Wang and M. Steinhart, *Chem. Soc. Rev.*, 2021, **50**, 6333–6348.

4580 | *Chem. Soc. Rev.*, 2022, **51**, 4537–4582

This journal is © The Royal Society of Chemistry 2022

220 Y. J. Lim, J. Lee, T.-H. Bae, J. Torres and R. Wang, *J. Membr. Sci.*, 2020, **611**, 118407.

221 X. Lu and M. Elimelech, *Chem. Soc. Rev.*, 2021, **50**, 6290–6307.

222 Z. Kang, H. Guo, L. Fan, G. Yang, Y. Feng, D. Sun and S. Mintova, *Chem. Soc. Rev.*, 2021, **50**, 1913–1944.

223 R. Górecki, D. M. Reurink, M. M. Khan, V. Sanahuja-Embuena, K. Trzaskuś and C. Hélix-Nielsen, *J. Membr. Sci.*, 2020, **593**, 117392.

224 L. Sharma, L. Ye, C. Yong, R. Seetharaman, K. Kho, W. Surya, R. Wang and J. Torres, *J. Membr. Sci.*, 2022, **654**, 120551.

225 Y. Zhao, Y.-N. Wang, G. S. Lai, J. Torres and R. Wang, *Environ. Sci. Technol.*, 2022, **56**, 5179–5188.

226 X. Li, C. H. Loh, R. Wang, W. Widjajanti and J. Torres, *J. Membr. Sci.*, 2017, **525**, 257–268.

227 N. A. Pham, D. Y.-F. Ng, K. Goh, Z. Dong and R. Wang, *Desalination*, 2021, **520**, 115347.

228 S. Lim, N. Akther, T.-H. Bae, S. Phuntsho, A. Merenda, L. F. Dumée and H. K. Shon, *Desalination*, 2020, **485**, 114461.

229 Y. Lin, H.-C. Wu, Q. Shen, L. Zhang, K. Guan, T. Shintani, K.-L. Tung, T. Yoshioka and H. Matsuyama, *Desalination*, 2020, **493**, 114649.

230 Q. Xue and K. Zhang, *J. Membr. Sci.*, 2021, **640**, 119808.

231 X. Wang, Q. Li, J. Zhang, H. Huang, S. Wu and Y. Yang, *J. Membr. Sci.*, 2020, **603**, 118036.

232 J. L. Fajardo-Diaz, A. Morelos-Gomez, R. Cruz-Silva, A. Matsumoto, Y. Ueno, N. Takeuchi, K. Kitamura, H. Miyakawa, S. Tejima, K. Takeuchi, K. Tsuzuki and M. Endo, *Desalination*, 2022, **523**, 115445.

233 F. Wang, T. Zheng, P. Wang, M. Chen, Z. Wang, H. Jiang and J. Ma, *Environ. Sci. Technol.*, 2021, **55**, 5324–5334.

234 L. Xu, T. Yang, M. Li, J. Chang and J. Xu, *J. Membr. Sci.*, 2020, **610**, 118111.

235 J. Lee, F. Zhou, K. Baek, W. Kim, H. Su, K. Kim, R. Wang and T.-H. Bae, *J. Membr. Sci.*, 2020, **623**, 119017.

236 Y. Lin, Q. Shen, Y. Kawabata, J. Segawa, X. Cao, K. Guan, T. Istirokhatun, T. Yoshioka and H. Matsuyama, *Chem. Eng. J.*, 2021, **420**, 127602.

237 J. Li, L. Li, Y. Xu, J. Zhu, F. Liu, J. Shen, Z. Wang and J. Lin, *Chem. Eng. J.*, 2022, **427**, 132070.

238 Q. Zhao, D. L. Zhao and T.-S. Chung, *J. Membr. Sci.*, 2021, **625**, 119158.

239 L. Liu, X. Xie, S. Qi, R. Li, X. Zhang, X. Song and C. Gao, *J. Membr. Sci.*, 2019, **580**, 101–109.

240 Z. Yang, P.-F. Sun, X. Li, B. Gan, L. Wang, X. Song, H.-D. Park and C. Y. Tang, *Environ. Sci. Technol.*, 2020, **54**, 15563–15583.

241 P.-F. Sun, Z. Yang, X. Song, J. H. Lee, C. Y. Tang and H.-D. Park, *Environ. Sci. Technol.*, 2021, **55**, 13219–13230.

242 X. Wu, M. Ding, H. Xu, W. Yang, K. Zhang, H. Tian, H. Wang and Z. Xie, *ACS Nano*, 2020, **14**, 9125–9135.

243 M. J. Park, C. Wang, D. H. Seo, R. R. Gonzales, H. Matsuyama and H. K. Shon, *J. Membr. Sci.*, 2021, **620**, 118901.

244 G. S. Lai, Y. Zhao and R. Wang, *J. Membr. Sci.*, 2022, **650**, 120405.

245 Z. Wang, Z. Wang, S. Lin, H. Jin, S. Gao, Y. Zhu and J. Jin, *Nat. Commun.*, 2018, **9**, 1–9.

246 M. Di Vincenzo, A. Tiraferri, V.-E. Musteata, S. Chisca, R. Sougrat, L.-B. Huang, S. P. Nunes and M. Barboiu, *Nat. Nanotechnol.*, 2020, **16**, 190–196.

247 M. Di Vincenzo, A. Tiraferri, V.-E. Musteata, S. Chisca, M. Deleanu, F. Ricceri, D. Cot, S. P. Nunes and M. Barboiu, *Proc. Natl. Acad. Sci. U. S. A.*, 2021, **118**, e2022200118.

248 Y. Jiang, S. Li, J. Su, X. Lv, S. Liu and B. Su, *J. Membr. Sci.*, 2021, **635**, 119523.

249 C. Li, S. Li, J. Zhang, C. Yang, B. Su, L. Han and X. Gao, *J. Membr. Sci.*, 2020, **604**, 118065.

250 J. Zhang, S. Li, D. Ren, H. Li, X. Lv, L. Han and B. Su, *Sep. Purif. Technol.*, 2021, **268**, 118649.

251 W. Zhao, H. Liu, Y. Liu, M. Jian, L. Gao, H. Wang and X. Zhang, *ACS Appl. Mater. Interfaces*, 2018, **10**, 34464–34474.

252 X. Zhu, X. Zhang, J. Li, X. Luo, D. Xu, D. Wu, W. Wang, X. Cheng, G. Li and H. Liang, *J. Membr. Sci.*, 2021, **635**, 119536.

253 D. L. Zhao, W. S. Yeung, Q. Zhao and T.-S. Chung, *J. Membr. Sci.*, 2020, **604**, 118039.

254 B. Zhao, Z. Guo, H. Wang, L. Wang, Y. Qian, X. Long, C. Ma, Z. Zhang, J. Li and H. Zhang, *J. Membr. Sci.*, 2021, **625**, 119154.

255 R. Dai, H. Han, T. Wang, X. Li and Z. Wang, *J. Membr. Sci.*, 2021, **628**, 119267.

256 Z. Li, R. Valladares Linares, S. Bucs, L. Fortunato, C. Hélix-Nielsen, J. S. Vrouwenvelder, N. Ghaffour, T. Leiknes and G. Amy, *Desalination*, 2017, **420**, 208–215.

257 M. Xie, W. Luo, H. Guo, L. D. Nghiem, C. Y. Tang and S. R. Gray, *Water Res.*, 2018, **132**, 90–98.

258 A. Güvensoy-Morkoyun, S. Kürklü-Kocaoğlu, C. Yıldırım, S. Velioğlu, H. E. Karahan, T.-H. Bae and Ş. B. Tantekin-Ersolmaz, *Carbon*, 2021, **185**, 546–557.

259 L. Xu, B. Shan, C. Gao and J. Xu, *J. Membr. Sci.*, 2020, **593**, 117398.

260 Y. Kang, M. Obaid, J. Jang and I. S. Kim, *Desalination*, 2019, **470**, 114125.

261 Z. C. Ng, W. J. Lau, G. S. Lai, J. Meng, H. Gao and A. F. Ismail, *Desalination*, 2022, **526**, 115502.

262 C. Wang, M. J. Park, D. H. Seo and H. K. Shon, *Sep. Purif. Technol.*, 2021, **254**, 117604.

263 V. Berned-Samatán, C. Rubio, A. Galán-González, E. Muñoz, A. M. Benito, W. K. Maser, J. Coronas and C. Téllez, *J. Membr. Sci.*, 2022, **652**, 120490.

264 S. Qi, W. Fang, W. Siti, W. Widjajanti, X. Hu and R. Wang, *J. Membr. Sci.*, 2018, **555**, 177–184.

265 N. Hanikel, M. S. Prévot and O. M. Yaghi, *Nat. Nanotechnol.*, 2020, **15**, 348–355.

266 J. Kamcev, M. K. Taylor, D. M. Shin, N. N. Jarenwattananon, K. A. Colwell and J. R. Long, *Adv. Mater.*, 2019, **31**, 1808027.

267 H. B. Park, J. Kamcev, L. M. Robeson, M. Elimelech and B. D. Freeman, *Science*, 2017, **356**, eaab0530.

This journal is © The Royal Society of Chemistry 2022

Chem. Soc. Rev., 2022, **51**, 4537–4582 | **4581**

268 Y. Chun, L. Qing, G. Sun, M. R. Bilad, A. G. Fane and T. H. Chong, *Desalination*, 2018, **445**, 75–84.

269 A. Bianco, Y. Chen, E. Frackowiak, M. Holzinger, N. Koratkar, V. Meunier, S. Mikhailovsky, M. Strano, J. M.-D. Tascon and M. Terrones, *Carbon*, 2020, **161**, 373–391.

270 J. Wang, X. Jin, C. Li, W. Wang, H. Wu and S. Guo, *Chem. Eng. J.*, 2019, **370**, 831–854.

271 H. Zhang, J. Hou, Y. Hu, P. Wang, R. Ou, L. Jiang, J. Z. Liu, B. D. Freeman, A. J. Hill and H. Wang, *Sci. Adv.*, 2018, **4**, eaaq0066.

272 X. Li, H. Zhang, P. Wang, J. Hou, J. Lu, C. D. Easton, X. Zhang, M. R. Hill, A. W. Thornton, J. Z. Liu, B. D. Freeman, A. J. Hill, L. Jiang and H. Wang, *Nat. Commun.*, 2019, **10**, 2490.

273 A. A. Uliana, N. T. Bui, J. Kamcev, M. K. Taylor, J. J. Urban and J. R. Long, *Science*, 2021, **372**, 296–299.

274 R. Epsztein, R. M. DuChanois, C. L. Ritt, A. Noy and M. Elimelech, *Nat. Nanotechnol.*, 2020, **15**, 426–436.

275 M. Zhang, K. Guan, Y. Ji, G. Liu, W. Jin and N. Xu, *Nat. Commun.*, 2019, **10**, 1253.

276 S. Sahu, M. Di Ventra and M. Zwolak, *Nano Lett.*, 2017, **17**, 4719–4724.

277 C. Lu, C. Hu, C. L. Ritt, X. Hua, J. Sun, H. Xia, Y. Liu, D.-W. Li, B. Ma, M. Elimelech and J. Qu, *J. Am. Chem. Soc.*, 2021, **143**, 14242–14252.

278 C. Hannesschlaeger, A. Horner and P. Pohl, *Chem. Rev.*, 2019, **119**, 5922–5953.

279 F. Sheng, B. Wu, X. Li, T. Xu, M. A. Shehzad, X. Wang, L. Ge, H. Wang and T. Xu, *Adv. Mater.*, 2021, **33**, 2104404.

280 X. Li, H. Zhang, H. Yu, J. Xia, Y.-B. Zhu, H.-A. Wu, J. Hou, J. Lu, R. Ou, C. D. Easton, C. Selomulya, M. R. Hill, L. Jiang and H. Wang, *Adv. Mater.*, 2020, **32**, 2001777.

281 C. Cheng, G. Jiang, C. J. Garvey, Y. Wang, G. P. Simon, J. Z. Liu and D. Li, *Sci. Adv.*, 2016, **2**, e1501272.

282 W. Li, W. Wu and Z. Li, *ACS Nano*, 2018, **12**, 9309–9317.

283 K. Guan, S. Wang, Y. Ji, Y. Jia, L. Zhang, K. Ushio, Y. Lin, W. Jin and H. Matsuyama, *J. Mater. Chem. A*, 2020, **8**, 25880–25889.

284 S. Jiao, L. Liu, J. Wang, K. Ma and J. Lv, *Small*, 2020, **16**, 2001223.

285 S. Zhang, B. Zhang, H. Liang, Y. Liu, Y. Qiao and Y. Qin, *Angew. Chem., Int. Ed.*, 2018, **57**, 1091–1095.

286 Z. Zhang, A. Simon, C. Abetz, M. Held, A. L. Höhme, E. S. Schneider, T. Segal-Peretz and V. Abetz, *Adv. Mater.*, 2021, **33**, 2105251.

287 A. Fang, K. Kroenlein, D. Riccardi and A. Smolyanitsky, *Nat. Mater.*, 2019, **18**, 76–81.

288 E. T. Acar, S. F. Buchsbaum, C. Combs, F. Fornasiero and Z. S. Siwy, *Sci. Adv.*, 2019, **5**, eaav2568.

289 T. Kitao, Y. Zhang, S. Kitagawa, B. Wang and T. Uemura, *Chem. Soc. Rev.*, 2017, **46**, 3108–3133.

290 C. R. Kim, T. Uemura and S. Kitagawa, *Chem. Soc. Rev.*, 2016, **45**, 3828–3845.

291 J. P. Thiruraman, K. Fujisawa, G. Danda, P. M. Das, T. Zhang, A. Bolotsky, N. Perea-López, A. Nicolaï, P. Senet, M. Terrones and M. Drndić, *Nano Lett.*, 2018, **18**, 1651–1659.

292 A. Esfandiar, B. Radha, F. Wang, Q. Yang, S. Hu, S. Garaj, R. R. Nair, A. K. Geim and K. Gopinadhan, *Science*, 2017, **358**, 511–513.

293 T. E. Culp, B. Khara, K. P. Brickey, M. Geitner, T. J. Zimudzi, J. D. Wilbur, S. D. Jons, A. Roy, M. Paul, B. Ganapathysubramanian, A. L. Zydney, M. Kumar and E. D. Gomez, *Science*, 2021, **371**, 72–75.

294 R. Zhang, Y. Liu, M. He, Y. Su, X. Zhao, M. Elimelech and Z. Jiang, *Chem. Soc. Rev.*, 2016, **45**, 5888–5924.

295 Y. J. Lim, Y. Ma, J. W. Chew and R. Wang, *Desalination*, 2022, **533**, 115771.

296 Y. Okamoto and J. H. Lienhard, *Desalination*, 2019, **470**, 114064.

297 A. G. Fane, R. Wang and M. X. Hu, *Angew. Chem., Int. Ed.*, 2015, **54**, 3368–3386.

298 X. Tong, S. Liu, J. Crittenden and Y. Chen, *ACS Nano*, 2021, **15**, 5838–5860.

299 D. L. Zhao, S. Japip, Y. Zhang, M. Weber, C. Maletzko and T.-S. Chung, *Water Res.*, 2020, **173**, 115557.

300 M. B. Gohain, R. R. Pawar, S. Karki, A. Hazarika, S. Hazarika and P. G. Ingole, *J. Membr. Sci.*, 2020, **609**, 118212.

4582 | *Chem. Soc. Rev.*, 2022, **51**, 4537–4582

This journal is © The Royal Society of Chemistry 2022